# Stony Brook University

**Development of the Optimal Radiochromic Film Dosimetry**

**System for Measurement of IMRT Radiation Beams**

A Dissertation Presented

by

**Jameson Todd Baker**

to

The Graduate School

in Partial fulfillment of the Requirements

for the Degree of

**Doctor of Philosophy**

in

**Biomedical Engineering**

Stony Brook University

December 2008

**Stony Brook University**

The Graduate School

**Jameson Todd Baker**

We, the dissertation committee for the above candidate for the

Doctor of Philosophy degree,

hereby recommend acceptance of this dissertation

**Lawrence Reinstein, Ph.D.**
Professor Emeritus
Department of Radiation Oncology

**Terry Button, Ph.D.**
Associate Professor
Department of Radiology

**F. Avraham Dilmanian, Ph.D.**
Associate Professor of Research
Department of Radiation Oncology

**A. Rick Lubinsky, Ph.D.**
Assistant Professor of Research
Department of Radiology
Discipline in Physics

This dissertation is accepted by the Graduate School

Lawrence Martin
Dean of the Graduate School

ii

Abstract of the Dissertation

**Development of the Optimal Radiochromic Film Dosimetry System for**

**Measurement of IMRT Radiation Beams**

by

**Jameson Todd Baker**

**Doctor of Philosophy**

in

**Biomedical Engineering**

Stony Brook University

**2008**

The complex dose patterns that result in Intensity Modulated Radiation Therapy make the typical QA of a second calculation insufficient for ensuring safe treatment of patients. Many facilities choose to deliver the treatment to film inserted in a phantom and calculate the dose delivered as an additional check of the treatment plan.

Radiochromic films allow for measurements without the use of a processor in the current digital age. International Specialty Products developed Gafchromic EBT film, which is a radiochromic film having a useful range of 1 – 800 cGy. EBT film properties are fully analyzed including studies of uniformity, spectral absorption, exposure sensitivity, energy dependence and post exposure density growth. Dosimetric performance on commercially available digitizers is studied with specific attention on the shortcomings. Finally, a custom designed scanner is built specifically for EBT film and its unique properties. Performance of the EBT digitizer is analyzed and compared against currently available scanners.

## Dedication

Writing of this dissertation was done for my wife, Melissa, and our family to come. They were my motivation in finishing and without them I do not know if I would have finished. Melissa provided constant encouragement and support in completing the work. Everything from handling all the responsibilities that I could not spend time completing to countless nights without me around. All with much grace and understanding of my absence. For this, I am much indebted to her. She is the best wife around.

Much appreciation also goes towards my parents. I know that everything they did was for my siblings and myself. Constantly striving to support the family. In my education, they were extremely supportive. The expectation that I performed to my abilities was crucial, as I usually desired to take the easier path. So much of what they did I could never repay and for that all I can say is thanks. So, Thank you!

# Table of Contents

# List of Figures

# List of Tables

# List of Equations

## List of Acronyms

| | |
|---|---|
| A/D | Analog to Digitial |
| BCC | Batch Calibration Curve |
| CCD | Charged Coupled Device |
| EBT | External Beam Therapy |
| EPID | Electronic Portal Imaging Device |
| IMRT | Intensity Modulated Radiation Therapy |
| MLC | Multileaf Collimator |
| OD | Optical Density |
| PSF | Point Spread Function |
| SDC | Single Dose Calibration |
| SSD | Source to Surface Distance |
| QA | Quality Assurance |

## Acknowledgments

I would like to thank International Specialty Products for their help throughout the entire research project. They provided Gafchromic EBT film, funds to cover the expenses of building the EBT digitizer and technical insights into properties of the EBT film. Specifically, I would like to recognize David Lewis and Carl Listl. David Lewis was an excellent resource for information on film handling and properties. He took the time to have many conversations and offered excellent advice. Carl Listl provided technical assistance in the production of the EBT digitizer. His help was crucial in covering all the aspects necessary to build the EBT digitizer.

# 1 Background & Significance

## 1.1 Introduction

In the 1990's Intensity Modulated Radiation Therapy (IMRT) began to be used in a clinical setting as a complex form of treatment for cases that were difficult to successfully treat with conventional methods. IMRT is implemented through the use of Multi Leaf Collimators (MLCs), as a means of shaping a radiation beam. A MLC consists of metal (usually Tungsten) sheets stacked against each other and oriented so that the plane formed by the sheets is parallel to the axis of the radiation beam. Each sheet can slide independently from the other. When used in conjunction with a second set on the opposite side of the radiation beam, complex shapes can be formed. IMRT is the combination of many shapes, otherwise known as segments. Combining segments together forms complex patterns of radiation. This generates a customized dose distribution for each patient. A single dose distribution from one direction is not very useful. However, the cumulative effect of combining several fields from different angles allows for the tumor to receive a uniform dose, while avoiding patient anatomy that will be harmed by excessive radiation levels.

Determining the segment shapes requires a complex computer algorithm that can yield erroneous results. Additionally, the transfer of treatment files, misplacement of the MLC leaves by the MLC controller and a number of other errors can yield a treatment to the patient that differs from the expected dose distribution. It is, therefore, important that a well defined quality assurance (QA)

program is established[1,2] that will detect errors, so patients are not treated with incorrect treatment parameters.

Historically, QA of a conventional treatment plan is accomplished through the use of an independent calculation, along with a port film for a visual confirmation of the jaw positions in relation to the patient. Due to the added complexities involved with the leaf sequences, IMRT does not lend itself to a similar process. A comprehensive solution for IMRT QA would be a comparison of the dose delivered using the actual treatment setup and software, to ensure transfer accuracy from the planning system, with the expected results of the treatment planning system (TPS).[3]

## 1.2 IMRT QA Techniques

### 1.2.1 Dynamic log file analysis

One form of IMRT QA utilizes the dynamic log files generated by the MLC controller during radiation delivery when using MLCs. These files record the position of the MLC leaves and the dose delivered while in that position at regular intervals.[4,5] Comparing this information with the expected positions and doses in the MLC files allows for a limited QA, which includes the transfer accuracy of the plan and the ability for the linac to deliver the specified dose pattern. However, it does not to consider that the MLC controller often has an inaccuracy in the positioning of the leaves. Additionally, there is no second check on the TPS

calculations.  Most IMRT QAs solve these shortcomings through an actual dose measurement.

The use of a secondary calculation on the patient's CT is not common at this time, but it would be possible to use the dynamic log files as an input for a forward calculation.  If this calculation was completed on the same CT used in the IMRT planning, a comparison could be made of the two.  One challenge is obtaining an accurate match between two dose calculation algorithms, as each has its own set of errors.  The comparison of two calculations will yield a summation of the errors as the difference, in addition to inaccuracies in delivery.[6] Studies have been made using a Monte Carlo technique as the second calculation and the doses to 95% and 5% of the volume were compared.  These resulted in dose errors up to 5.9%, but typically in the 2.5-3% range.[7]  The same calculations were completed using the MLC file rather than the dynamic logs.  Dose errors had a maximum value of 1.5% and typically were 0.3%.[7]  When using the dynamic log files the increased error shows it is important to take into consideration the delivery systems ability to provide the planned dose.

1.2.2  2D arrays

One of the most convenient methods of measuring a radiation dose distribution is through the use of a two-dimensional array.  These consist of many measuring points spread around a plane located at depth within a phantom.  Measurement is usually performed with 256 to 1000 ion chambers or diodes.  The distance between the measurement points vary from about 5 mm to 10

mm[8,9].  This allows for fast setup, easy measurement and accurate results in the measurement locations.

Studies were completed on the dosimetric accuracy of PTW's device 2D Array Seven29, which utilizes 0.125 cm$^3$ ion chambers.  Reproducibility was found to be 0.2% short term and 1% otherwise, but those included setup and machine output fluctuation errors.  Dose measurement was found to be linear between 2-500 cGy.[10]  Although each measurement point can determine dose very accurately a problem arises with the spacing between the measurement points.  Most MLC leaves are either 3 or 5 mm wide and move in increments that are sub millimeter in size.  If a leaf were to fall between the detectors in the array, its position would be impossible to determine accurately.  It is possible to perform a shift in the 2D array and complete a measurement a second time for more accurate results, but the efficiency and convenience of the system is then lost[9].  The end result is that the 2D array measurement system is a good system, but the poor special resolution can cause errors in the results.

1.2.3  Electronic portal imaging devices

Electronic Portal Imaging Devices (EPIDs) are very similar to using a 2D array, but are different in that the measurement points are not within the phantom being irradiated.  Instead the phantom exit dose is measured.  Collecting exit dose means that a back projection dose calculation method must be performed to obtain a dose measurement.  This means that from the port image the exit fluence must be determined.  The dose to the phantom can then be found based

on the knowledge of the phantom shape and energy absorption along the path from the source to the particular pixel in the EPID.[11]

The EPID, being fixed to the gantry, will always measure the entire field being delivered provided that the field is not bigger than the EPID. This is different from a 2D array in that when the array plane and the gantry are aligned on the same axis only a line profile will be measured for that field at various depths. Full knowledge of the dose distribution of all fields allows for the calculation of a 3D volume, rather than just a plane. This enables a more complete analysis of the dose distribution. This additional information is beneficial in a research setting or when a more detailed study is necessary.

There are several drawbacks to an EPID IMRT QA method. First, there is a difference in the dose calculation algorithm between the treatment planning system and the particular back projection method used to determine phantom dose. This means that comparison errors could be caused by lower accuracy in the QA algorithm, but would have to be viewed as delivery errors[12]. Second, the fluence needed for the back projection is not directly measured by the EPID. Included in the measurement are scatter and glare that must be removed before an actual fluence pattern is found. Even when a fluence pattern is obtained it does not guarantee an energy deposition (or dose), which is dependent on the energy spectrum of a particular photon beam.[13,14] Finally, a smaller problem would be the neglect of gantry and detector sag yielding a misalignment that interferes with the calculation results.[12]

1.2.4  Film

Silver based radiation sensitive films have existed in radiography and radiation dosimetry for many years.   These films require a processor or a dark room for development of the film, much like photography film from a camera. Radiochromic films have a radiosensitive dye embedded into the film, which automatically darkens after exposure to radiation or even slight sensitivity to light in the 400 nm range and shorter.

A much more detailed discussion of radiation sensitive film is to follow, but the major advantage to film is the resolution that it provides.   When measurements are performed at lower resolution, errors in dose can occur between the measurement points.  Unfortunately, film involves more steps before a dose is determined and the accuracy of the measurement is not as precise as a two-dimensional array if a strict procedure is not followed.

## 1.3   Radiation Sensitive Films

1.3.1  Radiographic film

Most radiographic films are constructed by laminating a polyester base with radiosensitive emulsion.  The active components of the emulsion are silver halide crystals, which often consist of silver bromide and silver iodide.  Radiation ionizes the silver halide crystal and creates what is known as a latent image. The sensitivity of the film is dependent on the ratio between the sliver bromide,

silver iodide and other components in the emulsion (iodine, chlorine, etc.) in addition to the size of the crystals, which typically range from 1 – 3 $\mu m$.[15] Film sensitivity is characterized by the sensitometric curve, also known as the H&D curve. Figure 1 shows an example of an H&D curve for EDR2 film. Silver based films yield a linear response in a dose vs. optical density (OD) graph. OD is determined through Equation 1. By definition the transmission in the OD formula is measured with white light and has a specific geometry. For simplicity, OD is used to talk about the absorbance of any light spectrum without a predefined geometry. As the film has fewer silver halide crystals that are not ionized, the radiation incident on the film cannot ionize more crystals, so the response of the film will begin to roll off. In this region it is still possible to measure dose, but the density will not grow linearly.

$$OD = -\log(T) = -\log\left(\frac{I_o}{I}\right)$$

**Equation 1 – Optical Density where T is the light transmission, $I_0$ is the incident light and I is the transmitted light.**

Processing the film is a critical element in dosimetry using radiographic film. Temperature, chemical concentrations and time are all major components in determining the final OD that a particular dose will yield. The initial step in processing a film is developing. In this step the latent image or the ionized silver halide molecules are reduced to metallic silver and unexposed silver halide grains remain unaffected. Developing is done with a basic solution of Hydroquinone, Metol or Phenidone. The nest step is fixing, which is the process of washing away the undeveloped crystals while allowing the metallic silver to

7

remain in the emulsion of the film.  Sodium and ammonium thiosulfate perform the fixing in an acidifier to neutralize the developer solution that was transported with the film.  The developer and fixer need to be replenished with developing the film and time due to oxidation.  The temperature of the solutions greatly affects this rate due to a greater amount of oxidation.  A high temperature means more replenishing must occur, but processing time is reduced.  It is necessary to find a balance between time, temperature and replenishment rate.  How well a specific processor maintains these variables will affect how accurate a particular OD is between films in a single or multiple developing sessions.  In the final step of processing, the film must be washed to remove the chemicals and dried.[15]
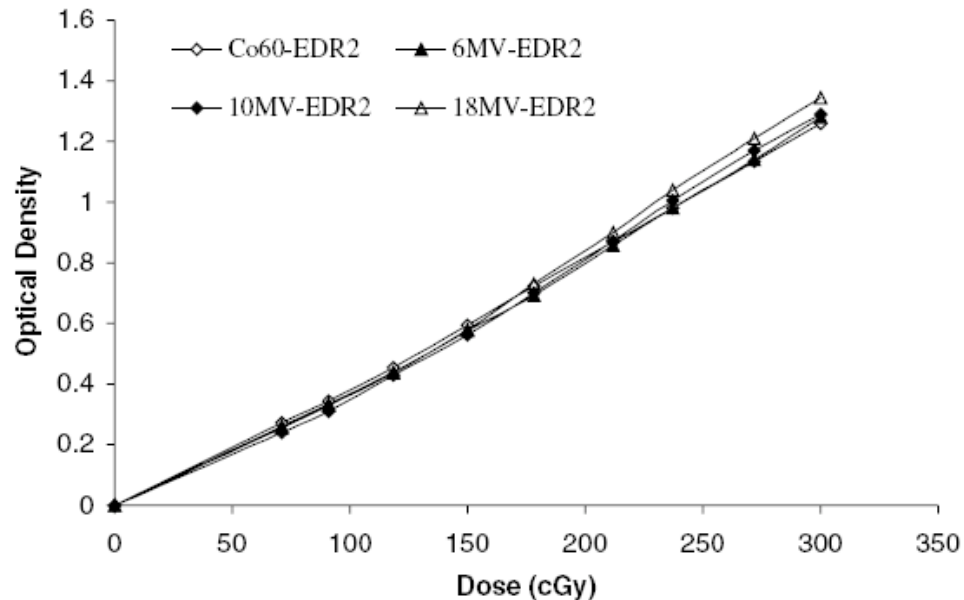


**Figure 1 – Kodak EDR2 H&D curve.**[16]

Radiographic dose measurement is also dependant on the photon energy incident on the film.  Photon absorption in high energy photon beams is primarily dependant on electron density.  As the photon energy drops to values below 200 keV interaction becomes photoelectric dependant.  The major deciding factor in

8

absorption for the photoelectric effect is the atomic number, whish is proportional to $Z^3$. Film measurements are usually performed in a water equivalent phantom with an effective atomic number of approximately 6.5, compared to water at 7.22.[17] Knowing that radiographic film contains silver, which has an atomic number of 47, it is necessary to know the effects that low energy photons have on film measurements. Figure 2 shows the increased response of Kodak XV film at energies below 200 keV. Clearly, as the spectrum of the exposing radiation changes, the resulting OD of the film will vary. This means that the best results can only be achieved when films are exposed at the same field size, depth in phantom, energy and distance from the radiation source[16,18] as is shown in Figures 1, 3 and 4, because all will change the energy spectrum incident on the film.
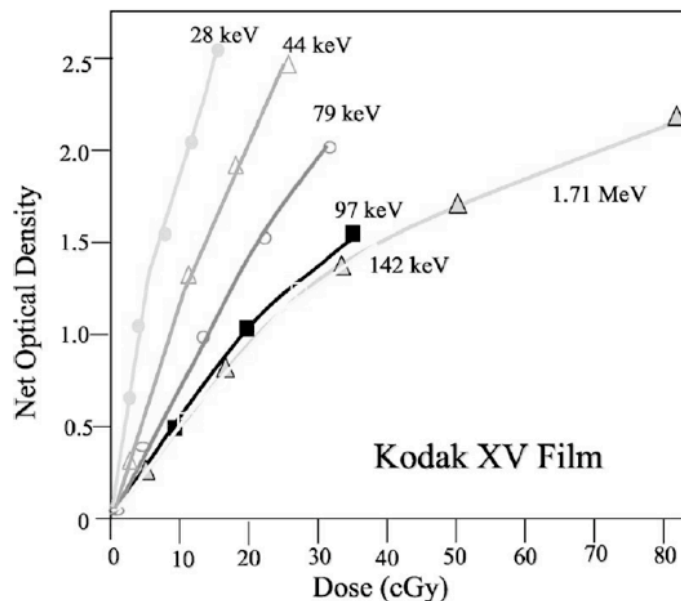


**Figure 2 – Low energy photon dependence of Kodak XV film[15] where netOD = OD – OD_{0 Gy}.**
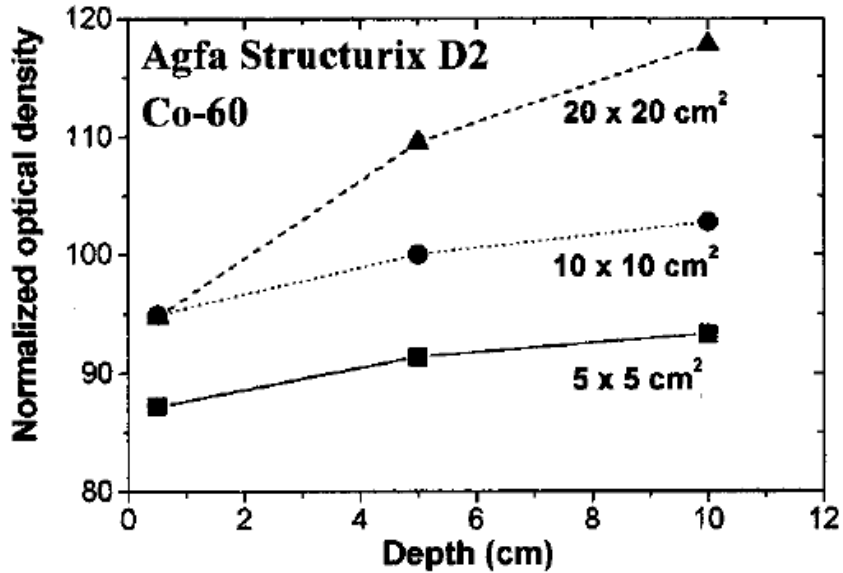
**Figure** 3 – **Variation in radiographic film OD with field size[18] at 0.4 Gy. Normalized to 10x10 cm² at 5 cm depth.**
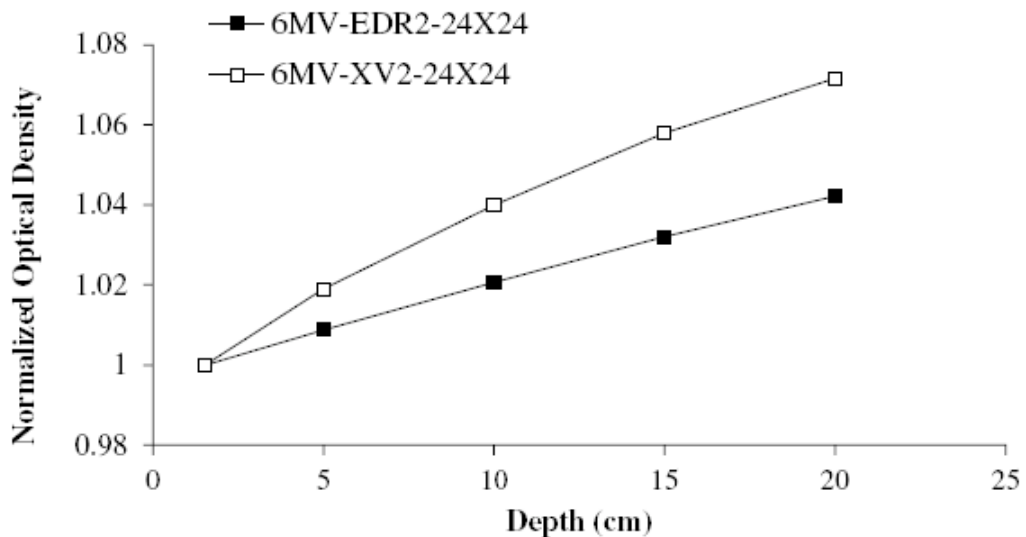


**Figure 4 – Variation in OD with depth for Kodak EDR2 and XV film[16] at doses of 300 and 80 cGy respectively and a field size of 24x24 cm².**

1.3.2  Radiochromic film

Radiochromic films have existed for many years and are primarily produced by International Specialty Products (Wayne, NJ).  Historically, the radiochromic films available were Gafchromic HD-810 or MD-55.  These have useful ranges between 10 – 400 Gy or 2 – 100 Gy respectively.[19]  There was

10

also a Gafchromic HS which was about twice as sensitive as MD-55,[20] but this film is no longer available. All of the films have an active layer composed of the same photosensitive dye that darkens when photons of sufficient energy are incident on the film. Different dose ranges are generated by changing the thickness or adding multiple active layers. The active layers are laminated onto a clear polyester base and multiple layers can be glued together. The MD-55 film is sandwiched between clear polyester yielding a tough outer layer. This makes it more difficult to damage the film and yields a resistance to water.[21, 22]
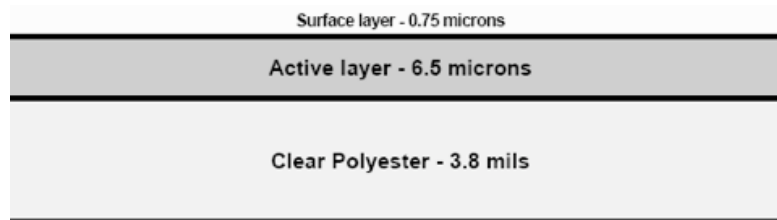


Figure 5 – Gafchromic HD-810 construction.[21]
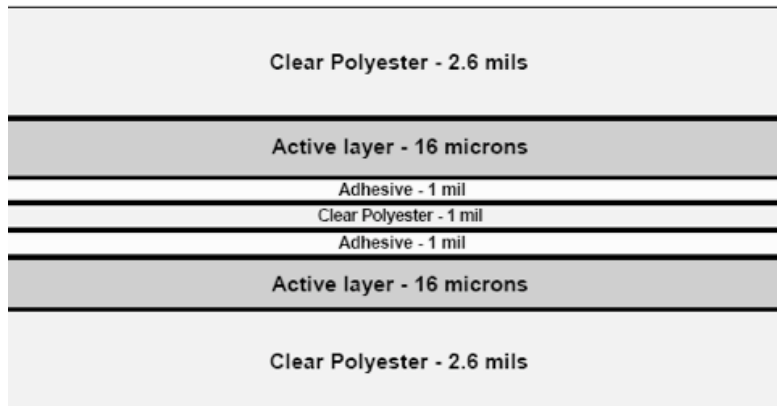


Figure 6 – Gafchromic MD-V2-55 construction.[22]

Unlike radiographic films, radiochromic films do not have uniform absorption of visible light. The spectral absorption has two peaks at 614 and 674nm.[23] The 674 nm peak is has much stronger absorption than the 614 nm. This affects the light source and detector that is ideal for measuring the response of the film. An unirradiated film will allow close to uniform light to pass through at

all visible wavelengths.   As the exposure dose increases, photon absorption in the 600 – 700 nm range increases while it remains nearly constant below 500 nm, as seen in figure 7.  Typically, the greater change in the signal measured by a system with a variation in the input the more accurate results.   In the case of film dosimetry, the signal is determined by a light source, film and detector.   The input is dose.  Measurement with white light would have much less signal change as the dose increases compared to a system that measures a single wavelength at 674 nm.  This is due to the unabsorbed light washing out the signal.
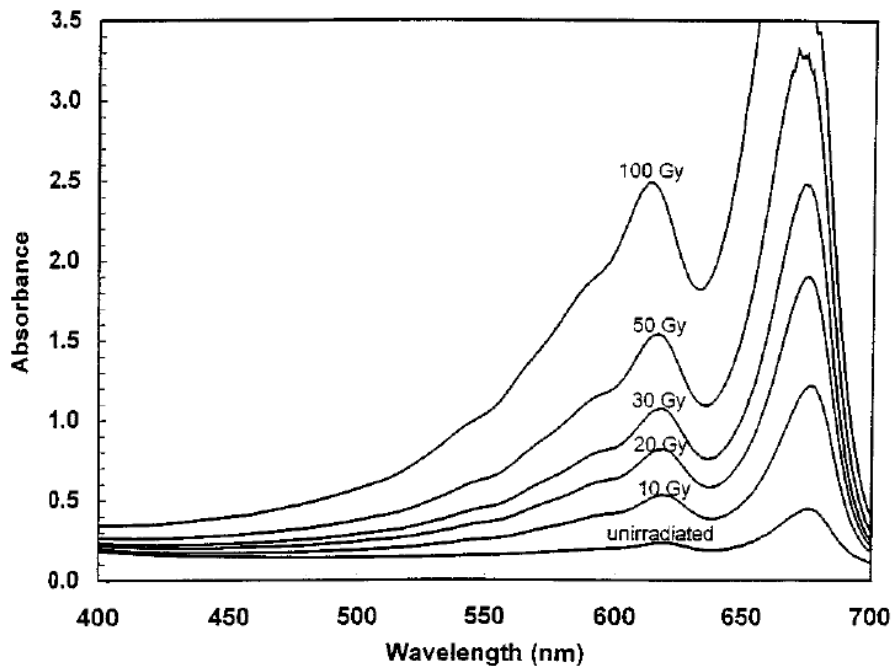


**Figure 7 – Spectral Absorption of Gafchromic MD-V2-55 film for 0, 10, 20, 30, 50, 100 Gy.**[23]

Due to the variable absorption of light with wavelength, a H&D curve must be accompanied by the type of light used during measurement of the film. Figures 8 and 9 show the dose response for MD-55 and HD-810 when a Nuclear Associated Radiochromic densitometer 37-443 reads the film with a narrow band pass light source centered at 660 nm.[21, 22]   The radiation energy exposing the

film would also have a significant effect on the sensitometric curve. Figure 10

shows that when low energy radiation exposes the film its response is reduced

by about 40%[24]. Energy dependence is shown by the change in OD for a

specific radiation source relative to the change in OD for $^{60}$Co at an exposure of 1

Gy. For exposures at energies of 75, 100 and 225 kV the response in the film is

significantly less than what $^{60}$Co generates. Energies of 6 and 18 MV show a

smaller response than $^{60}$Co as well. A possible cause for the decreased

response from linear accelerators is the low energy component of the beam,

where $^{60}$Co primarily yields energies of 1.17 and 1.33 MeV of $^{60}$Co. The variable

response requires that the measurement conditions be similar to that of silver

based films. Specifically, Calibration and measurement films must all be

exposed under the same conditions (depth, orientation and source spectrum) for

best results.
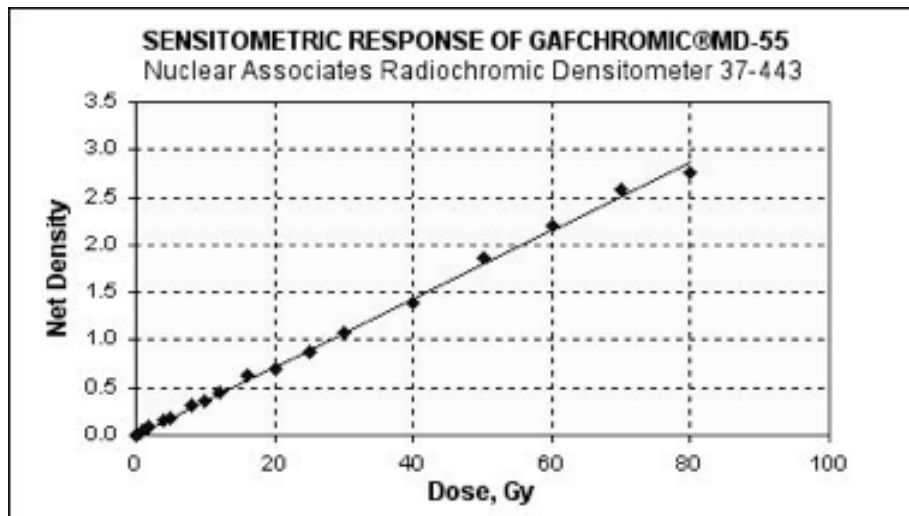


**Figure 8 – Sensitometric curve for Gafchromic MD-55 using a Nuclear Associates Radiochromic Densitometer 37-433.**[22]
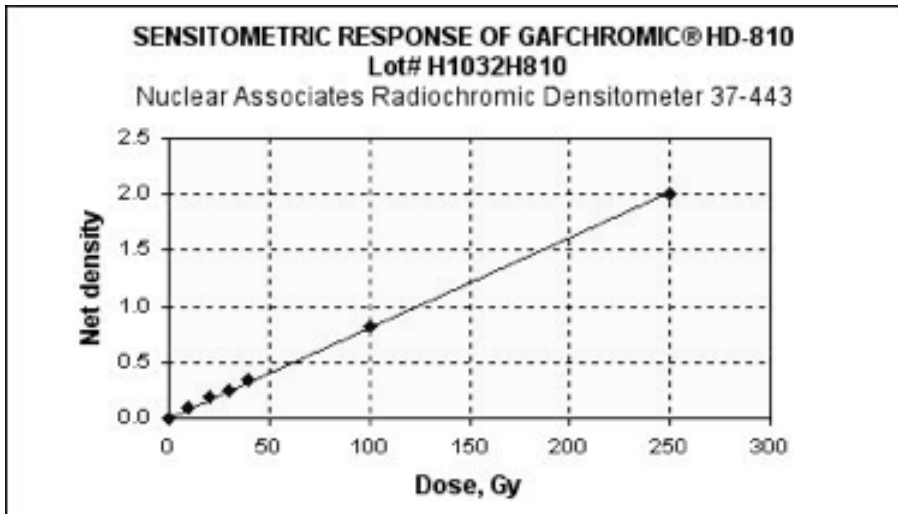
**Figure 9 – Sensitometric curve for Gafchromic HD-810 using a Nuclear Associates Radiochromic Densitometer 37-443.**[21]
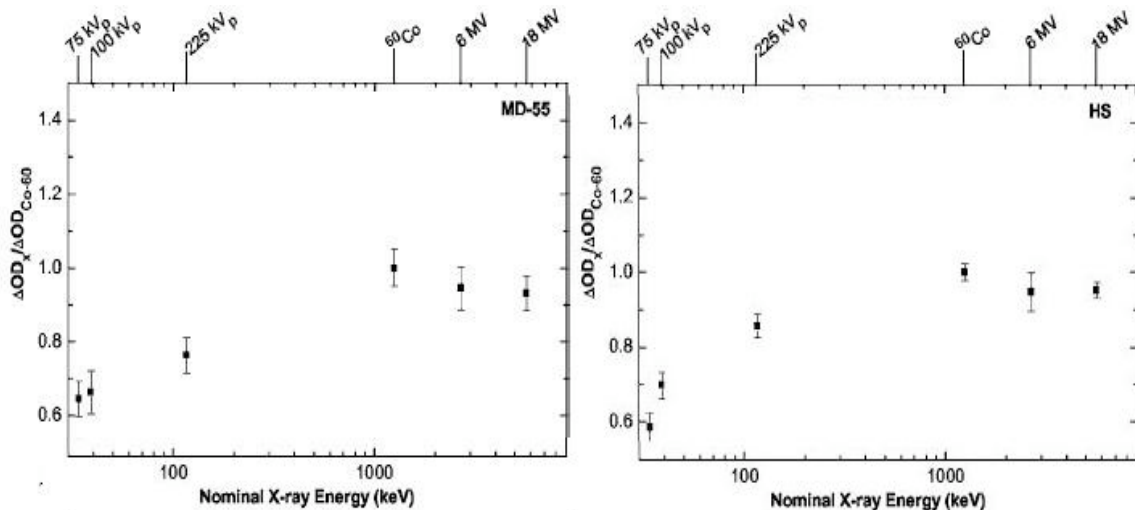


**Figure 10 – Energy dependence of MD-55 and HD-810 displayed as a change in OD at various photon energies relative to $^{60}$Co for an exposure of 1 Gy**[24].

After exposure darkening of radiochromic film begins immediately. In the case of Gafchromic MD-55 it can extend beyond 50 hours before the OD is within 1% of its final value.[25] This is very different from radiographic film where final development can take place within 5 min of exposure. The post exposure density growth is an inconvenience when performing measurements and prohibits measurements under some time restrictions. Optical density growth can be seen in Figure 11 in addition to the results of a rapid color stabilization

14

technique. In this method the films are maintained at 45 °C for 2 hours within 30 minutes of exposure. All optical densities measurements are normalized to a reading that occurred 3 hours after exposure. The rapid color stabilization technique reduces the required time to wait before measurement, but 3 hours are still needed before variations less than 1% are seen.
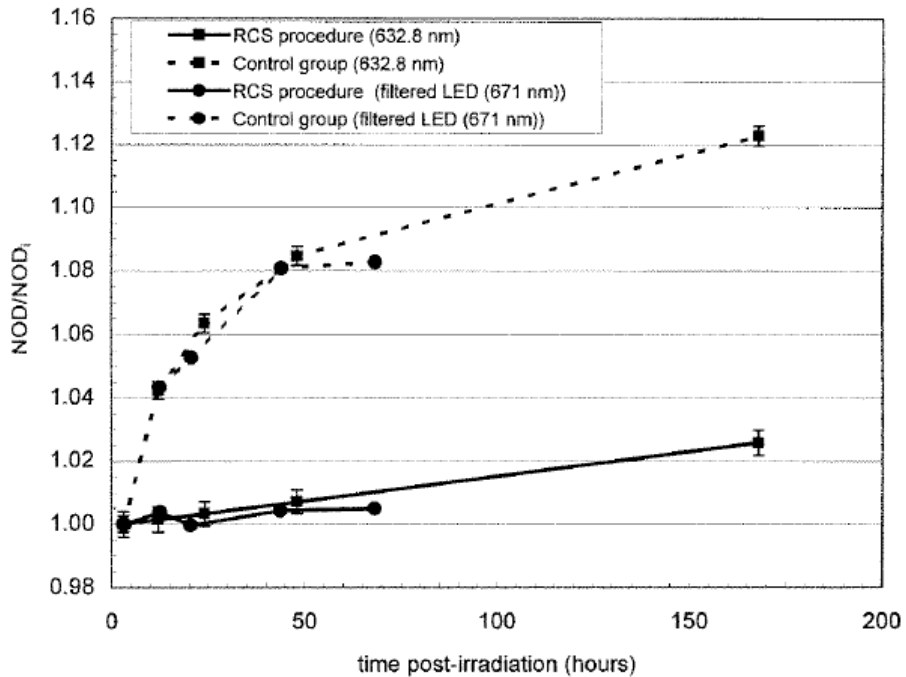


**Figure 11 – Gafchromic MD-55 post exposure density growth at 632.8 and 671 nm for a control group and rapid color stabilization procedure where the film is at 45°C for 2 hours after exposure.**

## 1.4   Film digitizers

Analysis of QA films must be completed through the use of a computer, unless the desired results are only point doses. The film digitizer is used in the final step of creating dose conversion curves and reading the films. Errors in measuring the OD of the film greatly affect the dose measurement. Factors such

15

as uniformity, input-output response, noise, geometric distortion, spatial resolution and low contrast discrimination all affect the scan quality and subsequent dose accuracy.[26] Uniformity measures the response at a fixed OD across the scan plane of the digitizer. Just like film has a characteristic curve that relates dose to OD, a digitizer will have an input-output response that converts the input or the OD of the film into some output value. Sometimes the output is related to OD, but often it is an indication of the incident light on the detector. Noise is generated through light output fluctuation, film granularity, electrical and quantum noise if low light levels are incident on the detector. Geometric distortion can occur through optics that stretch or compress the image uniformly or inaccurate movement of the film/detector during the scan, because most digitizers are limited to either a point or one dimensional simultaneous measurements. Spatial resolution is affected by the point spread function (PSF) of the scanner and ultimately determines how much detail can be seen in the images. Often a low OD region of the film would cause a higher OD region to be digitized at a lower OD, due to the light leaking into the high OD region. Finally, low contrast discrimination is determined mostly through the combination of input-output response and noise of the digitizer. Typically, low contrast discrimination diminishes at higher ODs.

Most digitizer can be place into two main categories. Either they are point based or incorporate a charged coupled device (CCD) into the design. A point based system often has a laser as a light source, but it could incorporate another

system that illuminates a single point at a time. Laser systems can raster horizontally while the film is moved vertically to perform the scan. Optics before the film focus the laser and cause the raster action. Collection of the light after the film is often accomplished with a light collection tube. Another design for a laser system is to shift the film in two dimensions and have a fixed light source. This provides more accurate results because the light always passes perpendicular to the film, but makes scan times much longer.

Devices using a CCD have a linear array of solid state detectors that simultaneously read the film. Two dimensions are measured through either transporting the film or the light source. Light sources may vary, but must illuminate an entire row of the film. Less common is a two dimensional detector that measures the entire film at once. Often this is with a very broad light source that illuminates the entire film as evenly as possible and then a camera that takes a picture. Each setup has its own set of problems and are discussed later.

```
┌──────────────┐      ┌──────────────┐      ┌──────────────┐
│ Light Source │ ───▶ │    Optics    │ ───▶ │     Film     │
└──────────────┘      └──────────────┘      └──────────────┘
                                                    │
                                                    ▼
                      ┌──────────────┐      ┌──────────────┐
                      │ A/D Conversion│ ◀── │    Optics    │
                      └──────────────┘      └──────────────┘
```
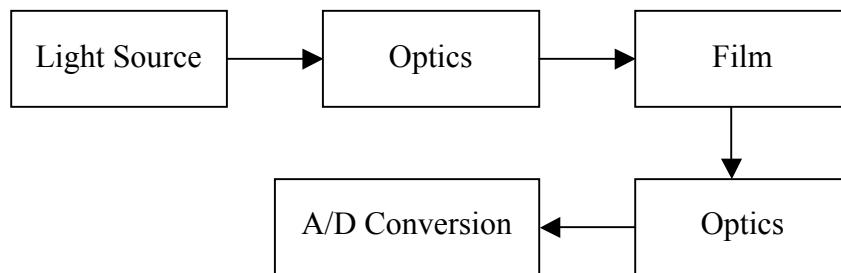
**Figure 12 – Block diagram of typical digitizer configuration. The optics either before or after the film may not be present in a particular system depending on the specific design.**

## 2 Gafchromic EBT Film Properties

### 2.1 Gafchromic EBT construction

Manufacturing the film consists of laminating the 17 microns thick active layer on a 97 microns clear polyester base. The active component consists of fibers that tend to align in the direction of lamination. (The lamination direction is across the shorter dimension of the film.) On top of the active layer is a surface layer that is 3 microns.[27] The final product is constructed through sandwiching two active layers between the clear polyester with no adhesive. Lamination of the active layer is not completely uniform perpendicular to the lamination direction. To increase uniformity in this direction, rolls of film are cut in the direction of lamination. When the two active layers are combined the middle portions are matched to the outside of the opposite side. Therefore, if there is a gradient in the thickness of the active layer the two will combine to cancel out the gradient.[28]



**CLEAR POLYESTER - 97 microns**

**ACTIVE LAYER - 17 microns**
SURFACE LAYER - 6 microns
**ACTIVE LAYER - 17 microns**

**CLEAR POLYESTER - 97 microns**
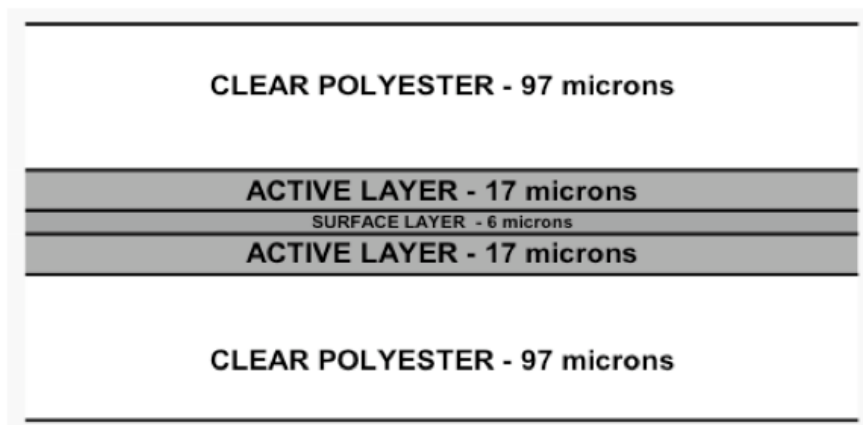
**Figure 13 – Gafchromic EBT film construction.[27]**

## 2.2 Uniformity

As mentioned previously, irrespective of the technique used in measuring a two dimensional plane, it is critical to have the same response in one region as another with a set of input parameters.  For radiochromic film this means that the optical density generated due to a fixed amount of radiation must be equivalent in all regions of the film.  This requirement must hold true between films when they are going to be compared against each other.  In IMRT QA, measurements across a plane are taken and then these values are analyzed with respect to a calculated value.  IMRT QA does not analyzed films against each other, but a calibration must be made by exposing a separate film, therefore each film must have the same response.

### 2.2.1  Uniformity test setup

The most critical procedure in measuring the uniformity of film is exposing it at a consistent and determined level.  This is completed with a phantom at an extended SSD of 500 cm.  Film is at a depth of 5 cm and backscatter of 10 cm is used, which is depicted in figure 13.  As discussed later, the center 16x16 cm region is analyzed, correcting for the extended SSD shows that the center 3.2x3.2 cm of the radiation beam are used when looking at the isocenter.  An exposure with a much more even distribution is achieved using this method.  Correction for variations in the exposure is achieved through the use of ion chamber measurements in a 5x5 grid with a spacing of 4 cm on the same plane

as the film.  The center location in the grid falls on the central axis of the radiation beam.
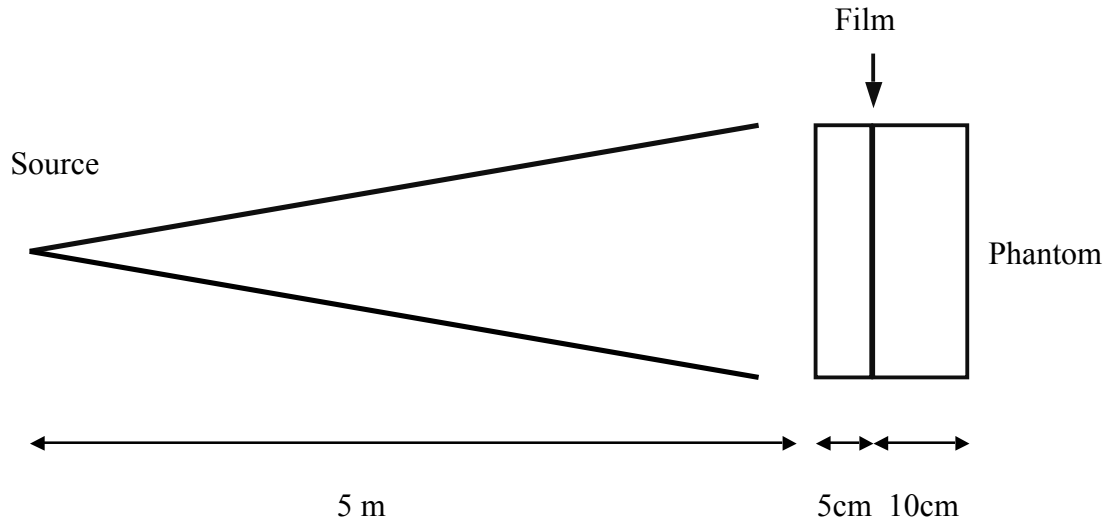


**Figure 14 – Uniformity test setup with a phantom at an SSD = 5 m, film depth = 5 cm and backscatter > 10 cm.**

Five films were exposed to doses of 90 cGy and 260 cGy and measured in the same grid positions as the ion chamber measurements.  Readout of the film was performed using a Macbeth (Grand Rapids, MI) TD932 point densitometer, retrofitted with a 635 nm band pass filter that has a 10 nm transmission width. Optical density precision of the point densitometer was 0.01, which did not yield enough accuracy in the dose.  To increase the precision the voltage output of the densitometer was measured using an IOTech (Cleveland, OH) DAQBoard 2005 that had a 16 bit A/D converter.  Using the A/D converter yields a maximum quantization dose error of 5.6E-6% as opposed to 4.8% of the standard densitometer.  The system performs a measurement 95% of the time with a certainty in dose error less than 1.5% and 1% for 100 cGy and 300 cGy respectively.

2.2.2 Uniformity results

The test setup creates a method of exposing the film with minimal variation in dose, but there will still be some fluctuation from region to region. Table 1 shows the percent variation from the central axis at the same points used for comparison of the films. Overall, the variation in the exposure from the minimum to maximum value is 1.41%.

|  | -8 cm | -4 cm | 0 cm | 4 cm | 8 cm |
|---|---|---|---|---|---|
| 8 cm | 0.02% | 0.30% | 0.43% | 0.46% | 0.32% |
| 4 cm | -0.11% | 0.02% | 0.04% | 0.19% | 0.17% |
| 0 cm | -0.06% | -0.04% | 0.00% | 0.17% | 0.28% |
| -4 cm | 0.17% | 0.47% | 0.55% | 0.68% | 0.64% |
| -8 cm | 0.83% | 1.21% | 1.30% | 1.30% | 1.04% |

**Table 1 – Exposure variation expressed as a percentage deviation from the central axis for a 25x25 cm grid with 4 cm spacing.**

Uniformity measurements were performed after the films were allowed to stabilize overnight. Using the point densitometer system each point in the 5x5 grid was measured. The pixel value then converted to dose using a $4^{th}$ order polynomial curve that was generated from a film exposed at the same time. Measured doses were then scaled by the values in Table 1, so that the variations in the exposing doses would be removed. Intrasheet deviations were found by comparing each measurement point to the average value for that sheet. The maximum difference from that value and the standard deviation of all the errors is shown in Table 2. Intersheet uses the same data points, but the comparisons are completed based on a specific grid location. For each grid location the average dose from the five films is found and the error is the difference from that value. Again the results are shown in Table 2. It should be noted that the error

21

of the measurement system is responsible for a significant contribution of the measured variations.

| Intrasheet | | | | Intersheet | | |
|---|---|---|---|---|---|---|
| Dose Level | Error | | | Dose Level | Error | |
| Average (cGy) | Max (cGy) | Std (cGy) | | Average (cGy) | Max (cGy) | Std (cGy) |
| 90 | 2.04 | 0.84 | | 90 | 3.60 | 0.69 |
| 260 | 5.54 | 2.13 | | 260 | 4.23 | 1.24 |

**Table 2 – Intrasheet and intersheet uniformity displayed as the maximum and standard deviation from the central axis measurement point.  All errors are after exposure correction.**

Gafchromic EBT film shows a significant improvement over Gafchromic MD-55-2, which has shown intrasheet uniformities differences up to 15%.[29]  For the majority of measurements the intersheet error is less than the Intrasheet. This may seem unexpected compared to radiographic film where the coating process is very even, but processing causes a film to film variation.  EBT skips the processor, so the intersheet variation is low for films from the same production lot and handled in a similar fashion.   Laminating does cause fluctuations for EBT film.

## 2.3   Spectral absorption analysis

Gafchromic EBT film's color has pink tones as an unirradiated film, but as the exposure increases the appearance turns towards more of a blue/purple. This means that the absorption in the visible light spectrum starts uneven and strengthens by different amounts dependant on the wavelength of the light. Analysis of past versions of radiochromic film (MD-55 etc.) show that there are

two peaks in the absorption spectrum at 610 and 670 nm.  The 670 nm peak has absorption of approximately double the 610 nm.[30]  The active component in EBT film resembles previous versions so it was expected that the absorption peaks would appear similarly.

2.3.1  Absorption spectrum test setup

A sheet of film was cut into 2x2 cm squares and irradiated to doses of 0, 0.5, 1, 2, 3, 4, 5, 6, 8 and 10 Gy.  Analysis was performed using a Beckman (Fullerton, CA) DU640B photospectrometer.  Films read where always placed with the direction of lamination oriented in the vertical direction.  The photospectrometer was set to perform measurements at a rate of 240 nm/min with a step size of 0.2 nm.

In addition to the standard spectral absorption measurements the effects of a polarized light source and film temperature on the absorption spectrum were investigated.  Films will typically be measured within 4 °C of room temperature, so measurements at 18 and 26 °C were taken.  Temperature was maintained by placing an insulated box inside the photospectrometer with a temperature controller.  The uncontrolled temperature always fell within the 18 – 26 °C range so a method of heating and cooling was necessary.  For 26 °C, a resistor and a fan were placed within the insulated box.  When the temperature fell below the 26 °C the controller allowed current to flow through the resistor and the fan circulated the air.  Cooler temperatures (18 °C) were maintained using the same method except the resistor was replaced by ice.

Polarized light source measurements were achieved through the use of a polarizer located in the light path before the film. While keeping the polarizer stable, with the axis of polarization oriented vertically, the film was rotated in 10° increments and a measurement of visible light was performed.
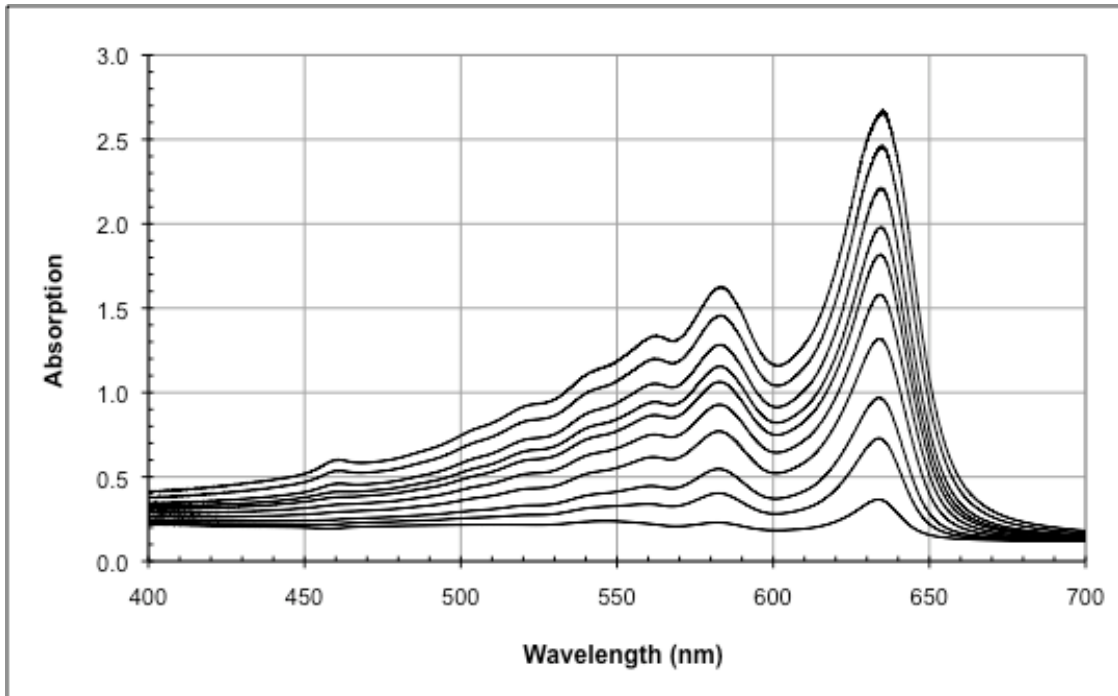


**Figure 15 – Gafchromic EBT absorption spectrum for doses of 0, 0.5, 1, 2, 3,4, 5, 6, 8 and 10 Gy.**

2.3.2  Spectral analysis results

The absorption spectrum shows two peaks at 583 and 635 nm, as shown in Figure 15. The steep falloff in the absorption at wavelengths longer than 635 nm reveals the importance of measuring the film at the proper wavelengths. A light source will have significant degradation in signal at higher doses if measurements with wavelengths above 650 nm are used. Figure 16 shows the sensitometric curve at a wavelength of 635 nm. Even though the EBT film is rated for use up to 8 Gy[27] it still exhibits significant absorption increase beyond

10 Gy. This demonstrates that when the measurement wavelength is paired accurately with the absorption peak, it is possible to achieve a greater dynamic range and have an increased signal in the measurement system.
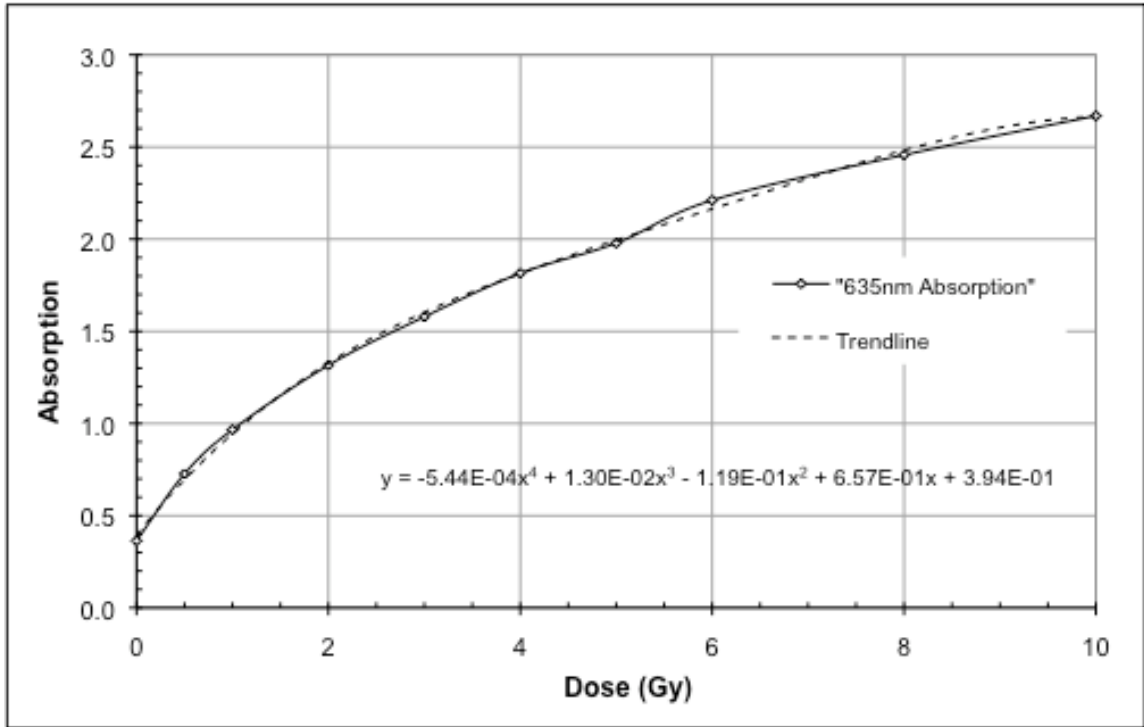


**Figure 16 – Gafchromic EBT film sensitometric curve based on the peak absorption wavelength (635 nm) as seen by a Beckman DU 640B photospectrometer.**

2.3.3  Temperature and polarization effects on absorption spectrum

Looking at the absorption spectrum for Gafchromic EBT film at 18 and 26°C have two major effects due to temperature as shown in Figure 17. As the temperature increases there is a shift in the peak wavelength by 2 nm over the 8°C range. In most cases this aspect will not be very important, but if measurements are taken in the 640 – 660 nm range this would significantly change the absorption. When looking at 640 nm the absorption change is 0.3 between the two temperatures, so that is about a 0.04 per degree. This translates into about 2.4% change in dose per degree. Also, the absorption peak

will increase by about 0.05 OD. Fortunately, the shift in the absorption peak and the rise in absorption will tend to cancel out at 635 nm, placing more importance on using a system solely at a wavelength of 635 nm.
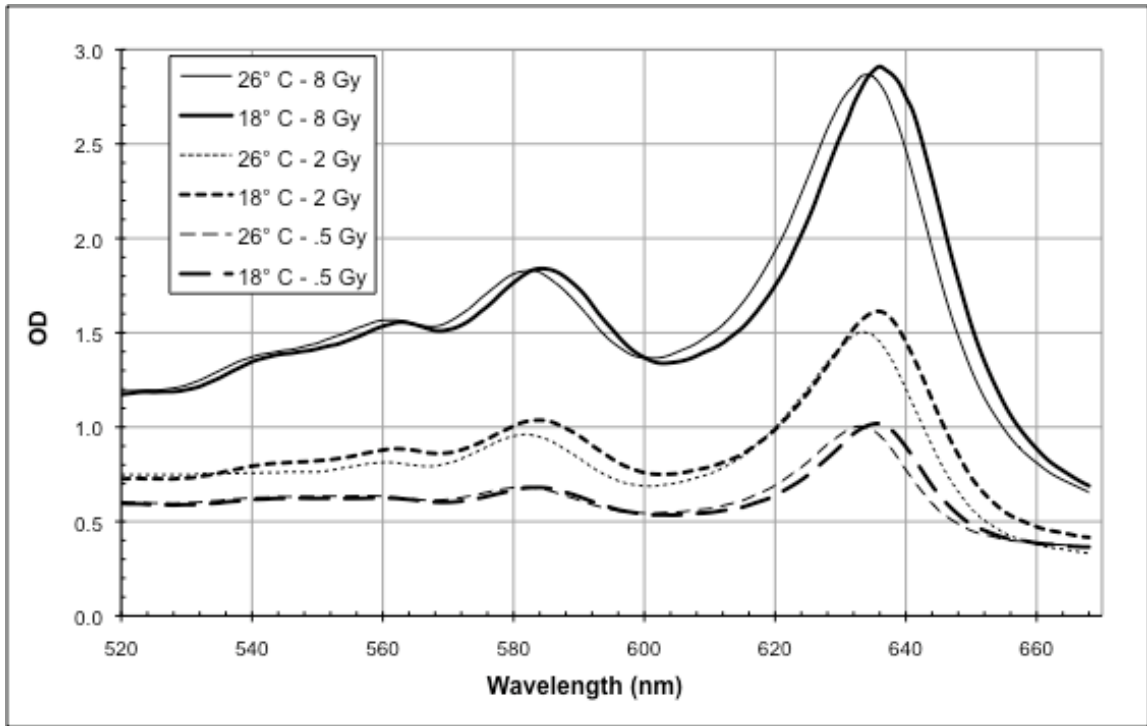


**Figure 17 – Gafchromic EBT absorption spectrum at temperatures of 18° and 26°C for 0.5, 2 and 8 Gy. Major peak shifts 2 nm, but most prominent is the increased absorption.**

Rotating the angle of polarization of the light with respect to the lamination direction has a profound affect on the final absorption. Figure 18 shows the results of a 90° rotation on a 3 Gy film. The 0° scan has noise around the peak due to the polarizer decreasing the light intensity. A change in absorption of 0.85 is seen over the 90° range. Effects of this magnitude would not be seen unless the films are rotated 90° between scans and a highly polarized source is used. Although, fluctuations of approximately 0.1 to 0.2 OD are observed in a scan of an unexposed film with a polarized light source. The cause of the polarizing effects stem from the laminating of the fibers in the active layer. Fibers tend to

align in the direction of lamination. Although, regional variations will occur that have a shift in the rotation or a change in the percentage of fibers aligning in the lamination direction. The variations in fiber orientation account for the change in the detected OD within a film. This makes measurements with a linearly polarized light source ineffective.
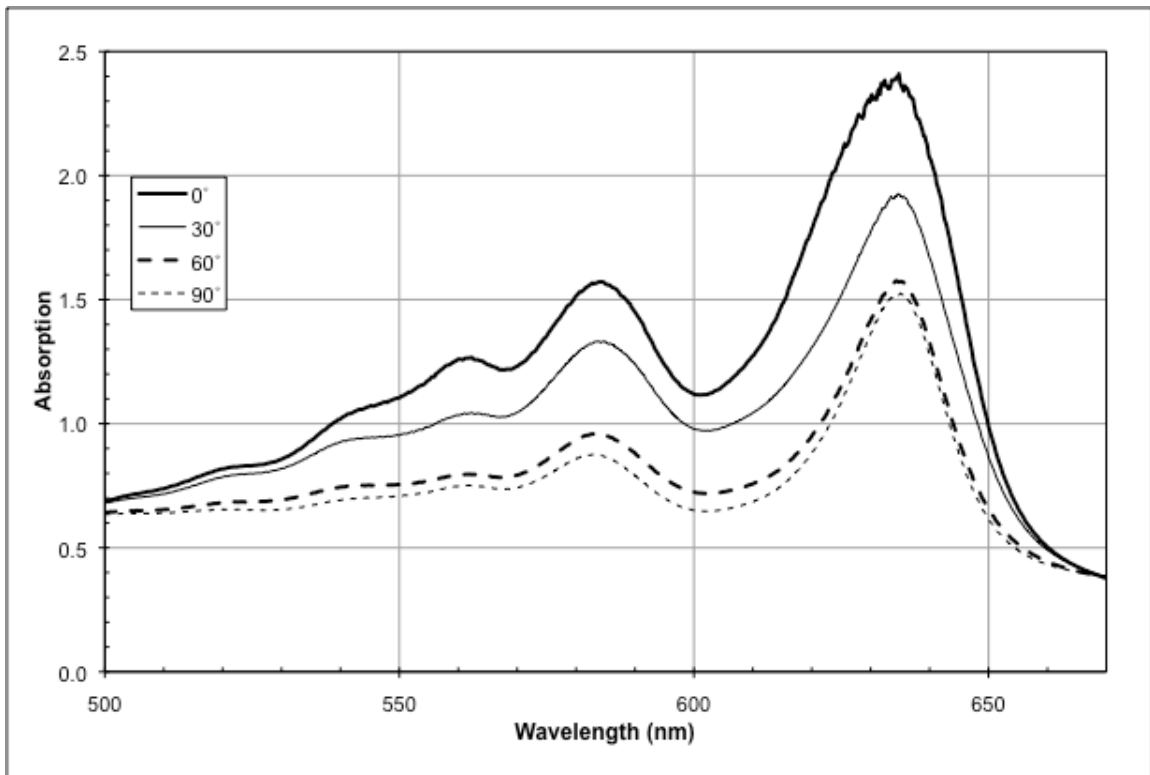


**Figure 18 – Gafchromic EBT absorption spectrum for polarized light source. 0° means that the light is polarized in the direction of lamination. The data shown is for a dose of 3 Gy.**

## 2.4 Gafchromic EBT energy dependence

As discussed previously, radiographic films show an energy sensitivity about 300% higher at 28 keV compared to 1.71 MeV (Figure 2), and MD-55 and HD-810 films have 60% of the response at low energies as compared to an

exposure from [60]Co (Figure 10). Even though IMRT is in the megavoltage range, a significant portion of the exposure to the film is due to the low energy portion of the spectrum. This photon energy dependence limits the methods in which the film can be used. To be as accurate as possible, any calibration curve is only precise for a given field size and depth. Unfortunately, IMRT is composed of many different field sizes and depths (when treatment gantry angles are used) and it is impossible to avoid the errors introduced due to the energy variations. When using Gafchromic EBT film for IMRT QA one should also understand how it is dependent on energy.

2.4.1 Energy dependence experimental setup

The test performed used photons in the clinical energy range. Exposures for 6 and 15 MV were made at their respective nominal $d_{max}$ of 1.5 and 3 cm in solid water at an SSD of 100 cm. Ion chamber exposures of 100 MU at the respective depths ensured accurate knowledge of the dose delivered to the film. The geometric depth of the ion chamber was shifted towards the source by 0.6 * $r_{cav}$ when converting from ionization to dose as described in TG-51.[31] The ion chamber used was a PTW pinpoint ion chamber with a volume of 0.015 cc. At each energy the films where irradiated with 3x3 cm fields with 50, 100, 200, 300, 400, 600 and 800 cGy to $d_{max}$. Film analysis was executed using the Macbeth TD932 point densitometer with the 635 nm band pass filter and A/D converter as described in the film uniformity section.

2.4.2  Energy dependence results

Figure 19 shows the dose response curves for 6 and 15 MV. The curves fall within the measurement accuracy of the system. Therefore, there is no distinguishable difference in the response of the energies.  The variations in the delivered dose are due to the 6 MV exposure depths being slightly shy of $d_{max}$. Other studies have also shown no measurable difference for energies down to the 20 keV range[24] and are shown in Figure 20.
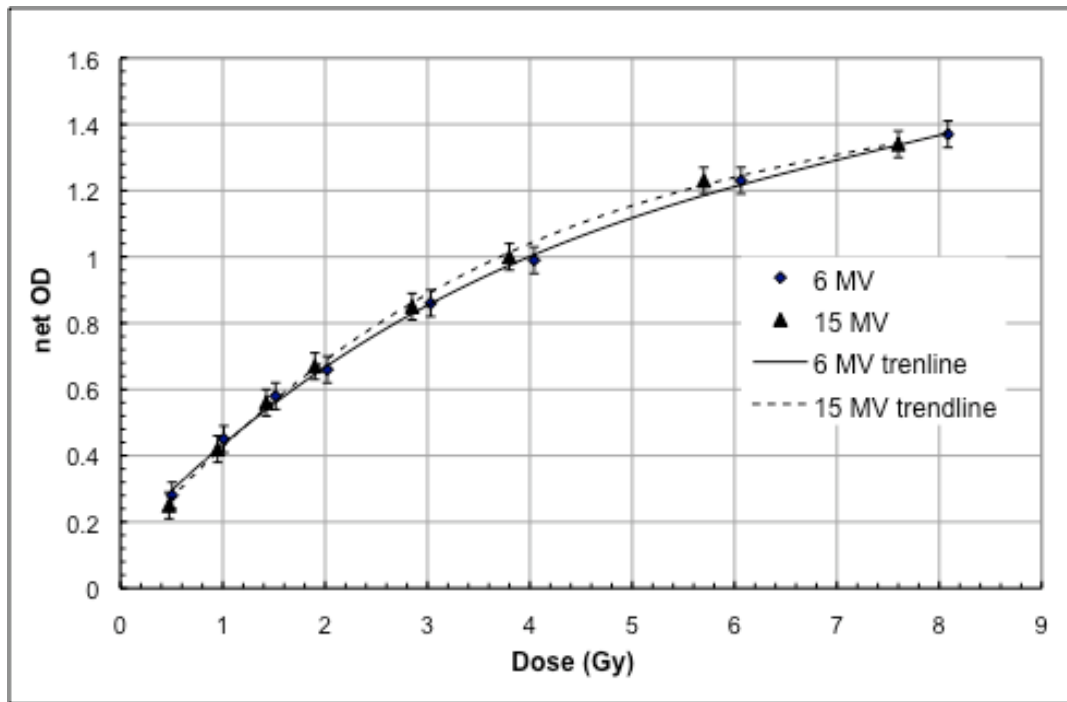


**Figure 19 – Energy dependence of Gafchromic EBT film for clinically available photons. Error bars represent 1σ.**

Elimination of the energy dependence of EBT film is due to the effective atomic number of 6.98 being nearly equal to water, which is 7.42. Table 3 shows the composition of EBT film.  Note that the Chlorine has an atomic number significantly higher and increases the response at lower energies.  MD-55 and HD-810 effective atomic energies are lower causing a decrease in the

29

photoelectric effect when compared to water.  With minimal energy dependence,

EBT film can be much more user friendly.  An accurate depth dose profile can be

taken without correction for increased or decreased response at depth.  Also, a

single calibration film can be used when performing IMRT QAs with multiple

exposure energies and still obtain accurate results while saving time.
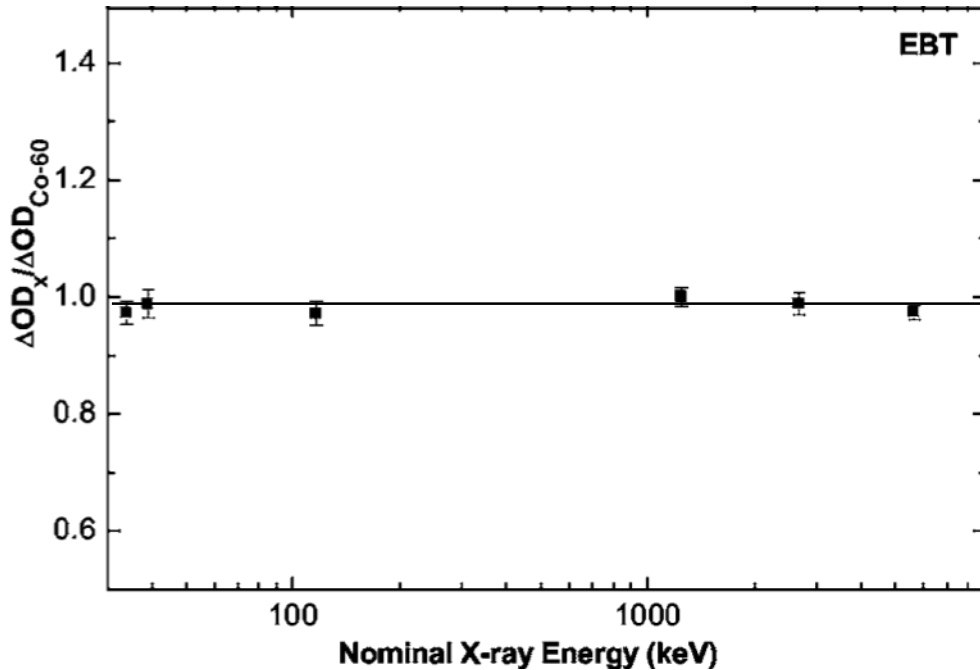


Figure 20 – $\Delta$OD/Gy of EBT film for energies of 75 kV – 18 MV normalized to $\Delta$OD/Gy for Co$_{60}$.  Error bars represent 1$\sigma$.[24]

| Atomic Composition | | | | | | Zeff = $[\sum \alpha i \ (Zi)a]^{1/a}$ |
|---|---|---|---|---|---|---|
| C | H | O | N | Li | Cl | |
| 42.3% | 39.7% | 16.2% | 1.1% | 0.3% | 0.3% | 6.98 |

Table 3 – Atomic composition and the effective atomic number of Gafchromic EBT film.[27]

## 2.5   Single dose calibration method

One may think that removing the processor from the film measurement

procedure would eliminate the need for repeated calibration.  Factors such as

post exposure density growth[32] and temperature dependence of the absorption spectrum[33] cause valid calibration curves to vary with post exposure measurement time. As a result a general calibration film is not always valid. These factors do not change the shape of the calibration curve, but they do scale it. We investigate the possibility of scaling a calibration curve using a single dose calibration (SDC) method. The SDC method involves performing a one time batch calibration curve (BCC) generation for an entire lot of Gafchromic EBT film, and using a film exposed to a known dose to scale the BCC. Doing so would save time from the typical method of exposing a dose pattern.[34]

2.5.1 Gafchromic EBT post exposure density growth

Post exposure density growth was found by using five calibration films with exposure levels of 22, 43, 84, 147, 209 and 291 cGy measured at 0.7, 1.3, 1.9, 3.3, 9.2, 21.0 and 51.9 hours post exposure. Films were measured on the Macbeth system described earlier and then converted to OD.

Figure 21 shows the change in the sensitometric curve in post exposure time for film 1. Most of the film darkening occurs in the first several hours, but there is a noticeable darkening between 21 and 52 hours post exposure. The growth in OD is greater at higher ODs, but is about the same as a fraction of the final OD. Although the film may continue to darken for a couple days, it is necessary to understand that this does not pose a problem. The rate of change in OD is an important factor. Upon measuring the film, the difference between the post exposure measurement time of the first and last film exposed must result

31

in an insignificant amount of OD growth.  Either waiting enough time before measurement or staggering the measurement times with the exposure times can remove the OD growth effects.
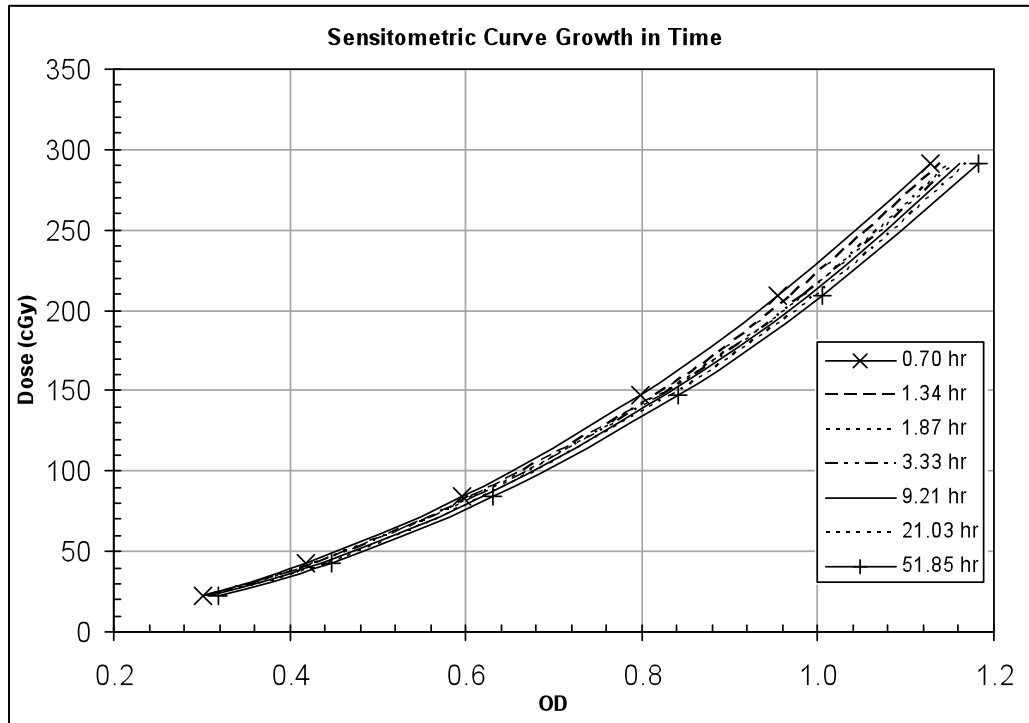


**Figure 21 – Shows the stretching of the calibration curve for film 1 in time due to the post exposure density growth.  Note that all curves tend to be centered at the zero dose point.**

### 2.5.2  Single dose calibration curve generation

Using the five films and measurements from the post exposure density growth, a BCC is generated from film 1 measured at 3.3 hours post exposure. This curve would typically only be valid for use with films that are measured at approximately the same time lapse from the exposure time.[35] However, scaling can make the BCC applicable to any measurement time for which it is scaled. Although scaling the calibration curve has been talked about, scaling was actually performed on the measured net ODs before conversion to dose, so the

measurement films fit the BCC. In this study, scaling is accomplished with an exposure from one of the calibration points in the curve.

### 2.5.3 Single dose calibration procedure

Calibration with the SDC method is performed by the following procedure:

1) Calculate the net OD for the initial calibration curve values.

2) Generate the BCC using the cubic formula in Equation 2 and record A, B and C. Note that since the equation is based from the net OD there is no $netOD^0$ term.

$$Dose = A*netOD^3 + B*netOD^2 + C*netOD$$

**Equation 2 - The equation used to fit the calibration curve.**

3) Convert Equation 2 so that the net OD is calculated as opposed to dose. This involves solving Equation 2 for net OD and yields three solutions. Two of the solutions are non-real and can be discarded. Equation 3 shows the formula for the third real solution as long as the value under the square root is positive, which is likely unless one of the dose measurements that make the calibration curve is not accurate.

$$netOD = \frac{X^{1/3} + 2^{2/3}\left(B^2 - 3AC\right)}{54^{1/3}AX^{1/3}} - \frac{B}{3A}$$

*where*

$$X = -2B^3 + 9ABC + 27A^2 Dose + \sqrt{4\left(-B^2 + 3AC\right)^3 + \left(2B^3 - 9ABC - 27A^2 Dose\right)^2}$$

**Equation 3 - Equation used to calculate the net OD. Found by solving for netOD from Equation 2 and taking the only non-imaginary solution. A, B and C are the same as what are found for Equation 2.**

The first three steps can be completed at any time prior to analysis of the measurement films. Steps 4 – 6 are to be completed on the measurement films.

4) Calculate the OD scaling factor by exposing a region to a known dose and finding the net OD of the region. The scaling factor is the result of Equation 3 when the known scaling dose is inserted divided by the measured net OD of the region.

5) Multiply the net ODs of the measurement films by the OD scaling factor to get a scaled net OD.

6) Calculate the doses on the measurement films by inputting the scaled net OD into Equation 2.

### 2.5.4    Single dose calibration accuracy

Scaling allows for effective dose calibration with the use of a single dose exposure. Figure 22 shows five measured calibration curves from five films, at 21 hours post exposure, in a graph of OD divided by dose verses dose. Viewing a graph in this fashion causes differences in the calibration curves to be amplified and gives a measure of the linearity of the film. A horizontal line would indicate a linear response. From the graph it is apparent that the film's response is not linear with a variation of 0.0035 to 0.007 OD/cGy. This demonstrates that the film is twice as sensitive at 20 cGy compared to 290 cGy. The inconsistency in OD per cGy between films at each dose level has a maximum value at 22 cGy of 0.00049 OD/cGy. This means that when comparing two sheets, the sensitivity at a particular dose level will not vary by more that 0.00049 OD/cGy.

Examining a single film's calibration curve over time shows how the sensitivity at a particular dose level can vary. This is shown in Figure 23. The

maximum change in sensitivity is found to be 0.00068 OD/cGy at 43 cGy. This

value is higher than what is seen from film to film, but it is also important to note,

at higher dose levels, this variation remains large. When comparing between

films, at a set time after exposure, the differences in the sensitivity decreases

significantly as the dose increases. As a result, the calibration curves are very

similar. After scaling, the effects of post exposure density growth are nearly

removed as seen in Figure 24. The range of the sensitivity variation is from 0

OD/cGy at the scaling dose of 209 cGy to 0.00025 OD/cGy at the 44 cGy level.

At all dose levels the variation is less than the film to film variation. This means

that the error introduced using the SDC method for calibration are less than what

is introduced by the film to film variation. Although the errors will be combined,

the addition of the error from the SDC method is not significant.
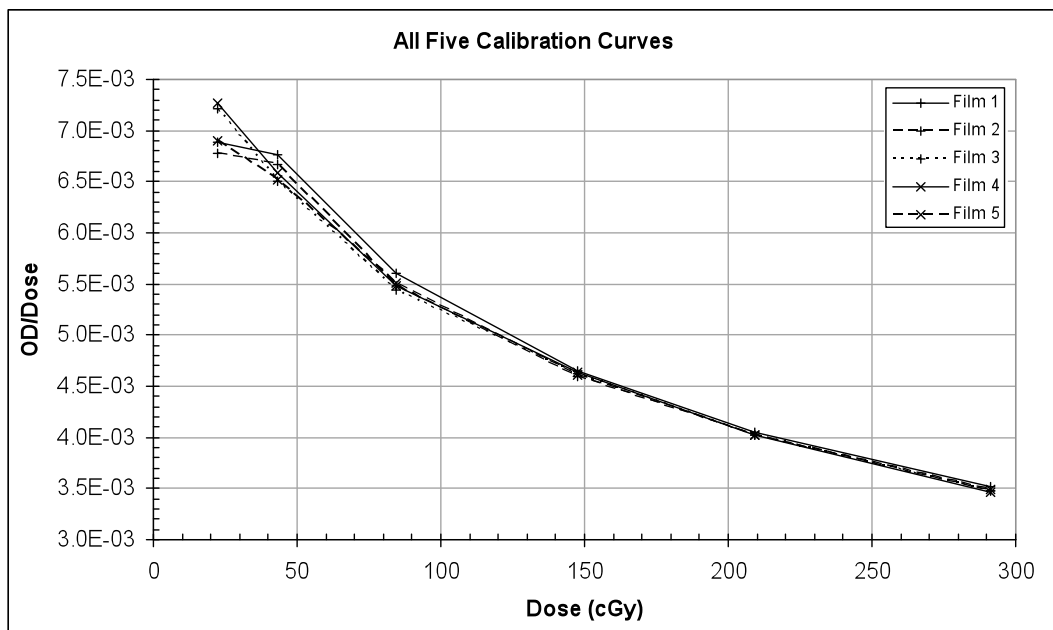


**Figure 22 - The response of 5 films prior to scaling at 21 hours post exposure. The vertical axis is shown as OD/Dose, so that the errors are enhanced. A horizontal line would indicate a linear response to the film.**

Proper selection dose to use as the scaling dose is critical. The use of error summation for each calibration curve at all post exposure measurement times was used to determine the best scaling dose. Figure 25 shows the results of the error summation. Although the actual value of the summation does not matter, how the values relate to each other is relevant. When scaled by 22 cGy the cumulative error is 18.7, which is compared to the result for 209 cGy of 2.3. This shows that over an 8 fold increase in dose error is found when scaling is performed by 22 cGy compared to a 209 cGy exposure. Empirical testing demonstrates that the best scaling dose for applications up to 300 cGy is approximately 210 cGy. The result for scaling at 290 cGy is nearly the same and is within experiment error. It is unknown whether the error will continue to remain low or will increase again, but by looking at the pattern that is formed from scaling with lower doses it is likely that the error will rise as the scaling dose increases. If the maximum exposure dose is significantly different from the 300 cGy seen here, it would be beneficial to choose a different scaling dose. A safe rule of thumb may be to use a scaling dose at 80% of the maximum calibration dose.

Figure 25 also demonstrates BBC generation through the average of 5 calibration curves and hopefully generating a very accurate BCC. At all scaling dose levels the cumulative error generated from the averaged BBC was lower, but when the scaling dose was at an optimum value, the decrease in error was insignificant. This shows that while it is important to get an accurate BBC, there appears to be little benefit in taking the average of many curves.
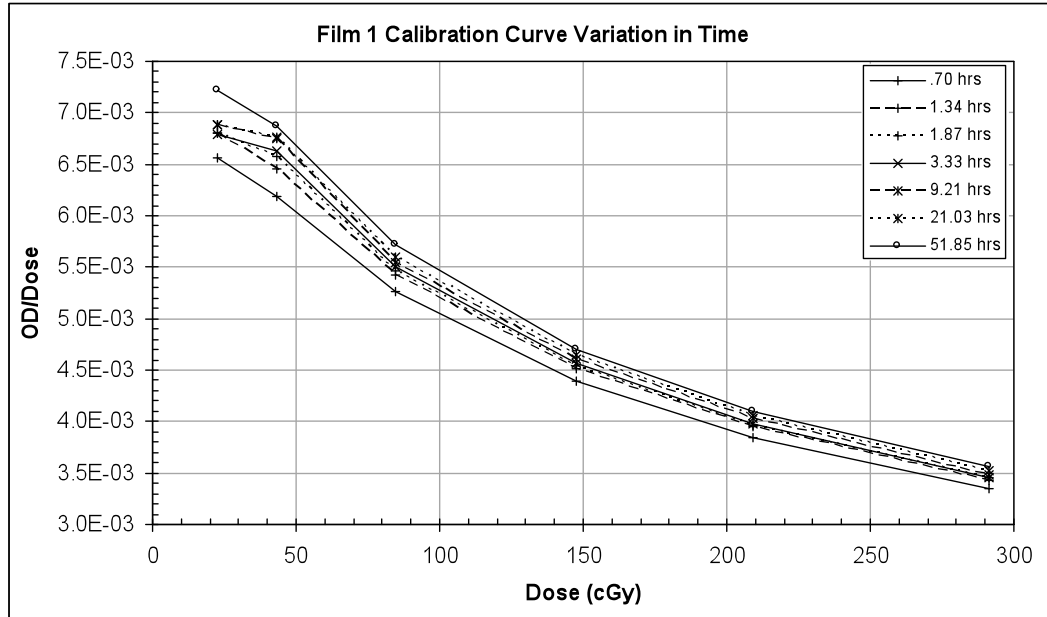
**Figure 23 – The same as Figure 22, except that it shows how film 1 changes in time. Note how the responses vary significantly in time and there is a general trend of the values increasing.**
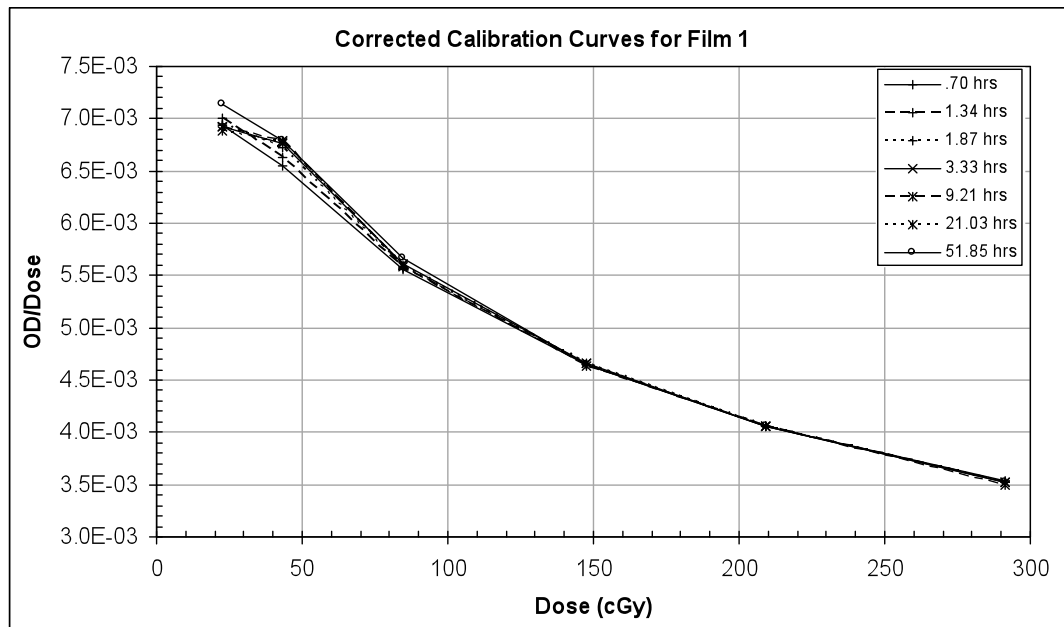


**Figure 24 – The change in Film 1 with time after scaling with the 209 cGy exposure. At all dose levels the difference between the min and max values of OD/Dose is less than that found in the measurements of figure 3.**

The results above are meaningful in providing insight to how well the SDC method performs. However, the most important issue is the final calculated dose values. After scaling the ODs, at all post exposure measurement times and

converting to dose, the average dose error of all dose levels as a percentage of 200 cGy is 0.53% or 1.06 cGy.  Performing the same dose conversion and average error calculation, but neglecting to scale, resulted in a dose error of 3.87%.  These final results show that the SDC method is capable of calculating doses accurately.
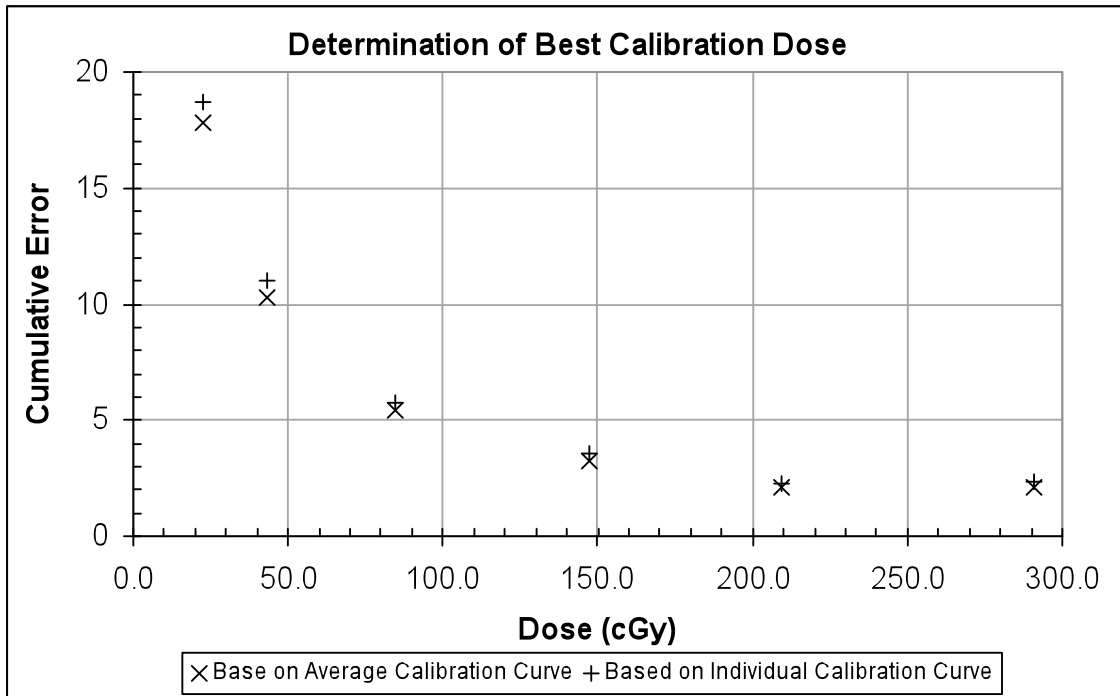


**Figure 25 – A figure of merit was calculated through the summation of errors to determine the best scaling dose (x-axis).  The numbers are irrelevant except that they are linearly in relation to each other.  The scaling dose of 209 cGy yields the best results, although the 291 cGy is only slightly higher and is within experimental error.  When the BCC is generated using an average of different curves the results tend to be slightly better.**

# 3 Commercial Digitizers

## 3.1 Specific aim of digitizer studies

Most commercially available digitizers are designed for medical use with radiographic film or for the general public with the goal of photographic imaging or document copying. In the medical field, scanners are typically of high expense and high quality, due to the low volume of sales and the manner in which they are used. Digitizers for the general public vary significantly, but as a general rule are designed to be lower cost and higher volume. This can result in lower quality of electronics, which translates into higher noise levels and more error in dose measurement.

In nearly all cases of available digitizers, Gafchromic EBT film was not a consideration or was an after thought in the design. As a result most digitizers do not work optimally for EBT's specific qualities. The purpose of the following research is to find where the available digitizers fail with regard to performance with EBT film, so that an optimal scanner can be created.

## 3.2 Digitizers analyzed

One of the most commonly used digitizers for radiographic film is produced by Vidar Systems (Herndon, VA). At the time of study their latest model was the DosimetryPro 16. A 16-bit CCD is the sensor of the system. There are enough detectors on the CCD to perform scans at 300 dpi for the full

width of the 14". The light path starts at the white light fluorescent tube that is about 4 cm from the film with a slit that limits the height of the light field at the midpoint to ~1 cm. The film to detector distance is 40 cm. Optics in the light path focus the light and limit the analyzed height so that it is not measuring the full illuminated region. A 2D scan is achieved through movement of the film passed the sensitive area. The pixel size is variable and can be set to 89, 187 or 356 $\mu$m.[36]

A HeNe laser based system called the Lumisys (Currently General Electric in Fairfield, CT) Lumiscan 75 has a 632.8 nm light source and is paired very accurately with the peak absorption wavelength of the EBT film. This greatly increases the signal to noise ratio generated by the digitizer. The light path exits the laser and passes through a beam splitter. One path goes to a monitoring system that accounts for any fluctuations in the laser output. Following the beam splitter, the second path is reflected by a mirror that causes the light to raster across the film. After the film a collection tube directs the light towards a photomultiplier tube with a 12 bit A/D converter. The spot size of the laser is 0.1 mm.[37]

The Howtek (Now Aztek, Inc in Irvine, CA) MultiRAD 460 is a red LED based digitizer with peak wavelength of 662 nm. The light path is similar to the Vidar DosimetryPro 16. After the LEDs there is a diffusing plate, which makes the separate LEDs a continuous light source. The diffusing plate is placed in close proximity to the film. Afterwards, an optics system focuses the light on a

CCD, which has 8000 elements.  This results in pixel sizes of 87 microns.  The A/D converter is 12 bit. There is also a closed feedback loop that monitors the light intensity and adjusts the voltage to the LEDs, to ensure constant light output.[38]

Three professional quality flatbed color scanners with a transparency setting were also analyzed.  The Mircrotek (Hsinchu, Taiwan) 9800XL, Epson (Longbeach, CA) 1640XL and Epson 10000XL all have similar configurations.  The light source is a cold cathode tube.  In flatbed scanners the film is not transported, but the light source moves with a stationary detector.  This arrangement forces a more complex arrangement in the post film light path to enable a constant film to detector distance.  This is necessary for the optics to keep their focus.  All scanners are 1600 dpi resolution and have three channel red, green and blue color detectors.  The Microtek is 48 bit (3 x 16 bit) while the 1640XL is 42 bit (3 x 14 bit).  Eventually, the 10000XL was used over the 1640XL because it incorporates a 48 bit detector.

## 3.3   Reflective scanners

The transparent nature of film lends itself to measurement in a transmission mode, which is the most commonly used method.  Reflective scanning is another possible method.  It has the advantage of the optical path traversing through the film twice and therefore could increase the sensitivity

observed. A study incorporating MD-55 film measured using the HP (Palo Alto, CA) Scanjet 4570c looks into the effectiveness of the reflective scanning technique.[39] Important findings were in the results for the precision, which is the repeatability of the measurements, and the accuracy in determining the exposure dose. Precision for transmission mode yielded a consistent 0.27 Gy standard deviation while reflection increased linearly between 0.1 and 1 Gy for doses between 5 and 50 Gy.[39] Accuracy yielded more consistent results between the two techniques with values between 0.18 and 0.283 Gy depending on method used to determine the accuracy, but neither transmission or reflective proved to perform better.[39] It is important to note that accuracy may be more dependant on the calibration curve that the digitizer. Reflection did have performance advantages in the uniformity across the scan plane and temporal stability.[39]

## 3.4  EBT sensitivity on various digitizers

When digitizing films for IMRT QA the ultimate goal is to achieve a dose map across the plane of the film with a high degree of accuracy. One of the greatest contributors towards the precise measurement is the signal to noise ratio (SNR). Noise is typically determined by the design of the amplifier and the stability of the light source. Signal is the change in the detected intensity of the light per unit dose given. A larger SNR will result in a more precise dose measurement. This makes optimizing the signal strength imperative. In this

section signal responses for the Lumisys Lumiscan 75, Vidar DosimetryPro 16, Epson 1640XL, Howtek MultiRAD 460 and the Macbeth TD932 point densitometer retrofitted with a 635 nm band pass filter with a 10 nm width are determined.

Measurements were performed on 1" squares from a single sheet of film. Each square was exposed individually with a 15 MV beam at 100 cm SSD, depth of 3 cm and a 10x10 cm field size to doses of 50, 100, 150, 200, 300, 400, 600 and 800 cGy. For analysis, films were attached to another film in a cutout region, so that they could be passed through rollers of a digitizer. An example image from the scan is shown in Figure 26. Each measurement point is an average of 100 pixels and is then converted to OD through the use of a curve determined with a neutral density step wedge.



**Figure 26 – Example of scan obtained from the Vidar DosimetryPro 16 for determination of the digitizer sensitivity.**

Looking at the results in Figure 27 the match of the HeNe light source of the Lumisys digitizer, with the absorption peak of EBT film, yields a very sensitive system. When compared to the result of the spectrophotometer in Figure 15 the Lumisys achieves the maximum signal possible. There is a dip in the signal response at 150 cGy, which is not an accurate representation of the dose response curve and is talked about in section 3.7. The Macbeth point densitometer has a strong response, but includes a 10 nm width in the

measurement spectrum. Including wavelengths other than ideal cause the sensitivity to decrease. It is possible to predict the signal based on the absorption spectrum and the light source used. This was completed on MD-55 film using a white light system, the Howtek and Lumisys digitizers.[37] Another step lower in sensitivity is seen with the Epson using the red color channel in a color scan. The green channel was also considered, because the exact wavelengths used in each color channel are not known. If the red was centered above the absorption peak the green channel could have performed better. Responses with white light sources show to be nearly identical, as seen with the Epson grayscale scan and the Vidar. The Howtek shows minimal response and should not be used for IMRT QA. For this reason the Howtek digitizer is not considered in other test.
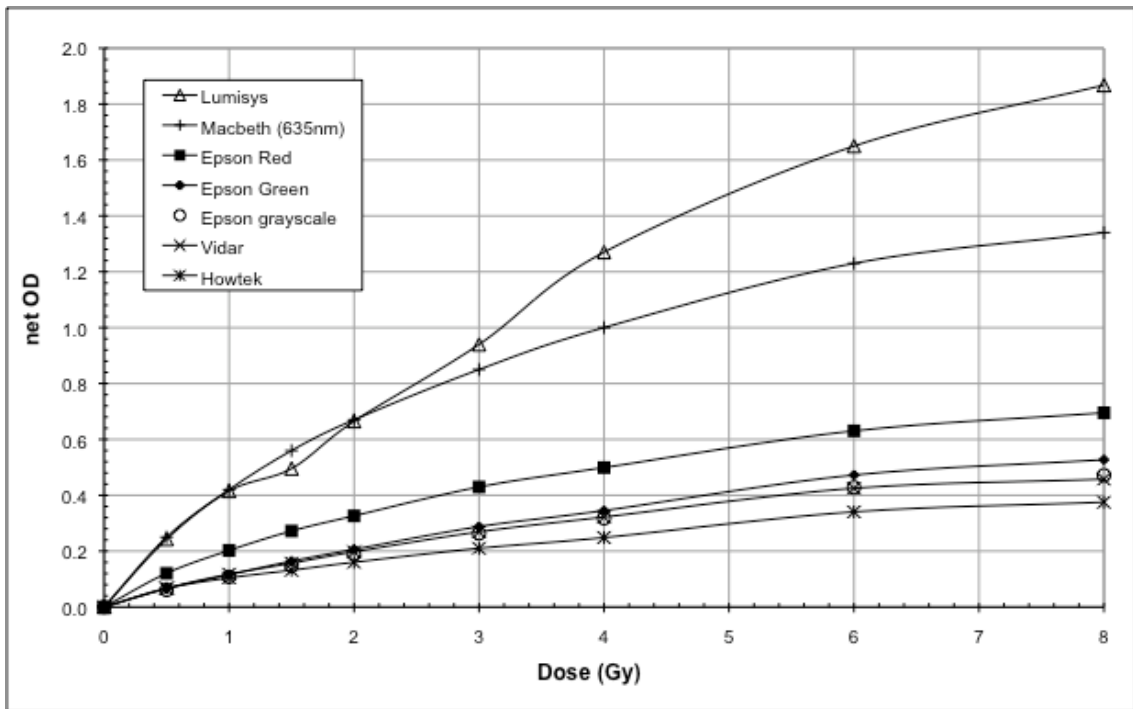


**Figure 27 – Sensitivity to EBT film on various digitizers.**

44

## 3.5   Digitizer noise

In the previous section the importance of a high SNR was discussed. Using a system that obtains a high signal response is important for generating a favorable SNR, but if the hardware that amplifies the signal is of low quality or the intensity of the transmitted light is low a high noise level is inevitable.  This can easily negate the benefits of a large signal response.  A study was performed looking into the noise level on the Vidar, Microtek and Epson 1640XL.  The resulting OD error for each is shown in Figure 28.  These results show that the Microtek has a significantly higher noise level over the Epson and Vidar.  The resulting dose measurements on film would have a grainy appearance and a low degree of accuracy.
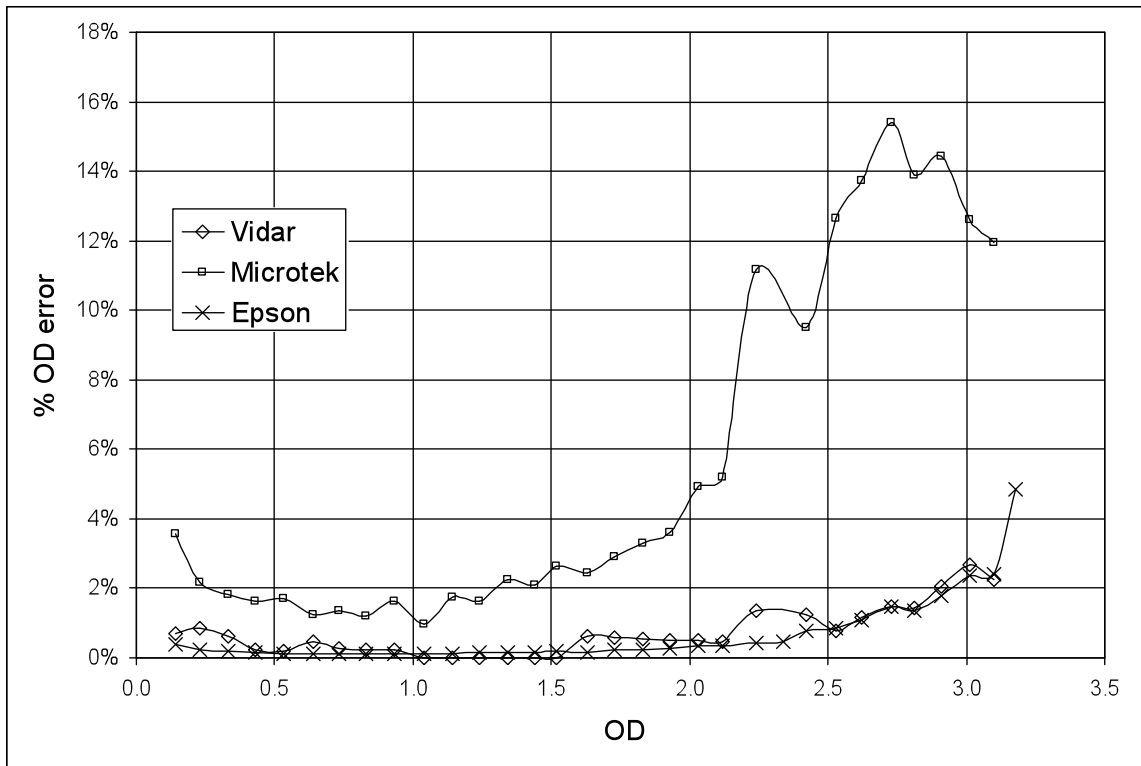


**Figure 28 – Digitizer OD error at various ODs for the Vidar DosimetryPro 16, Microtek 9800XL red channel and Epson Expression 1640XL red channel.**

45

Determining the percent OD error is completed by performing scans on the same neutral density step film with step sizes of approximately 0.1 OD. All scans were performed at 75 dpi and a region of 225 pixels was measured for each OD level. The average of the pixel values in each region for the Microtek and Epson are shown in Figure 29. Also recorded was the standard deviation of the pixel values. Knowing the equation for the pixel value curve to OD, the expected OD can be calculated from the average pixel value from the region. Finding the difference between that OD and OD for the average pixel value plus standard deviation yields the OD error. This error as a percentage of the expected OD is graphed in Figure 28.
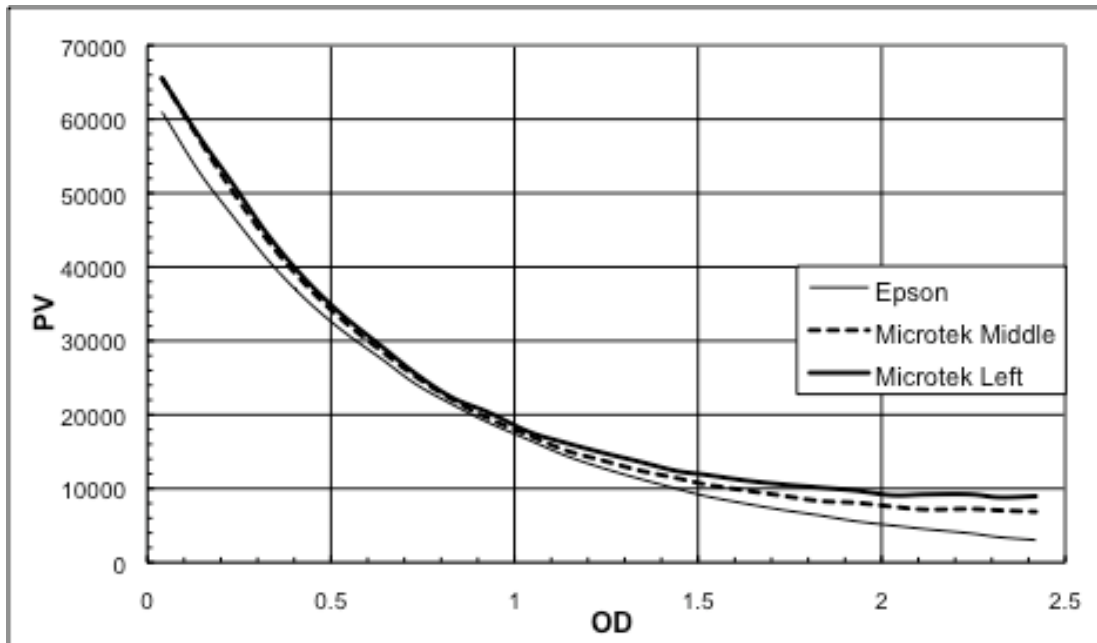


**Figure 29 – Neutral density response curves for Epson 1640XL and Microtek 9800XL on the middle and left side of the scan bed.**

The shape of the percent OD error curve is low in the middle and high at the min and max OD. Although, this effect is much more prevalent at high ODs. This is due to the change in pixel value with OD being far less significant at high

46

ODs. A consistent pixel value standard deviation will result in a much more significant OD error at regions in the curve with a slope that is low as in the high OD range. The percent error increases at low ODs, because the OD value that the error is being compared against is small and the error does not go to zero as OD goes to zero.

An increase in the error for the Microtek is observed due to two effects. At high ODs the slope of the curve is far less than what is seen for the Epson. This is shown in Figure 29. Most likely this is due to the intensity of the light incident on the step wedge. At higher ODs there is just not enough light transmitted to the detector to produce a signal, so the background signal due to light leakage and electron drift through the circuitry has more of a significant effect. The impact of the slope does not account for the higher noise at ODs below 1, because the Microtek actually has a larger slope. The average standard deviation in the pixel values for the Epson is 55, while the Microtek is 222. Microtek's larger slope cannot negate the effects of the high noise, so the resulting OD error is greater.

All these errors point to the fact that the Microtek's amplifier gain is larger than the Epson. A higher gain yields a greater slope when enough intensity is present, as in the low ODs. Noise is also amplified with gain. As a result the noise of the Microtek is much larger. The lower light intensity creates the demand for the higher gain. To avoid these effects, in design of a scanner, it is

important to have the current from the detector that is large enough to keep the gain of the amplifier low.

## 3.6 Dynamic Range Variation

Inspection of data for the Microtek in Figure 29 shows that at low ODs the pixel value is nearly identical when scanned on different regions of the film. At ODs above approximately 0.9 the sensitivity at the edge of the scanning bed decreases at a higher rate when compared to the middle. This is seen by the reduction in the difference of the pixel values for ODs of 1 and 1.5 on the edge compared to the center. In actual use, results would not have errors to this extent, because the ODs only reach about 0.9 when 8 Gy is delivered. Measuring doses of 8 Gy the error in the dose is 1.02 Gy.

Evidence points to the Microtek exhibiting this effect due to the light traveling through the color filter on the CCD at a $90°$ angle in the center, but not at the edges. Towards the sides of the scan bed the light is at some oblique angle to the color filter on the CCD and as a result traverses a greater thickness. This yields a greater attenuation and combined with the lower light output of the Microtek the scanner exceeds its dynamic range prior to the Epson.

## 3.7 Polarized light source artifacts

As shown, Gafchromic EBT film is a weak polarizer when measuring the absorption spectrum with a polarized light source. What was not mentioned is

that the direction of the polarization within a sheet of film is not consistent.  This

causes major film artifacts when digitizing with a polarized light source as shown

in Figure 30.  This is a scan with the Lumisys using the same film scanned by the

Vidar in Figure 26.  The Vidar does not show artifact variations in the pixel values

as are seen by the Lumisys.
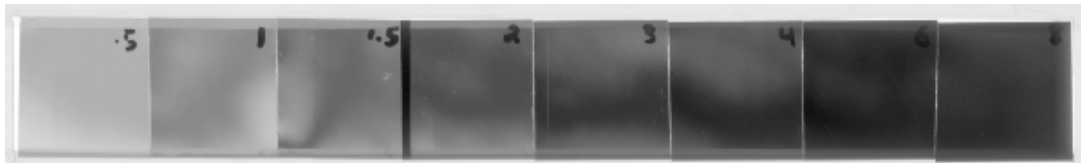


**Figure 30 – Polarized light artifact due to the inherent properties of the film acting as a polarizer as seen by the Lumisys Lumiscan 75.**

The exact amount of rotation in polarization direction is not known.  An

estimate is found through obtaining the optical density variation for the square in

Figure 30 marked with a 3, which is a 3 Gy exposure.  The ODs were found to be

between 1.6 and 2.3 OD.  Taking these values and comparing to the data shown

in Figure 18 an estimate in the rotation is found to be 60° for this particular

region.  These variations in the measured OD are clearly not an acceptable

amount of error to introduce into a measurement, so design criteria for an optical

system of a digitizer cannot have linear polarized light incident on the film or have

a detector that is sensitive to polarization.

## 3.8   Banding artifact

The Vidar DosimetryPro 16 exhibits a noticeable banding artifact as seen

in Figure 31.  This is not a problem with the manufacturing of EBT film, but is

caused by the transport mechanism of the Vidar digitizer.  As a film is read it is passed through a series of rollers that guide the film.  As the edge of the film is grabbed or released by a roller it causes a shift in the position and angle of the film.  A shift in the position and angle of the film causes the transmission detected by the CCD to be altered.

Figure 31 is a scan of an unexposed EBT film positioned with the bottom of the scan on the right of the image.  At about 2.5" (arrow) there is a shift in the pixel values from about 23000 to 26000.  This occurs as the leading edge of the film traverses past the last roller.  The positioning of the roller causes the film to flex and as a result the transmission increases.  Continuing to the top of the film at 0.2" from the edge (arrow) there is another shift in intensity.  When the film is not held in position by the roller just above the measurement area the tension caused by the bottom roller makes the film shift further.  The pixel values in this region are about 28000.  If the film did not have a change in bend during transport this artifact would not occur.



**Figure 31 – Banding artifact seen on Vidar DosimetryPro 16 visible on the top and bottom of the film.  Film is shown rotated 90° clockwise with contrast enhancement to show artifact.**

### 3.9   Light scattering affects

After developing radiographic film silver halide crystals scatter light isotropically due to the dimensions of the crystals being more or less uniform.  As

mentioned previously Gafchromic EBT film contains fibers as the active component. These fibers scatter light perpendicular to the long dimension of the fiber more than other directions. Due to the fibers aligning in the same direction, the film exhibits anisotropic scattering. More light scatters perpendicular to the lamination direction than parallel to it. This is evident by placing the film so that a bright light source is incident on the film, but so that your eyes are not in a line with the light source and film. The resulting light that is seen from the film is light that is scattered and not directly traversing the film. If the film is rotated it appears cloudier at a certain degree of rotation. The plane made by the light source, the film and your eyes is perpendicular to the direction of lamination within the film.

Light scatter has multiple effects on the performance of a digitizer. When determining the calibration curve there is a dramatic difference between two scans that are perpendicular to each other. The degree of the effect is specific for a digitizer. As seen in Figure 32 the calibration curves for the Epson scanned in landscape mode have pixel values that are significantly higher compared to portrait scan, and the difference is greater for the Vidar. When the film is oriented so that the lamination direction, and consequently the fibers, are parallel to the motion of the light source (or film depending on the transport mechanism), the light tends to scatter on the same plane of the light path to the CCD. Therefore, scattered light contributes to the measurements. Rotating the film causes the light to scatter away from the CCD and not be included in the

measurement. Ideally, the scattered light will not affect the measured values. The lamination direction is across the short length of the film, so the long dimension should be in the direction of transport, whether it is the film or the light source.
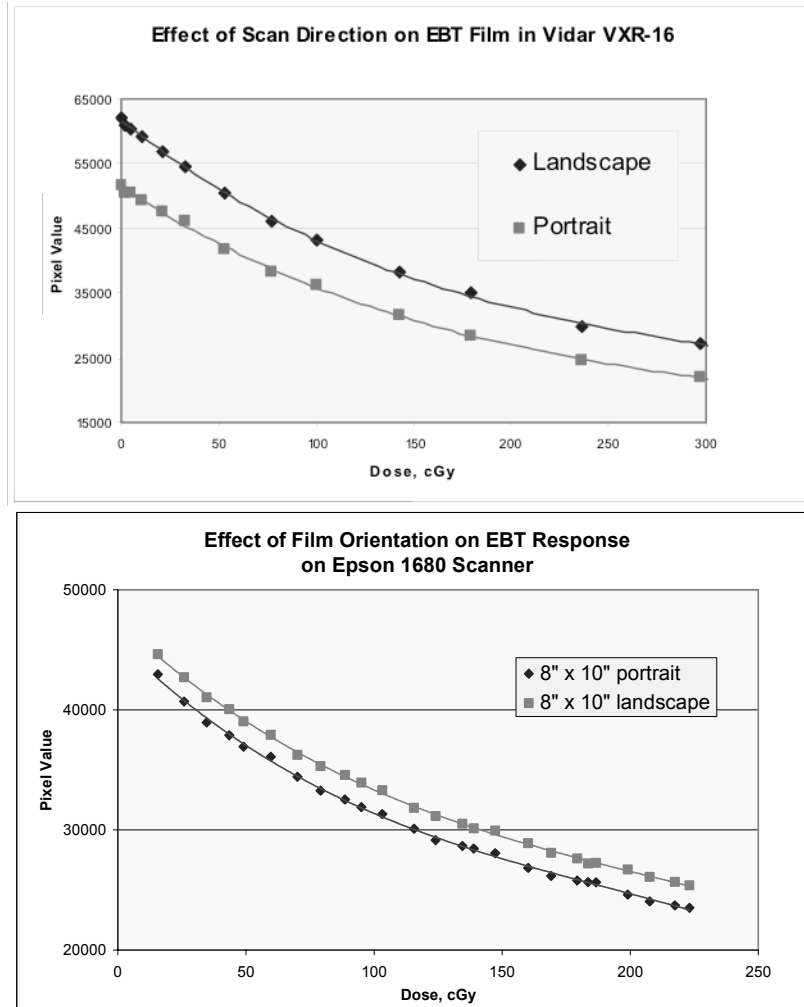


**Figure 32 – Light scatter effect on calibration curve for EBT film on the Vidar DosimetryPro 16 on top and the Epson 1680 scanner on bottom.[27]**

Typically, a digitizer with a greater distance between the light source and the film will show a greater sensitivity to scatter and will have an increased difference between the two calibration curves. Figure 33 shows a diagram of how the light scatter affects measurements. In the center of the film light from

either side of the light source is incident on the measurement point.  As the light

scatters the CCD sees an increased intensity.  On the edges scatter contribution

still exists, but only occurs from one side and results in a smaller effect.  As the

distance between the film and the light source increases, the length of tube that

can contribute to scatter increases so the effects are amplified.[40]
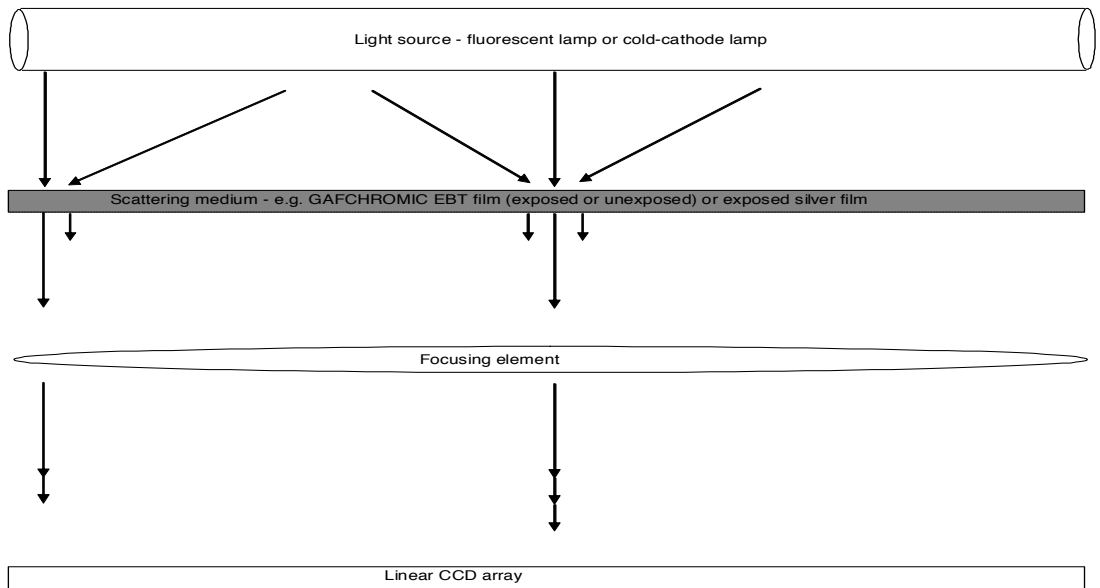


**Figure 33 – Light scattering diagram for a typical digitizer.[40]**

The greater scatter contribution towards the center of the film will cause

the pixel values at the edges to be less than the center as seen in Figure 34.

Corrections can be applied to reduce the scatter effect.  Averaging each column

in the profile and dividing by the average of the entire scan provides correction

factors for each column in the profile.  Figure 35 shows typical values for the

correction factors on a Vidar DosimetryPro 16.  Correction on a scanned image,

taken in the same location on the scanner as the image used to generate the

correction profile, is accomplished by dividing each pixel by the corresponding

correction factor determined by the column number. Radiographic film does not respond well to this method due to the increased scatter with dose. Increasing the scatter would necessitate increasing the correction factor and adds to the complexity required to correct this artifact. EBT film has consistent scatter with increasing dose.
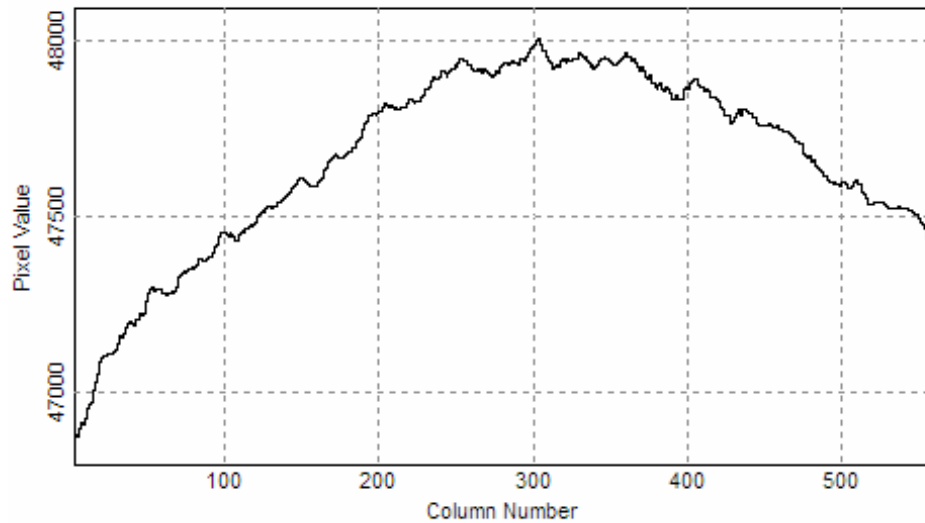


**Figure 34 – Profile of unexposed EBT film on the Epson 1680 shown as the average pixel value in a column.**[40]
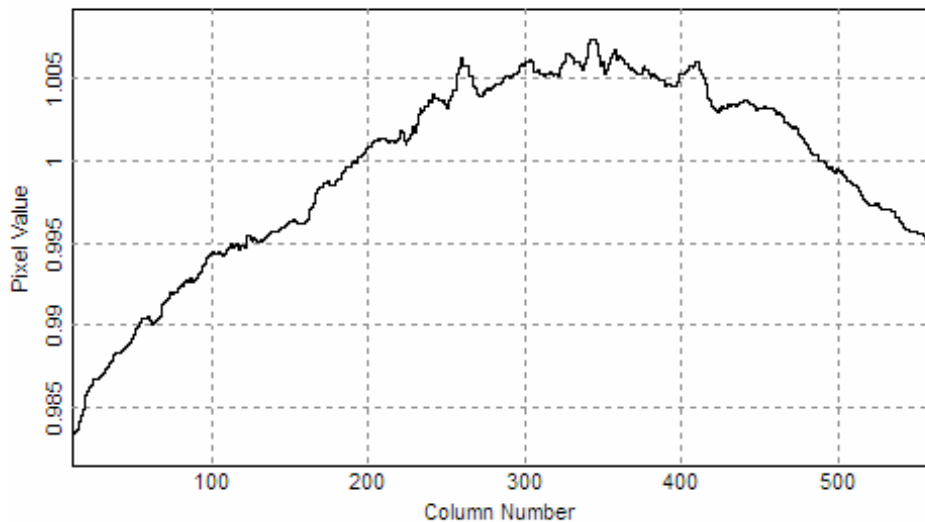


**Figure 35 – Scatter correction factors determined for the Vidar DosimetryPro 16.**[40]

## 3.10 Gafchromic EBT digitizer considerations

In designing the optimal digitizer for Gafchromic EBT film the primary goals are to determine the dose with very high accuracy to a dose up to 8 Gy (the manufacturer specified dose range) in a reasonable scan time. This time is different depending on the use of the system. In the clinical setting, the time in which a scan is performed is important, as many tasks must be completed within a day. A scan time of about two minutes is a reasonable for clinical use. In research, the time is not as critical and a longer scan time is tolerable, but accuracy may be of greater importance.

Many factors contribute to dose uncertainties and they have been discussed in detail. Ideally, the dose error in the measurement system will be insignificant compared to error in the treatment planning system calculations. A very common algorithm used in calculations is the pencil beam model. Studies have shown that maximum errors can be minimized to 1.5% – 2%.[41,42] Therefore, keeping dose errors below 1.5% would yield results that are limited by the calculation algorithm rather than the dosimetry system.

Studies of the Gafchromic EBT film itself and how the film interacts with commercially available digitizers, yields methods that will allow for high dosimetric accuracy. First and foremost it is vital to obtain a high sensitivity to dose with the measurement system. Using a light source that is matched with the 635 nm absorption peak of EBT film is essential to achieving high sensitivity. A laser is capable of a very narrow band of wavelengths. Although, coherent

light causes moiré patterns to appear. Therefore, a laser which does not maintain the coherence, is ideal. Laser diodes have the tendency to lose coherence in a short distance and are capable of being tuned to a specific wavelength through control of the diode temperature. Changing the temperature of the diode alters the bandgap width in the semiconductor through thermal expansion.[43] The wavelength that the laser lases is shortened as the temperature decreases, due to the contraction of the semiconductor and a resulting decrease in the size of the bandgap.

The absorption range for 635 nm from 0 – 8 Gy is from 0.3 to 2.3 OD. This means that the transmission through the film at 8 Gy will be about 1/200 the intensity of 0 Gy. To achieve best results, the gain and error of the amplifier and A/D converter would not introduce uncertainty in the dose measurement more than approximately 1/10 of the total noise or 0.15%, based on the acceptable error discussed earlier. Noise levels this low will be difficult to yield at high dose values.

A common problem observed in commercial digitizers is the variation in measured dose, based on the location or rotation of the film in the digitizer. These types of effects are not tolerable when they yield results with errors large enough to interfere with dose comparisons in the system. Errors of this sort can arise from several sources. A change in the distance to the detector and/or angle of incident light on the film will yield effects seen in section 3.8. To eliminate

artifacts of this kind, the film within the measurement region may move about a plane normal to the light source, but no other shift is tolerable.

Anther source of measurement variation artifacts arise through illuminating large regions of the film or utilizing large light sources that appear differently across a scan plane, as discussed in section 3.9. To eliminate these artifacts it is necessary to make each measurement point appear exactly the same to the detector, regardless of the position within the film. Using a laser that illuminates a single point, which is measured by the same detector independent of the location on the film, helps to satisfy this requirement.

Lastly, to maintain measurement stability it is necessary to have the light interact with the film identically at all points. Section 3.7 demonstrates how a linearly polarized light source can interact poorly with film. Unfortunately, a laser and optics such as mirrors introduce polarization into the light source and is a good selection otherwise. Therefore, methods to remove the polarization or to generate circularly polarized light can be utilized to eliminate the polarization artifacts.

# 4 Electronics design

## 4.1 Design requirements

The specifications of an amplifier are determined by the application in which it will be used. Ultimately, a film measurement system that is capable of measuring up to 8 Gy with no more than 1.5% dose uncertainty is desired. To achieve this goal the error introduced by the amplifier must be kept to a small percentage of the total. This allows for drift in the laser output, variation in the gain due to temperature, and noise introduced through the optics and light scatter within the film to have a larger percentage of the final error. Fortunately, it is possible to keep the electronics noise low.

The A/D converter determines the desired output and specifications of the amplifier. An IOTech DAQBoard 2005 was chosen as the A/D converter for the system. It is capable of 16-bit accuracy for a range of 0 – 10 V. Therefore, the gain of the amplifier should be sufficient to yield a high dose resolution at 8 Gy for the A/D step size of 153 $\mu$V, but not yield more than 10 V when an unexposed film is scanned. To design for this, it is necessary to know how much current will be generated by the diode. This is dependant on both the light intensity incident on the detector and the detector efficiency. A Hamamatsu (Hamamatsu City, Japan) S3071 photodiode was used to convert the light into current. It has an efficiency of at 635 nm of 0.45 A/W. Calculating the laser power incident on the detector starts with the 6 mW laser. The orientation of the incident light on the polarized beam splitter is arranged so that the measurement system will receive

58

90% of the power. Ten percent was used to monitor the laser output. Converting the linearly polarized light into circular polarization has an efficiency of 58%. Before the light can be transformed into circular polarization it must be pass through a linear polarizer, which allows for 39% transmission. Reflections off of lenses, polarizers and other components could add an additional 5% loss, but is not accurately known. Finally, an unexposed film has an OD of about 0.35, but is dependant on the production lot. Taking all factors into account an approximate power incident on the detector is 1.2 mW. Therefore, the max current generated by the photodiode should be 530 μA. Once the current generated by the photodiode is determined, Equation 4 determines the gain necessary to yield 10 V and is found to be 42.2 kV/A.

$$Gain \ (V/A) = Output \ Voltage \ (V)/Current \ (A)$$

**Equation 4 – Desired amplifier gain is determined by the desired output voltage for an input current.**

The frequency response for design is determined by the scanning speed that is desired. The motion system determines at what frequency pixels are measured. More will be discussed about the motion system, but for now assume the required scanning frequency will be 30000 pixels/sec.

## 4.2 Amplifier configurations

### 4.2.1 Log amplifier

The characteristics of radiographic film exhibit a linear region in the sensitometric curve, until the film saturates. Typically, radiographic film will only be used in the linear region.[44] Gafchromic EBT film does not exhibit the same linear region and darkening response becomes noticeably less after 0.5 cGy as seen in Figure 27. This effect causes a decrease in the change of the transmission at higher doses. Also contributing to a loss in sensitivity to dose is the method in which transmission operates. A certain object that is transparent will let a determined percentage of light pass through. When light levels are low the absolute change in intensity cannot be the same as when there is an abundance of incident light. Therefore, as seen in Figure 29, as the OD increases the change in intensity per unit of OD decreases. The combination of these two effects cause the noise component to be a much greater percentage of the total signal at high doses, which results in a greater degree of dose measurement error at high dose values.

A solution to the decreased signal at high exposure levels is the use of a log amplifier. These amplifiers have greater gains at lower current levels. As a result there is more amplification at higher doses. This greater amplification makes it so that the fixed noise to output signal ratio is lower for a log amplifier than a linear amplifier. The fixed noise is the noise that will not increase under greater levels of amplification. This fixed noise is introduced with the A/D

converter, through op amps that occur after the majority of the amplification, electromagnetic noise and other sources.

Basic log amplifier design starts with a standard linear op amp with gain determined through the use of a single feedback resistor. However, the feedback circuitry utilizes a log transistor instead of a resistor. The transistor is situated in such that the collector is attached to the photodiode and the input to the op amp. Output of the amplifier connects to the emitter of the transistor to complete the feedback circuit and to a voltage divider that controls the voltage to the base.
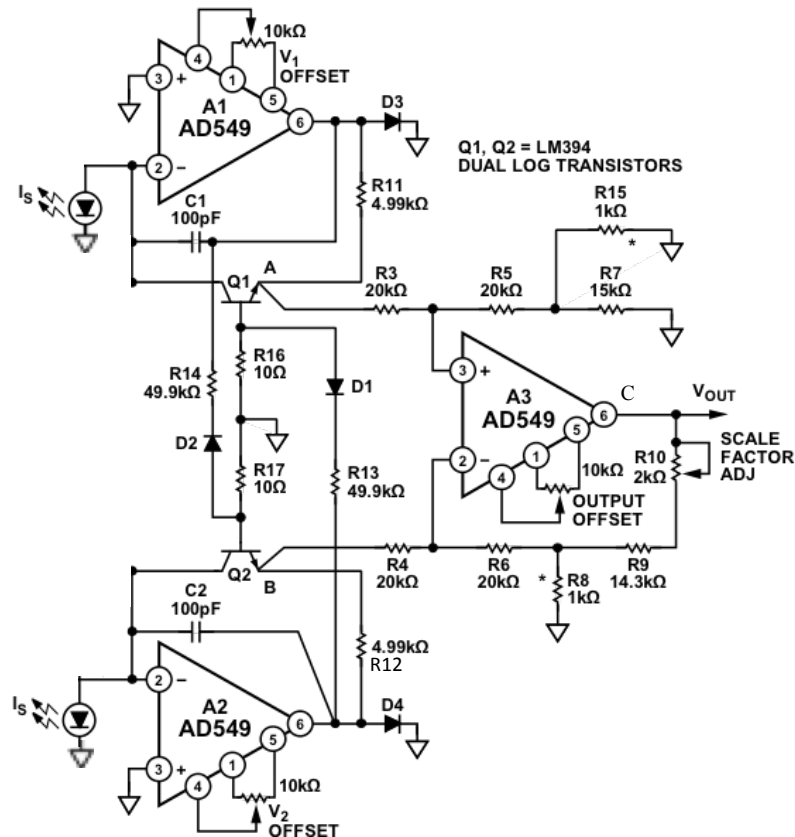


**Figure 36 – Log amplifier schematic with light intensity monitoring and correcting. Parts Q1 and Q2 must be a must be a match pair log transistor.**[45]

When considering a log amplifier for use with the EBT digitizer a more complex design with laser monitoring circuitry was considered. The schematic is

shown in Figure 36.   Monitoring the laser is achieved through the photodiode connected to op amp A2.   This is evident, because the output controls the voltage to the inverting input of A3.   As the light intensity increases on the monitoring photodiode, a stronger response is generated on the output and consequently on the inverting input of A2.   Voltage output of A3 would then correct back to the initial value.   The opposite is true for the photodiode on A1.

The overall circuit design of Figure 36 yields an output proportional to the base 10 log of the input currents $I_1$ and $I_2$.   The voltages are first generated at points A and B and are characterized by Equation 5.   Where $I_C$ is the collector current generated by the photodiode, $I_{ES}$ is the saturation current and kT/q defines the thermal voltage.   At room temperature the thermal voltage is 25 mV. A natural log output is generated through the variable gain of the transistors in the feedback loop.   Op amp A3 is a subtractor circuit with the output represented, with unity gain, by Equation 6.[45]   The subtractor circuit does not utilize unity gain and instead converts the natural log into log base 10.   Gain is determined with ratio between log and natural log seen in Equation 7 and the thermal voltage. Dividing the ratio by the thermal voltage yields 17.4 for room temperature. Realistically, the transistor will operate above room temperature and cause the thermal voltage to increase.   As a result, an approximate gain of 16 is desired to yield one volt per decade of input current.   The variable resistor R10 can be adjusted to fine tune the output for the actual operating temperature.   Final output

of the circuit is represented by Equation 8, assuming that the variable resistor is adjusted correctly.[45]

$$V_A, V_B = -(kT/q)\ln(I_C / I_{ES})$$

**Equation 5 – Voltage at points A and B found in Figure 36.  $I_C$ is the collector current determined by the photodiode current and $I_{ES}$ is the saturation current of the transistor. The thermal voltage of the transistor is kT/q and has a value of 25 mV at room temperature.[45]**

$$V_C = (kT/q)\ln(I_{C2} / I_{C1})$$

**Equation 6 – Output of unity gain subtractor circuitry found in Figure 36.  $I_{C1}$ and $I_{C2}$ are the collector currents and kT/q represents the thermal voltage of the transistors.[45]**

$$0.43429 = \log(X)/\ln(X)$$

**Equation 7 – Ratio between log and natural log.**

$$V_{out} = \log(I_{C2} / I_{C1}) \; Volts$$

**Equation 8 – Final output of Figure 36, where $I_{C1}$ and $I_{C2}$ are the collector currents of transistors Q1 and Q2.[45]**

The circuit is frequency compensated through elements R11, R12, C1 and C2.  Without the compensation, positive feedback may occur resulting in oscillations, overshoot and ringing.  Compensation in this circuit limits the bandwidth to 300 kHz, but values are not optimized for our photodiode and desired frequency response.  Elements R13, R14, R16, R17, D1 and D2 are used to compensate for the effects of emitter resistance that can degrade circuit accuracy above $I_C$ values of 100 µA.  Utilizing this setup 1% log conformance is achieved up to 1 mA.  The correct values for R13 and R14 are determined by the matched pair transistors used and are accurate for analog devices part number LM394.[45]

Although the log amplifier does yield excellent noise benefits the amplifier design was not chosen for use in digitizing the EBT film. Looking at Equation 6 the thermal voltage is part of the determination of the final output voltage. At room temperature a fluctuation in the transistor temperature of 3 °C results in approximately a 1% shift in the output voltage. It is possible to utilize a resistor with high temperature dependence for element R8 as compensation,[45] but significant dependence on temperature may still exist if R8 heats differently from the transistors. The difference in heating is unavoidable due to currents through the elements not being identical. Additionally, the bandwidth of the circuit is not stable due to the frequency compensation design. As the current decreases the bandwidth follows smoothly.[45] This effect is not as critical as the higher bandwidth, and therefore noise, is introduced with larger currents.

### 4.2.2 Composite amplifier

A composite amplifier design includes a modified integrator within the feedback loop of a photodiode amplifier that utilizes an op amp. The integrator limits the high frequency open loop gain, which only contributes to noise. Figure 37 shows the schematic of the amplifier. Values for the elements within the circuit are determined based on equations that utilize the desired circuit gain and a cutoff frequency.[46]

Analyzing the circuit at low frequencies is completed by making C1 an open circuit. This eliminates the effects of the feedback loop across A2. As light is incident on the photodiode it causes the noninverting input of A1 to be negative

and as a result the output of A1 decreases. With C1 being an open circuit the inverting input of A2 must be negative and therefore the output of A2 gets driven high. An increase in light intensity will cause an increase in voltage output. A2 at low frequencies will operate at its full open circuit gain. As the frequency increases C1 operates more as a short. This causes the gain of A2 to be controlled by the closed loop effects of R1 and R2 and is determined by Equation 9. Making $R_2/R_1 < 1$ causes a decrease in the gain at high frequencies. The final amplifier response is seen in Figure 38. A single stage amplifier gain is represented by $A_{OL1}$. At low frequencies the gain for the composite amplifier is greater, which enhances the signal. As the frequency increases above $f_{z2}$ the gain decreases below $A_{OL1}$ and as a result decreases the noise in the output.[46]
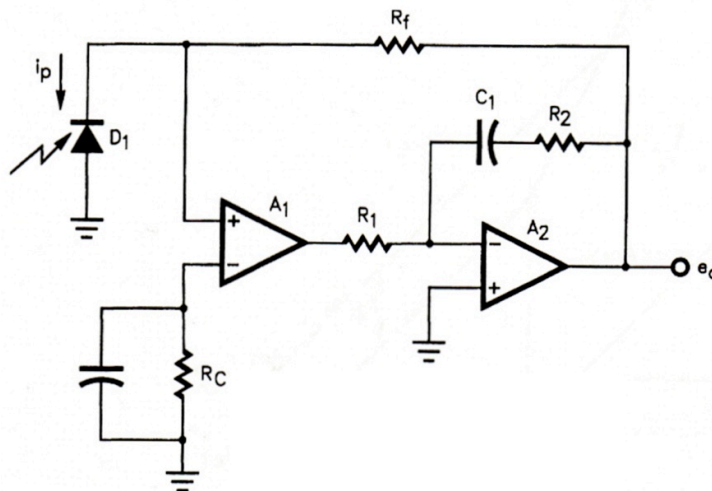


**Figure 37 – Composite amplifier design with a current to voltage converter.**[46]

Often in amplifiers the addition of the second op amp will add extra noise to the final output, but this is not the case for the composite amplifier. More will be discussed about amplifier noise in the section 4.4, but the input voltage noise of the op amp is a large determinate of the output noise. In the composite

amplifier case, the input noise of A2 is isolated from the circuit due to the large

gain of A1 and as a result does not contribute to the total output noise.[46]

$$A_{CL2} = -R_2 / R_1$$

**Equation 9 – Closed loop gain of A2 in the composite amplifier.[46]**

$$A_{OLc} = A_{OL1} * A_{CL2}$$

**Equation 10 – Composite amplifier gain.[46]**

$$f_{z2} = 1/(2\pi R_2 C_1)$$

**Equation 11 – Frequency that the gain reduction of $A_{CL2}$ begins to take effect.  Value is determined by the zero introduced with the integrator for the composite amplifier.[46]**
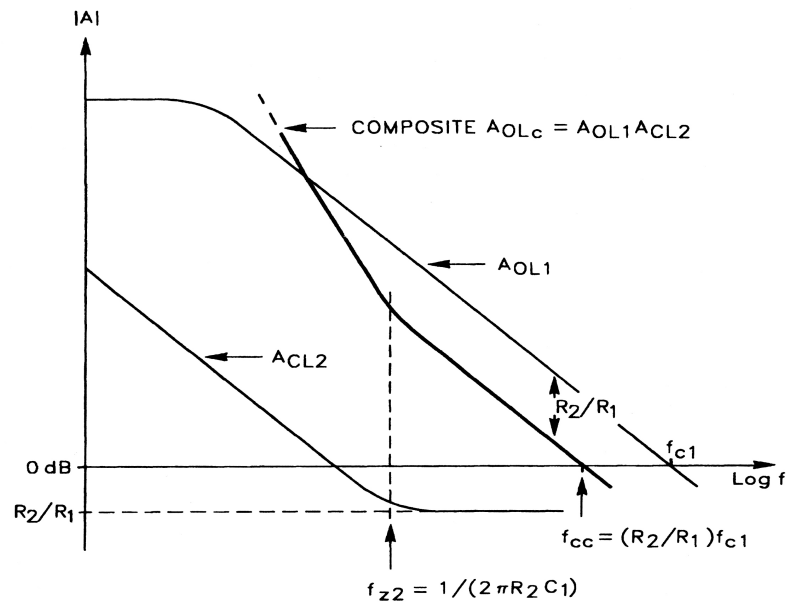


**Figure 38 – Frequency response of composite amplifier.[46]**

The gain of the composite amplifier is determined by Equation 10 and high

frequency noise reductions begin to take effect at $f_{z2}$, which is the zero frequency

across A2, and is determined by Equation 11.  Designing the composite amplifier

is determined through a set of equations and begins by calculating the $R_2/R_1$ ratio

with Equation 12.  Choosing a value for $R_2$ determines $R_1$.  The $R_2/R_1$ ratio can

be manipulated through the choice of a photodiode with a specific capacitance

and an op amp for A1 with a large unity gain crossover frequency, $f_{c1}$.  The introduction of a capacitor across $R_f$ will reduce the significance of the photodiode capacitance seen in $C_i$, but may limit the amplifier bandwidth due to the high value of $R_f$, which is determined by the amount of gain necessary for the amplifier.  Capacitor $C_1$ is the last major component to consider.  Its value can be determined through Equation 13.  Deviations from this value are possible, but instability may result if $C_1$ is lowered.  A decrease in $C_1$ increases the bandwidth of the amplifier and introduces a phase shift at higher frequencies.[46]  If the phase shift is great enough the feedback loop will result in positive feedback, causing the output to spike to the max value.  An increase in $C_1$ will cause a decrease in bandwidth and an increased reduction of noise.  Rc and the accompanying capacitor are optional.  If used, $R_c$ should equal $R_f$ to compensate for the input current of the op amp.

$$\frac{R_2}{R_1} = \frac{f_{pf}}{f_{c1}} * \frac{(C_i + C_s)}{C_s}$$

$$f_{pf} = 1/(2\pi R_f C_s)$$

**Equation 12 – Composite amplifier high frequency gain reduction.  $C_i$ = total input capacitance to ground for the noninverting input of A1, $C_s$ = the stray capacitance across $R_f$, $f_{pf}$ is the frequency of the pole introduced by $R_f$ and $C_s$, and $f_{c1}$ is the frequency of unity gain of A1 open loop gain.[46]**

$$C_1 = \frac{10R_f}{R_2} C_s$$

**Equation 13 – Composite amplifier final design equation determines the value for capacitor $C_1$.[46]**

A composite amplifier designed for this approach had to push the limits of the bandwidth due to the scanning frequency.  The photodiode has a large

sensitive area and consequently a big capacitance. This causes $C_i$ to be substantial, which necessitates a greater $C_1$ for stability. Unfortunately, this would not allow for the needed bandwidth. As a result Equation 13 could not be followed and an unstable circuit was designed. Although this design could be corrected through choosing a photodiode with a smaller capacitance, a dual stage amplifier was designed instead and yields good noise results, so it was not necessary to pursue the composite amplifier scenario.

4.2.3   Dual Stage linear amplifier

4.2.3.1   General schematic

When utilizing op amps a dual stage amplifier has the benefits of high gain and output current while maintaining low noise levels. Any single stage op amp cannot achieve this combination, because there is a tradeoff between output current and input noise within an op amp. If a single stage were to have a large output current then the input noise would have to be high. Any input noise on an op amp is multiplied by the feedback gain. In the case of a photodiode amplifier the gain must be large, therefore the output noise will be a significant amount of the signal.

A dual stage configuration can be seen in Figure 39. In this scenario, op amp A1 only has the requirements of supplying the current of the photodiode. The only gain in the circuit is found across A1. A2 is simply supplying output current. Since there is no gain in the feedback of A2 the input noise will not

increase at the output. If the second stage of the op amp were to have gain the

input noise of A2 could also contribute to the output noise significantly.
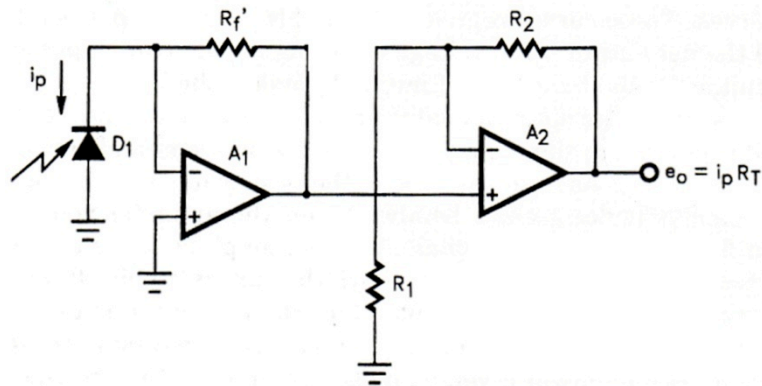


**Figure 39 – Dual stage amplifier uses a current to voltage converter with high gain and a voltage to voltage converter.** [46]

The DC analysis of the amplifier in Figure 39 starts with the current

generated by the photodiode, which has nowhere to travel except through the

feedback resistor across A1. The inverting input of A1 is tied to a virtual ground,

so the voltage on the output of A1 must be proportional to the current. This is

because of Ohm's law, which states that the voltage across any element must be

proportional to the current through it and is described by Equation 14. A voltage

defines the output of A1 with its input being a current. That makes stage 1 a

current to voltage converter. The noninverting input of A2 must be equal to the

output of A1. As long as R1 and R2 are equal the output of A2 is identical to A1.

This makes stage 2 a voltage to voltage converter. Although seemingly useless,

the second stage can be useful for increasing the output current and with the

addition of several elements it can be an active filter.

$$V = I * Z$$

**Equation 14 – Ohm's law equation where V is the voltage across an element, I is the current through the element and Z is the impedance. In the case of a resistor the impedance is the resistance in Ohms.**

4.2.3.2   Active filter stage design

The use of an active filter yields significant noise reductions due to limiting the bandwidth.   The Sallen-Key and Multiple Feedback (MFB) low pass architecture are considered for use in the active filter design.   Both are designed to be second order filters.   The cutoff frequency is the frequency at which the gain should begin to reduce.   A Butterworth filter is a description of the frequency response and can be designed in a Sallen-Key or MFB architecture.   Other filters implementable in both architectures are the Bessel and Chebyshev.   The filter type is determined by a quality factor Q.   Each filter design has a different frequency response for the same cutoff frequency.   Figure 40 shows the responses when designed for a cutoff frequency of 1 kHz.[47]   When properly designed each filter will have the same gain at the cutoff frequency.
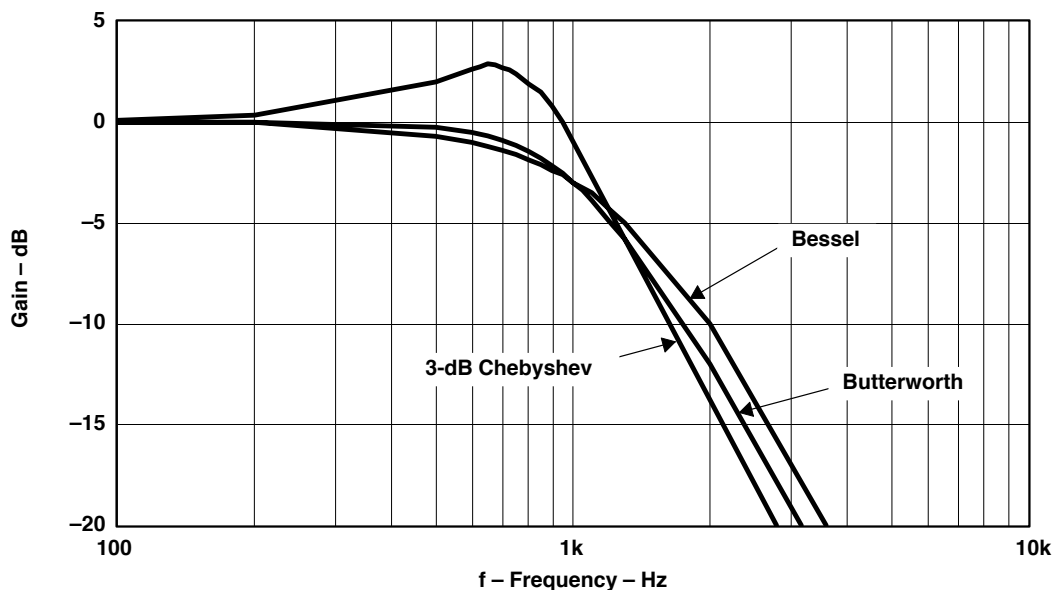


**Figure 40 – Frequency response for a 3 dB Chebyshev, Bessel and Butterworth filters.[47]**

A Butterworth function tends to show no significant attenuation prior to the cutoff frequency.   At the cutoff frequency there is -3 dB attenuation and thereafter

a -40 dB/decade attenuation for a second order filter.  The advantage of a Bessel

filter is described later, but the performance in the frequency response appears

worse than the Butterworth, due to its roll off significantly before the cutoff

frequency and a smaller attenuation per decade.  Lastly, 3 dB Chebyshev filter is

shown.  The 3 dB describes the increase in the gain around the cutoff frequency.

Although this gain increase will cause ringing, it allows for the attenuation per

decade to be greater than the Butterworth filter.[47]
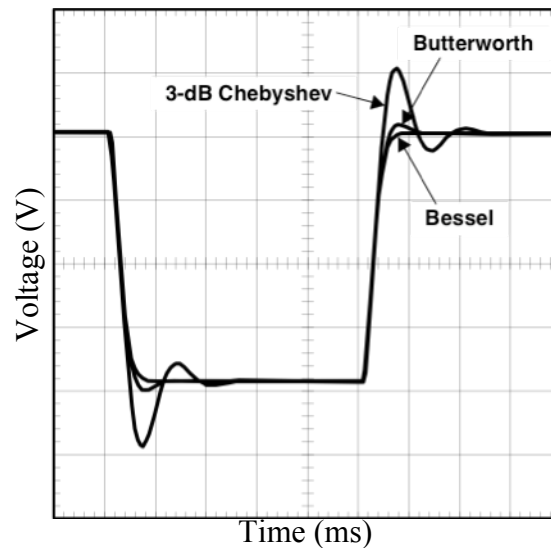


**Figure 41 – Impulse response of a 3 dB Chebyshev, Butterworth and Bessel filters.[47]**

Responses to an impulse signal further differentiate the three filter

designs.  Figure 41 shows the output of the 1 kHz filters with the frequency

responses seen in Figure 40.  The Bessel filter's output appears to be dampened

in that it has a slight curvature to the output near the end of the impulse.  This is

good for representing the input accurately, but as mentioned earlier, sacrifices in

the noise attenuation.   The Butterworth is a good tradeoff between noise

attenuation and accuracy in the response.   There is a noticeable degree of

ringing, but it is not too significant.  The 3 dB Chebyshev has considerable

ringing, but the best noise attenuation.[47] It should be noted that 3 dB Chebyshev

could be designed as a 0.05 dB and will have characteristics nearly identical to

the Butterworth filter. The dB could also be increased and have a stronger

ringing and attenuation or fall anywhere in between. In the case of an amplifier

for digitizing EBT film there will never be a situation where the film's OD changes

so quickly in a regions where dose is being measured to cause a ringing in the

output. This means a Chebyshev filter design would have the benefits of reduce

noise and no detriments, so a Chebyshev filter will be utilized.
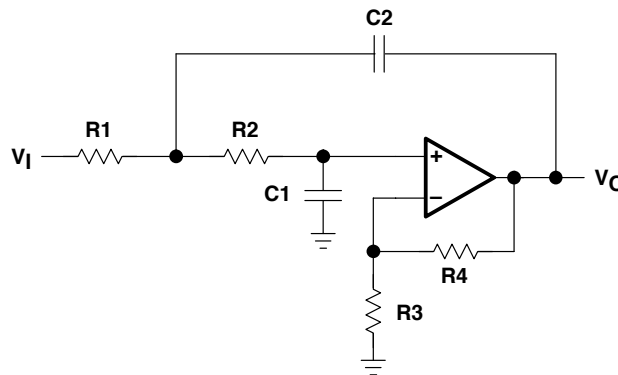


**Figure 42 – Low pass Sallen-Key active filter schematic.**[47]
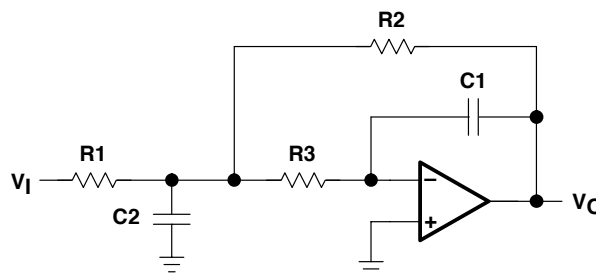


**Figure 43 – Low pass Multiple-Feedback active filer schematic.**[47]

As mentioned previously there are different architectures possible for

second order filters. Two of these are the Sallen-Key seen in Figure 42 and the

MFB in Figure 43. The difficulty to design and number of components is similar,

with the Sallen-Key using one additional resistor. However, there is a significant

72

difference in the magnitude of the attenuation at high frequencies shown in Figure 44. In many situations the time averaging effect of the A/D converter will average any high frequency noise, but the MFB design still yields better noise results and will be used.
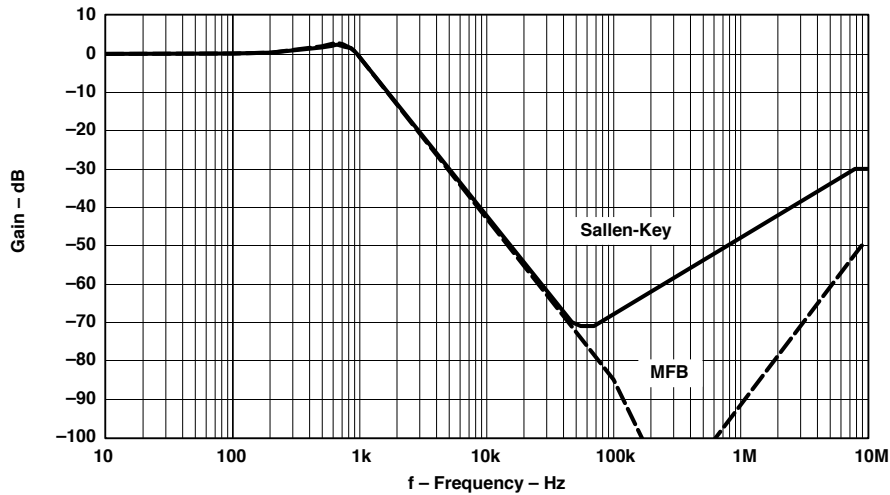


**Figure 44 – Frequency response for Sallen-Key and MFB architectures with a 3 dB Chebyshev filter.**[47]

### 4.2.3.3 Filter component values

Circuit design for the 3 dB Chebyshev MFB filter is governed by a set of design equations. Equation 15 shows the general form of the frequency response for a second order active filter. This general form is used in Sallen-Key, MFB and other architectures, which yields the gain for a specified frequency f. The cutoff frequency mentioned earlier is represented by $f_c$, K is the filter gain, Q is the quality factor and FSF is the frequency scaling factor.[47] Determining the values for K and $f_c$ are through the desired response of the amplifier. In the case for the EBT amplifier the gain of the filter is one, so Q is one and the desired cutoff frequency is 30000 Hz. Determining the value for $f_c$ is discussed in section 5.1. Finding the values for the FSF and Q are not as simple. As in most

73

electronic circuit design it is first necessary to know the polynomial used to describe the circuit. It is then possible to take the real and imaginary parts and substitute them into Equation 16. Since many basic filter types are used repeatedly it is possible to look in a filter design book and see tables used to design filters as in Table 4, which are values for a low pass MFB architecture implemented as a 3 dB Chebyshev filter. For the case of the EBT amplifier we are using a second order filter, so the FSF is equal to 0.8414 and Q is 1.3049.[47]

$$H(f) = \frac{K}{\left(\dfrac{f}{FSF * f_c}\right)^2 + \dfrac{jf}{Q * FSF * f_c} + 1}$$

**Equation 15 – General form of the frequency response of second order active filter, where $f_c$ is the cutoff frequency, j represents an imaginary number, Q is the quality factor, FSF is the frequency scaling factor and K is the gain factor.[47]**

$$FSF = \sqrt{Re^2 + |Im|^2}$$

$$Q = \frac{\sqrt{Re^2 + |Im|^2}}{2Re}$$

**Equation 16 – Formulas used to determine the FSF and Q. Re and Im represent the real and imaginary parts of the polynomial used to describe the filter being design.[47]**

| FILTER ORDER | Stage 1 | | Stage 2 | | Stage 3 | | Stage 4 | | Stage 5 | |
|---|---|---|---|---|---|---|---|---|---|---|
| | FSF | Q | FSF | Q | FSF | Q | FSF | Q | FSF | Q |
| 2 | 0.8414 | 1.3049 | | | | | | | | |
| 3 | 0.9160 | 3.0678 | 0.2986 | | | | | | | |
| 4 | 0.4426 | 1.0765 | 0.9503 | 5.5770 | | | | | | |
| 5 | 0.6140 | 2.1380 | 0.9675 | 8.8111 | 0.1775 | | | | | |
| 6 | 0.2980 | 1.0441 | 0.7224 | 3.4597 | 0.9771 | 12.7899 | | | | |
| 7 | 0.4519 | 1.9821 | 0.7920 | 5.0193 | 0.9831 | 17.4929 | 0.1265 | | | |
| 8 | 0.2228 | 1.0558 | 0.5665 | 3.0789 | 0.8388 | 6.8302 | 0.9870 | 22.8481 | | |
| 9 | 0.3559 | 1.9278 | 0.6503 | 4.3179 | 0.8716 | 8.8756 | 0.9897 | 28.9400 | 0.0983 | |
| 10 | 0.1796 | 1.0289 | 0.4626 | 2.9350 | 0.7126 | 5.7012 | 0.8954 | 11.1646 | 0.9916 | 35.9274 |

**Table 4 – FSF and Q factors for a MFB 3 dB Chebyshev active low pass filter.[47]**

Now knowing the values of $f_c$, K, FSF and Q, design can continue using Equation 17, which is only relevant for the low pass MFB architecture. Substituting into the general form of the frequency response with the equations for the factors, yields the frequency response for the low pass MFB filter shown in Equation 18. There are many solutions to the equations. Design starts by choosing a couple values and solving for the remainder. It is good to begin with values for $C_1$ and $R_2$. Best circuit performance will be found when capacitors are larger than the several hundred pF and resistances are in the $k\Omega$ to make stray capacitances and trace resistances negligible.[47] The remaining values are found by solving the equations. It is necessary to realize that the numerator of the Q equation is a constant. Solving for this using the equation for FSF*$f_c$ allows a solution to be found.

The filter for the EBT amplifier begins design with knowing the desired cutoff frequency of 30000 Hz and having a unity gain. Knowing that a low pass MFB 3 dB Chebyshev filter is desired, the FSF and Q are determined with Table 4 and are found to be 0.8414 and 1.3049. Finding the solution for the filter from Equation 17 yields Equation 19. Choosing values for $R_2$ and $C_1$ of 1 $k\Omega$ and 1 nF the remaining elements, after rounding to available components, are found to be $R_2 = 1$ $k\Omega$, $R_3 = 1.91$ $k\Omega$ and $C_2 = 2$ nF. If it is found that the initial values chosen for $C_1$ and $R_2$ yield undesirable values, trial and error will find acceptable numbers.

$$K = R_2 / R_1$$

$$FSF * f_c = \frac{1}{2\pi \sqrt{R_2 R_3 C_1 C_2}}$$

$$Q = \frac{\sqrt{R_2 R_3 C_1 C_2}}{R_3 C_1 + R_2 C_1 + R_3 C_1 K}$$

**Equation 17 – MFB substitution equalities, which make the general form frequency response specific for an MFB architecture.**

$$H(f) = \frac{-R_2 / R_1}{\left(j2\pi f\right)^2 + j2\pi f \left(R_3 C_1 + R_2 C_1 + \frac{R_2 R_3 C_1}{R_1}\right) + 1}$$

**Equation 18 – Frequency response of a MFB active filter, where j indicates a complex number, f is the frequency and the other values represent the components. Equation can be found by taking the general form in Equation 15 and substituting the values from Equation 17.[47]**

$$X = \sqrt{R_2 R_3 C_1 C_2} = \frac{1}{2\pi * FSF * f_c}$$

$$R_3 = \frac{X/Q - R_2 C_1}{C_1 (1 + K)}$$

$$C_2 = \frac{1/\left(2\pi * FSF * f_c\right)^2}{R_2 R_3 C_1}$$

$$R_1 = R_2 / K$$

**Equation 19 – Solution to low pass MFB filter. Found by solving Equation 17.**

Looking at Figure 44 the filters in the high end of the frequency spectrum begin to display a decrease in attenuation. In an ideal case, which is often the first stage of circuit design the gain would continue to decrease at high frequencies. In reality there are parasitic capacitances and resistance on the output of the op amp. Depending on those values at some frequency the gain

will begin to increase again at the rate of 40 dB/decade as is shown.  Inserting a

low pass RC filter will help to eliminate the effects and the results are shown in

Figure 45.[47]  Simulations of the MFB filter with the addition of the low pass RC

filter are shown in Figure 46.  At low frequencies there is a gain of 0 dB, which

represents the unity gain.  As the frequency moves towards $f_c$ an increase in the

gain represents the 3 dB Chebyshev design.  At the peak of the gain it is nearly 3

dB as designed.   Beyond $f_c$ there is close to a 54 dB/decade falloff when

measured between 50 and 500 kHz.  40 dB/decade is due to the second order

filter and the RC filter on the output contributes the other 15 dB/decade.

Typically, this value would be 60 dB/decade, but the output RC filter is designed

to have a cutoff frequency of 96 kHz.  If this value were lowered it would reduce

the gain near $f_c$ of the active filter, which is shown to be desirable.
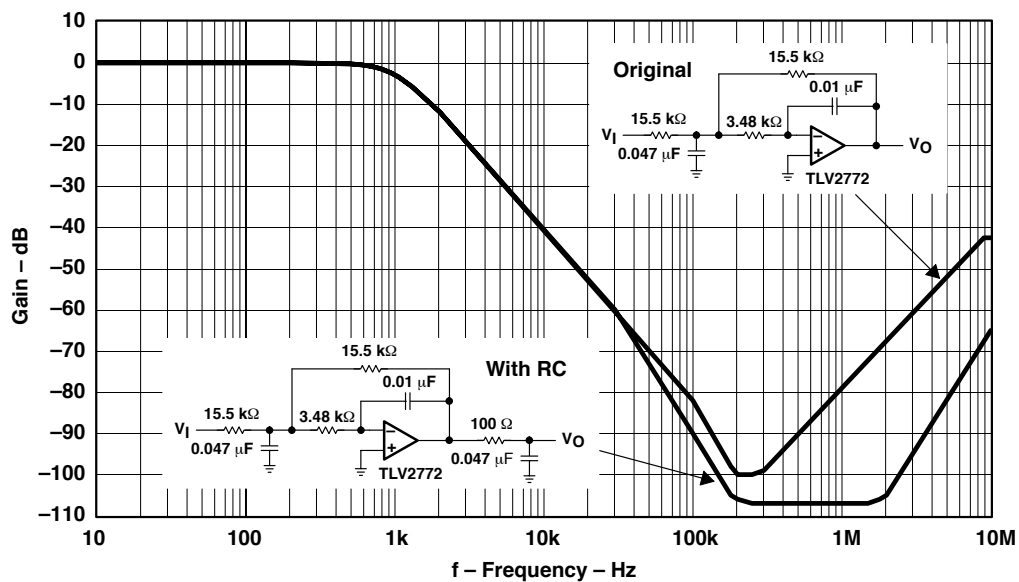


**Figure 45 – Effect of inserting a low pass RC filter to the MFB output.[47]**
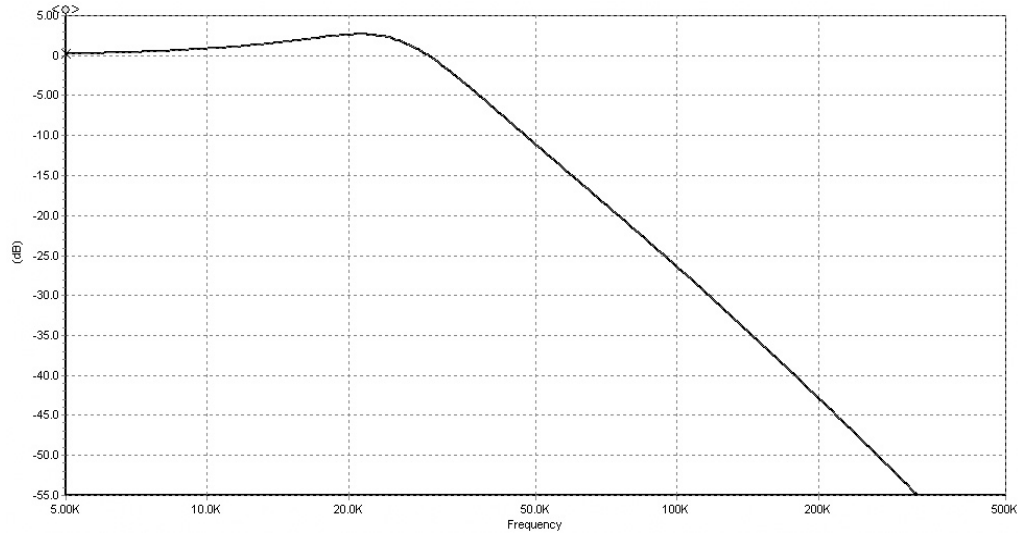
**Figure 46 – Simulation of designed MFB filter with the addition of the RC filter on the output. Simulations are completed on 5Spice software.**

### 4.2.3.4 Amplification stage design

Stage 1 of the amplifier is where the gain of the signal takes place. A feedback resistor of 42 k$\Omega$ will yield the desired gain for the calculated light intensity on the detector. A reproducible variable gain allows for adjustments to the amplification to account for errors in the calculated light intensity. These would be introduced through a variable fog OD level of the EBT film and errors in the expected attenuation of elements in the optical path. Having the gain be reproducible is important for being able to achieve the same amplification as a previous time with adjusting the gain in between. Using a variable resistance potentiometer could accomplish the different gains, but it would be close to impossible to adjust the gain back to the same value. Having the ability to adjust the gain digitally would be ideal. Replacing $R_f$ of Figure 39 with a resistor ladder allows for the desired reproducible variable gain through the use of switches on the ladder. Unfortunately, a feedback capacitance is necessary to maintain

stability in the amplifier and its use would be very complicated across a variable resistance. Introducing a feedback tee with the variable resistance as seen in Figure 47 simplifies the situation. In this case it is possible to put capacitors across $R_{ft}$ and $R_{f1}$ for stability, while inputting a 4 bit digital number into the switches. Table 5 shows the equivalent feedback resistance for the input values $0 - 15$.
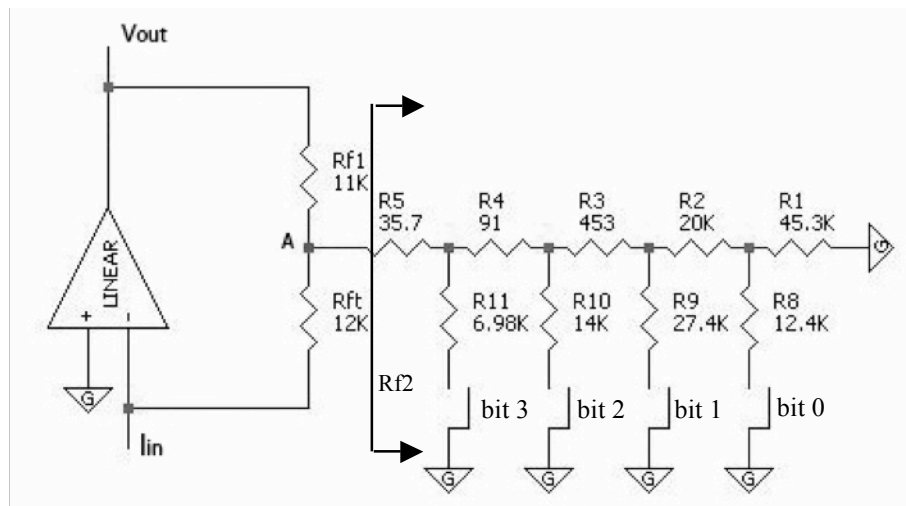


**Figure 47 – Stage 1 feedback resistance. Variable resistance controlled by a 4 bit input. Rf2 is the equivalent resistance of the ladder.**

| Input | Resistance | | Input | Resistance | | Input | Resistance | | Input | Resistance |
|---|---|---|---|---|---|---|---|---|---|---|
| 0 | 25 k | | 4 | 34.3 k | | 8 | 43.8 k | | 12 | 53 k |
| 1 | 27.4 k | | 5 | 36.6 k | | 9 | 46.1 k | | 13 | 55.3 k |
| 2 | 29.6 k | | 6 | 38.9 k | | 10 | 48.4 k | | 14 | 57.5 k |
| 3 | 31.8 k | | 7 | 41.1 k | | 11 | 50.6 k | | 15 | 59.6 k |

**Table 5 – Feedback tee resistance for inputs 0 – 15.**

Knowing that the estimated feedback needed is 42.2 k$\Omega$ and a desired ratio between the minimum and maximum gain is 2.5, the range in the feedback resistances should be 25 – 60 k$\Omega$. Calculation of the equivalent feedback resistance is determined through current analysis and is shown in Equation 20. $R_{f2}$ is equivalent resistance of the resistor ladder. With an input value of zero all

switches are open and $R_{f2}$ is equal to the sum of $R_1 - R_5$. Any other input value will result in a parallel resistor equation. Ideally, the final resistances will be equal steps between 25 – 60 kΩ for each input value. Determination of all resistor values was executed using a brute force method in Microsoft Excel. In the calculation, values of available resistors and current from the output of the op amp must be considered. It is necessary to take into account the increased output current of the op amp, so that it is not overloaded. This is determined using Equation 21.

$$R_{eq} = \frac{R_{ft}R_{f1}}{R_{f2}} + R_{ft} + R_{f1}$$

**Equation 20 – Equivalent feedback resistance across resistor tee.**

$$I_{opamp} = I_D \left( R_{ft} / R_{f2} + 1 \right)$$

**Equation 21 – Stage 1 output current draw. Current is increased over the diode current, $I_D$, due to the current through $R_{f2}$.**

A photodiode generates capacitance in the input of the op amp. This can lead to an unstable situation where positive feedback can occur due to a phase shift in the output. To avoid a phase shift that is too large, 0.47 nF capacitors are placed across resistors $R_{ft}$ and $R_{f1}$. The addition of the capacitors makes stage 1 act as a first order filter Bessel filter. The values of the capacitors are again chosen to have a cutoff frequency of approximately 30 kHz to match the second order filter of stage 2. Adding the filter to stage 1 has two effects on the frequency response shown in Figure 48 compared to stage 2 shown in Figure 44. At the cutoff frequency there is no longer an increase in the gain as seen in stage

80

2.  The Bessel filter of stage 1 counteracts the 3 dB Chebyshev filter in stage 2 and results in only a small increase in the gain.  Also, an addition of another first order filter generates an extra 20 dB/decade of attenuation above the cutoff frequency, yielding a total of 74 db/decade.
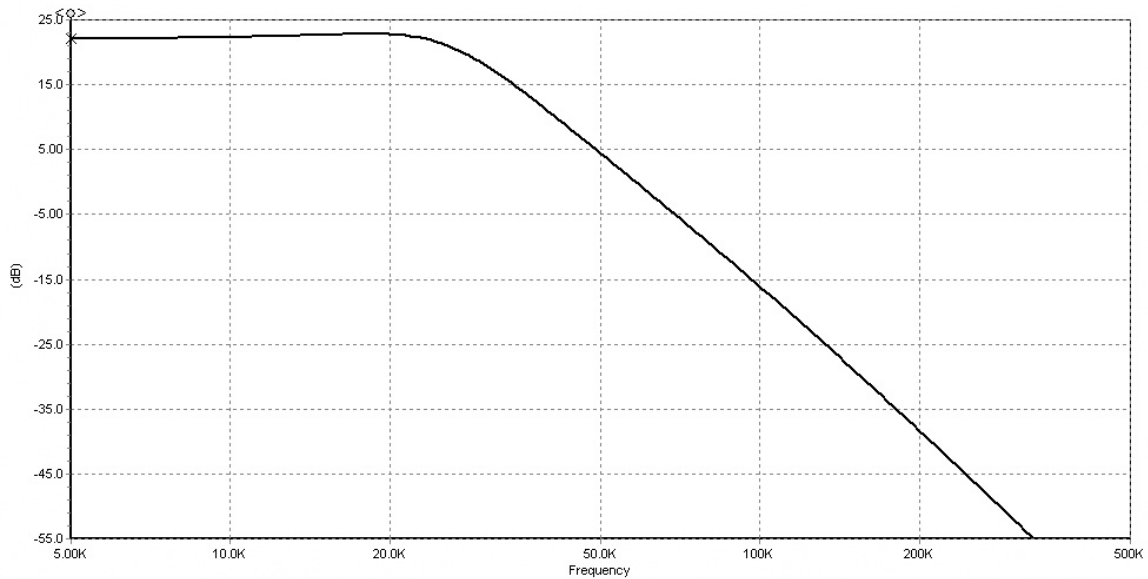


**Figure 48 – Total frequency response of the EBT amplifier determined through simulation.**

4.2.3.5    Dual stage amplifier noise analysis

There are five common sources of noise in op amp circuits.  Shot noise is due to charge being a discrete value, which leads to a statistical variation of the current across a potential.  Johnson noise is generated by thermal agitation of charge carriers.  Flicker noise occurs in all active devices and is brought about by many sources when dc current is involved.  Imperfections in semiconductor material cause burst noise and it represents sudden surges in current.  The last major noise source is called avalanche, which is due to reverse voltage across a pn junction yielding current pulses much like shot noise, but at much higher intensities.[48]

All noise sources in op amp circuits are calculated through determining the noise introduced with resistors, input voltage noise and input current noise multiplied by the gain of the amplifier. Current noise is determined through calculation of the Johnson noise, Shot noise and photodiode dark current. Equation 22 shows the formulas used to determine the current noise. Once the total input current noise is calculated it must be multiplied by the circuit gain to yield the output noise. Noise due to the discrete flow of electrons in resistors is found through the use of $E_{noR}$ in Equation 23, where K is the Boltzman's constant (1.38 x$10^{-23}$ J/°K) and T is the temperature in Kelvin.[46,48]

$$i_j = \sqrt{4kTB / R_{sh}} \quad Johnson \quad noise$$

$$where \quad R_{sh} = diode \quad shunt \quad resis\tan ce \quad and \quad B = bandwidth$$

$$i_{sd} = \sqrt{2qI_d B} \quad dark \quad current \quad noise \quad where \quad I_d = dark \quad current$$

$$i_{ss} = \sqrt{2qI_s B} \quad Shot \quad noise \quad where \quad I_s = photo \quad current$$

$$e_{noi} = \sqrt{i_j^2 + i_{sd}^2 + i_{ss}^2}$$

$$SNR = I_s / i_{total \quad noise}$$

**Equation 22 – Op amp input current noise. Must be multiplied by the gain of the circuit to determine the output noise.[46,48]**

$$E_{noR} = \left(1 + R_{f1} / R_{f2}\right)\sqrt{KTR_f \pi f_{pf}}$$

$$where \quad f_{pf} = \frac{1}{2\pi R_f C_S}, \quad R_f = feedback \quad resistance,$$

$$C_S = feedback \quad capacitance$$

**Equation 23 – Noise introduced due to the discrete effects of electron charge.[46]**
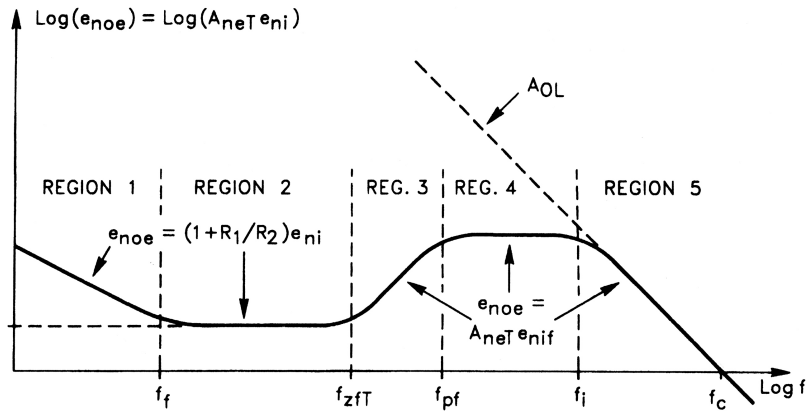
**Figure 49 – Input voltage noise frequency bands.**[46]

Much more involved is the calculation of the voltage noise, $E_{noe}$, as it is frequency dependent. Equation 24 shows the noise equations for the five frequency bands contributing to the input voltage noise and are displayed in Figure 49.[46] All elements in the circuit determine the magnitude of the noise introduced, but the op amp and diode will have the greatest affect on the final noise value. It is critical to choose an op amp with very low input voltage noise, as it is the primary determinant of the output noise.

Used in the circuit design is a Hamamatsu S3071 photodiode with a 5 mm diameter active region, which makes $C_i$ 128 pF. Stage 1 has an Analog Devices AD820B op amp and stage 2 is an Analog Devices AD745K. The AD820B has a very low input current noise of 0.8 $fA/Hz^{1/2}$ and the AD745K supplies a larger output current, but the input current noise is 6.9 $fA/Hz^{1/2}$. Stage 2 has unity gain, so there is no amplification of the current noise and as a result the affect of the current noise is negligible. Performing the noise calculations yields $E_{noi}$ and $E_{noR}$ of 96.6E $\mu V$ and 11.3 $\mu V$. To determine $E_{noe}$ it is found that $f_f$, $f_{pf}$, $f_{zf}$ and $f_i$ are 10 kHz, 30.78 kHz, 8.13 kHz, 1.44 MHz. Due to $f_{zf}$ being less than $f_f$, $E_{noe2}$ is 0. The

83

cutoff frequency of 30 kHz is less than the frequency ranges of $E_{noe4}$ and $E_{noe5}$ making their contribution to noise negligible. As a result only $E_{noe1}$ and $E_{noe3}$ are significant noise sources. Calculating the total RMS noise from the circuit yields 2.98 mV. A 16 bit A/D converter with a 10 V range gives a step size of 152 μV. The RMS noise is therefore 19.5 times the step size, therefore one standard deviation in the digital output should be about 20 steps of the A/D converter.

$$E_{noR} = \left(1 + R_{f1}/R_{f2}\right)\sqrt{KTR_f \pi f_{pf}}$$

$$\text{where } f_{pf} = \frac{1}{2\pi R_f C_S}, \quad R_f = \text{feedback  resistance,}$$

$$C_S = \text{feedback  capacitance}$$

$$E_{noe1} = \left(1 + R_{f1}/R_{f2}\right)e_{nif}\sqrt{f_f \ln\frac{f_f}{f_1}}$$

$$\text{where } f_f \text{ is the  corner  frequency  in } e_{ni} \text{ vs } \log(f)$$

$$f_1 \text{ is} \sim 0.01 Hz, \ e_{nif} \text{ is the  input  noise  at  the } f \text{ of  interest}$$

$$E_{noe2} = \left(1 + R_{f1}/R_{f2}\right)e_{nif}\sqrt{f_{zf} - f_f} \quad \text{where } f_{zf} = \frac{1}{2\pi R_f\left(C_i + C_S\right)}$$

$$E_{noe3} = \left(1 + R_{f1}/R_{f2}\right)\frac{e_{nif}}{f_{zf}}\sqrt{\frac{f_{pf}^3 - f_{zf}^3}{3}}$$

$$E_{noe4} = \left(1 + C_i/C_S\right)e_{nif}\sqrt{f_i - f_{pf}}$$

$$\text{where } f_i = f_{c1}C_S\left(C_i + C_S\right), \ C_i = \text{input  capacitance}$$

$$f_{c1} \text{ is the  open  loop  unity} - \text{gain  crossover  frequency}$$

$$E_{noe5} = \left(e_{nif}f_{cc}\right)\sqrt{\frac{1}{f_{pf}}} \quad \text{where } f_{cc} = \frac{R_{f2}}{R_{f1}}f_{c1}$$

$$E_{noe} = \sqrt{E_{noe1}^2 + E_{noe2}^2 + E_{noe3}^2 + E_{noe4}^2 + E_{noe5}^2}$$

$$E_{noi} = Gain * e_{noi}$$

$$E_{no} = \sqrt{E_{noR}^2 + E_{noi}^2 + E_{noe}^2}$$

**Equation 24 – Voltage noise calculation equations for op amp circuits.**[46,48]

## 4.3  PCB design

Once a schematic of a circuit is completed, the next step in design is the layout of components on a circuit board.  Location of the components, and the size of the copper traces can greatly affect the overall signal to noise ratio of the amplifier.  Any loop in a trace path introduces electromagnetically coupled current noise, as it acts similar to an inductor.  As a loop grows in the area, it encircles a larger electromagnetic flux and the current generated is proportional to the flux through the loop.  The smaller the signal current the greater the sensitivity to electromagnetic interference.[49]  Therefore, it is important that the loop formed by the input of the first stage and the photodiode be kept to a minimal size.  Decreasing the amount of electromagnetic flux in the area of the loop can also reduce current noise.  The use of ground planes can block the flux from entering the loop.  The PCB board used in construction of the amplifier is a four layer design with the top and bottom layers acting a ground.  All loops formed on the board are enclosed by the ground planes.

Trace size is also a consideration in construction, because the traces add resistance proportional to the length over the cross section area, as seen in Equation 25.  It is not a solution to just make the trace sizes extra large, because they also act as capacitors and can change the frequency response of the amplifier.  Capacitance is determined using Equation 26.  Fortunately in the dual stage linear amplifier design there is considerable capacitance and resistance

already built into the design, which greatly simplifies the design, as stray impedance will not alter the function of the amplifier.

$$R = \rho * l / A$$

**Equation 25 – Resistance of a trace in a PCB board. ρ is the static resistivity, *l* is the length and A is the cross section area.[49]**

$$C = A\varepsilon / d$$

**Equation 26 – Parallel plate capacitance, where A is the area, *d* is the distance between the plates and ε is permittivity.[49]**

$$E_{noS} = \frac{A_{ne}\sqrt{(2i_s Z_L)^2 + PS_n^2}}{PSRR}$$

**Equation 27 – Power supply induced output noise, where $A_{ne}$ is the gain, $i_s$ is the op amp current, $Z_L$ is the power supply trace resistance and PSRR is the op amp power supply rejection ratio.[46]**

The output of an op amp is only as stable as the power supply voltage levels and the induced noise is known as power supply noise coupling. The output noise is determined through Equation 27.[46] There are two parts to the numerator, $PS_n$ is the noise at the output of the power supply and the other part is the voltage fluctuation due to resistance in the trace. The power supply rejection ratio (PSRR) for the AD820B op amp is $10^8$. Taking a gain of 42500 into account, the noise on the output is 0.425E-3 of the input power supply noise. This effectively eliminates the power supply as a noise source when compared to other sources. In cases of larger gain it would be necessary to reduce the noise at the power supply input. An efficient method of removing the noise is through the introduction of bypass capacitors. An LC circuit tied to ground acts as a filter

and reduces the noise for frequencies within the bandwidth of the amplifier.  The

noise reduction frequency is determined by the time constant of the LC circuit.[46]

## 4.4   Amplifier analysis

While performing theoretical noise calculations are important, final

performance must be determined through measurements.  Gain and frequency

response are found through the use of sinusoidal current sources attached to the

input of the amplifier.  To determine the output response, the gain in decibels is

calculated with the output to input ratio for applicable frequencies at input signal

intensities of 128 and 0.5 $\mu$A.  Figure 50 shows the resulting amplifier response

for an approximate feedback resistance of 44 k$\Omega$.  Comparing this to the

calculated response in Figure 48 there is a noticeable difference.  The shape

around the cutoff frequency does not experience the increase in gain at 20 khz.

This could be attributed to the tolerances on the capacitors adjusting the cutoff

frequency on stage 1 to a lower value.  The lower cutoff frequency negates the

increased gain of the 3 dB Chebyshev filter.

Further analysis determines the combined laser and amplifier signal noise.

Using the amplifier and the optics system as a point densitometer, repeated

measurements give average and one standard deviation results.  Table 6 shows

the results from approximately 300 measurements when the laser beam is

attenuated by EBT film exposed to 20, 100, 200, 400, 600 and 800 cGy.

87

Knowing the signal output intensity to dose relationship and the noise at one standard deviation, dose error is calculated and shown in Figure 51. Inspecting the dose uncertainty results, the accuracy due to the laser fluctuation and amplifier noise yields accuracy better than 0.25% of the measured dose for up to 400 cGy. Typically clinical use is limited to a max dose of 300 cGy, so the system should yield excellent results. The increased dose uncertainty at high dose levels is due to the saturation of the film and a decreased signal change at high doses. These numbers do not include one other noise source, which is due to the film and how it alters the transmitted beam when exposed at a constant level. The final dose accuracy including the noise due to the film will be analyzed in chapter 6.
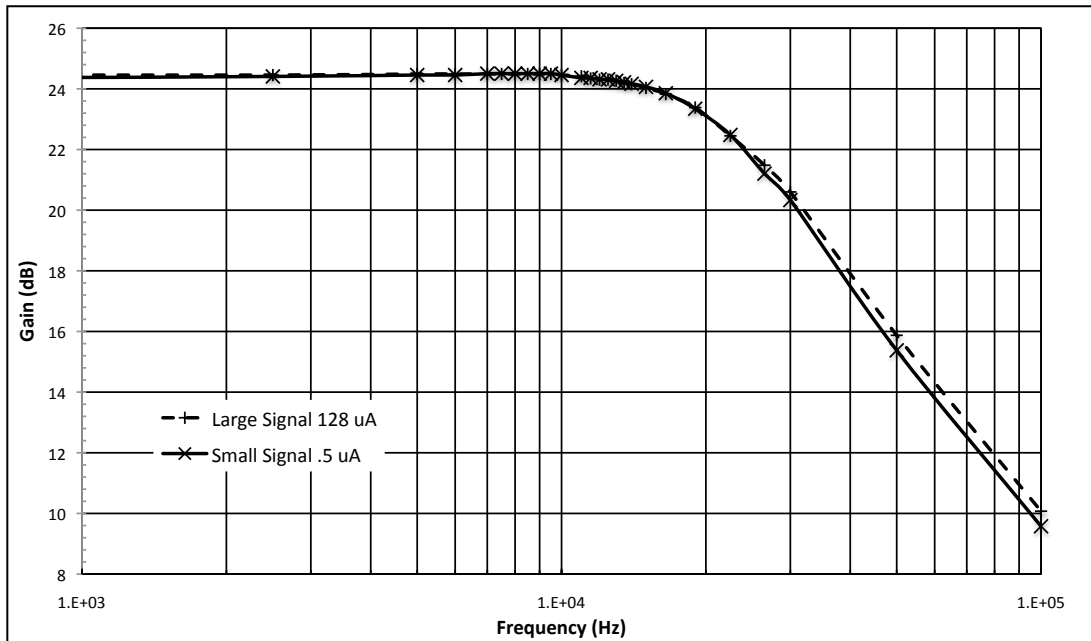


**Figure 50 – Measured frequency response of amplifier for input signal intensities of 128 and 0.5 μA.**

| Dose (cGy) | OD | Average | Std |
|---|---|---|---|
| 20 | 0.52 | 44600.28 | 30.05 |
| 100 | 0.97 | 15635.84 | 16.91 |
| 200 | 1.32 | 6942.89 | 12.96 |
| 400 | 1.82 | 2238.52 | 10.83 |
| 600 | 2.42 | 551.74 | 10.06 |
| 800 | 3.74 | 26.69 | 9.82 |

**Table 6 – Signal noise for the combined optics and amplifier system for various signal intensities.**
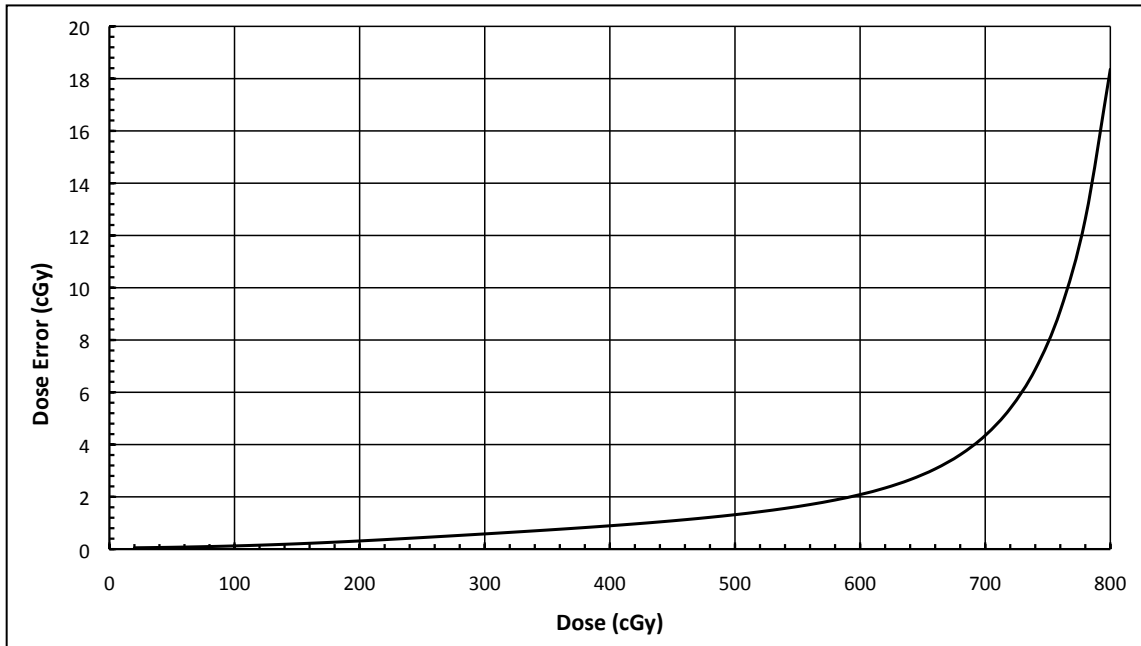


**Figure 51 – Dose error of the EBT system determined by the pixel value to dose relationship and the one standard deviation uncertainty in the output signal.**

# 5  Motion and Optics

## 5.1  Motion

The initial motion design was to incorporate a rotating platform as a means of scanning films with dimensions of 8x10 inches within two minutes in a radial scanning technique.  This design allows for the light path to always be perpendicular to the film while maintaining a pixel scan rate due to the continuous motion design.  A drum scanner approach could also achieve this, but it would be necessary to have an object such as glass in the light path, which would cause artifacts.  Using a platform technique could allow the film to be held in place through tension instead of support from below.  This would be feasible because, EBT film tends to have slight rigidness and the motion of the scanner would add to the support through centripetal forces as opposed to pulling the film out of position in a drum scanner.
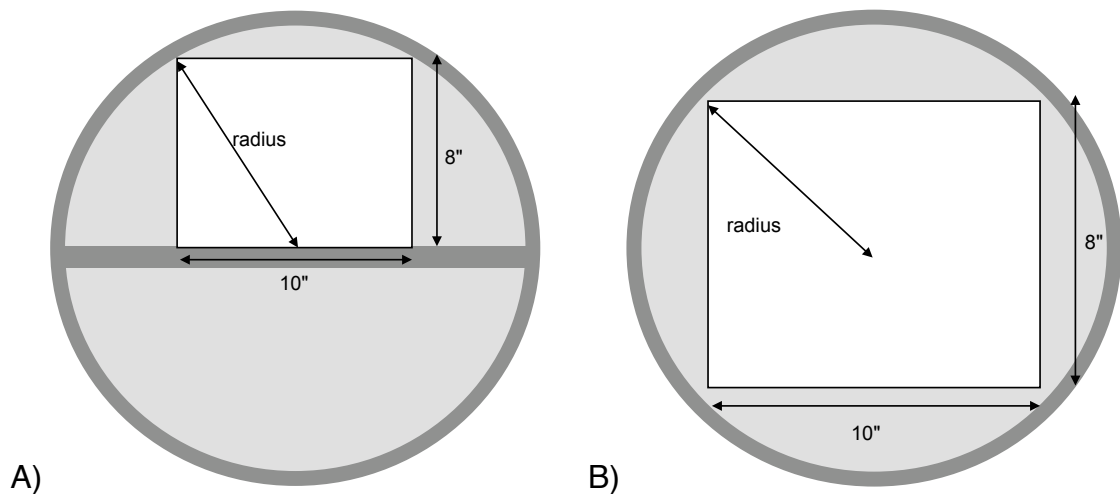


**Figure 52 – Rotating platform design possibilities.  A) can be used to digitize two films simultaneously to save scanning time.  B) allows for slower rotation speed, but requires accurate positioning at the center to avoid the possibility of not scanning the center region.**

Two platform designs were considered and are shown in Figure 52. Design B) digitizes one film at a time at a slower rotation speed, but may be subject to alignment problems, as the laser must pass through axis of rotation precisely to digitize the central region. Implementing design A) necessitates faster rotation speeds to scan the image in 120 seconds, but two images could be digitized simultaneously to reduce the effective scanning time.

The pixel measurement frequency is determined by the total scan time and the design utilized. Choosing the conditions that will yield the fastest scan rate is design A) with a scan time of 120 seconds and a resolution of 75 dpi. The radius of the platform will be approximately 10.5 inches yielding a circumference of 66 inches. Using 75 dpi, the number of pixels required at the circumference is 4950. A radius of 10.5 means the platform must rotate 788 times in the 120 seconds, which is 6.6 rotations/second. The number of pixels per second is then found by multiplying the rotational speed with the number of pixels per rotation and yields 32670 pixels/sec. This method was used to determine the cutoff frequency of the amplifier of 30 kHz. As long as the cutoff frequency is not significantly lower than the scan rate there will not be a noticeable blurring of a sharp edge, although sharp edges are not found in the high energy dose patterns of linear accelerators.

While scanning full sized films at times that are reasonable for clinical use is the ultimate goal, a prototype design was based on XY indexing and yields a proof of principle. All results presented were collected on the XY design. The

system is composed of two linear stages with a cantilevered platform that contains a 3.5"x3.5" aperture to allow for transmission scanning. The film resting over the opening is only supported on the edges and does not show significant sag in the center. To demonstrate that a rotational scanning technique is feasible, multiple scans of the same film were compared, when each scan has the film rotated within the digitizer with respect the other film placements.

## 5.2 Optics

### 5.2.1 Laser selection

The ideal light output from the laser would be a single wavelength of 635 nm and have polarized, but not coherent light. Coherent light produces moiré patterns due to internal reflections within the EBT film.[50] HeNe lasers produce a 632.8 nm wavelength, which meet the wavelength criteria, but they tend to yield coherent light for long distances from the laser source. Diode lasers lase in multiple modes producing a broader spectrum, but the output tends to lose the coherent qualities faster than HeNe.

Temperature control of the diode laser is a necessity to maintain 635 nm wavelength, which is primarily determined by the bandgap width of the semiconductor. Increasing temperature causes the optical path to lengthen, resulting in production of a longer wavelength.[51] Tuning of the wavelength does not occur as a constant change with temperature. After a section of smooth

adjustment of wavelength there is a jump in the wavelength that is cause by a change from one longitudinal mode to another, called mode hopping. The change in wavelength between operating modes is about 0.5 to 0.75 nm. Having a very particular wavelength may not be possible, because there are some wavelengths that are skipped in the switch between operating modes.[51] Figure 53 illustrates the different operating modes with temperature. Fortunately only the stability of the wavelength is crucial for the optics system and not having a precise wavelength of 635 nm, as a variation of several nm will not alter the observed sensitivity to a significant degree.
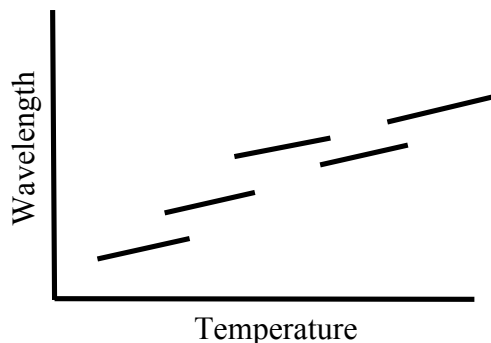


**Figure 53 – Laser diode wavelength selection with temperature. Laser operates in modes, which are apparent by the jump in wavelengths.**

The laser used in the digitizer is diode laser sold by Power Technology (Alexander, AR) with model number IQ1C. It is preconfigured with temperature control to have a stable wavelength of 635 nm using a peltier device. The output is 6 mW and has long term stability to within 1%. The active region of a laser diode has a rectangular shape and as a result the emitted beam will tend to be elliptical. Beam circularity optics within the laser makes the output have a Gaussian profile in all direction of approximately the same diameter of 2.5 mm. Divergence is specified to be less than one milliradian.

## 5.2.2 Circular polarization

Linear polarization occurs when an electromagnetic wave has a magnitude that varies, but the axis on which the amplitude fluctuates is constant. In circular polarization the opposite is true. The magnitude is constant while the axis on which the polarization appears on varies. Phase is determined by amplitude and angle for linear and circular polarization respectively. Just as in linear polarization, the distance between repeated phases determines the wavelength in circular polarization. An illustration of a circularly polarized wave is shown in Figure 54. The straight line represents the central axis of the beam. As the wave propagates the amplitude is shown as constant, while angle of the wave rotates around the central axis.
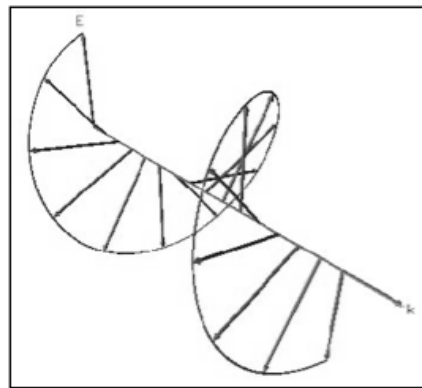


**Figure 54 – Circularly polarized light illustration.**[52]

Circular polarization is beneficial for digitizing EBT film due to the polarization affects shown in Figure 30. Measurements with linearly polarized light lead to fluctuations on an unexposed film, as the direction of the fibers in the active layer are variable. When light is polarized in the same orientation of the fibers the maximum transmission will occur. As it is not possible to control the placement of the fibers the light used for measurement must not be sensitive to

94

the fiber orientation.  Circular polarization accomplishes this task by averaging all polarization angles together.  The resulting transmission is neither the maximum nor minimum, but is constant for a given exposure.

Generating a circularly polarized light source is accomplished with a quarter waveplate also known as a quarter retarder.  The basic principle of a waveplate is that the index of refraction is different for one polarization compared to another.  For generation of circular polarization it is necessary to have the maximum index perpendicular to the minimum index.  A higher index of refraction causes light to propagate slower than a low index.  The axis on which light travels faster is the fast axis and the other is the slow axis.[53]  A quarter waveplate is one where the light emerging will have a $\lambda/4$ wavelength shift between the axis.  This requires that a quarter waveplate be designed for a specific wavelength as the shift is an absolute distance and not relative to the wavelength.  The resulting waves polarized to each axis are shown in Figure 55.[54]
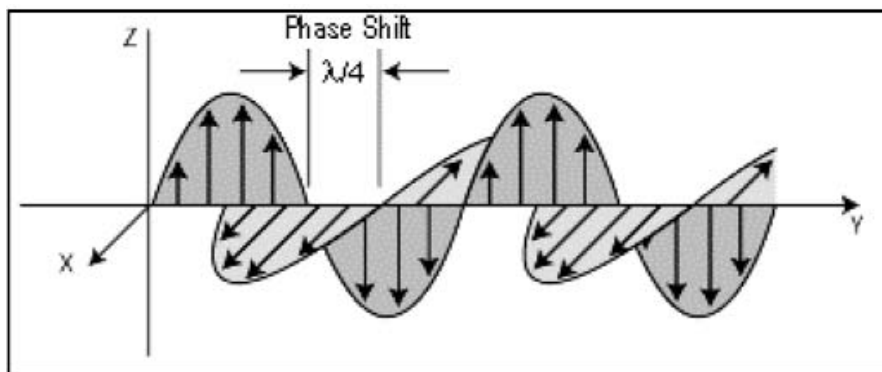


**Figure 55 – Quarter wavelength shift in perpendicular axis causes circular polarization given that the two axes have equal intensity.[54]**

Simply passing light through a quarter waveplate design for the desired wavelength will not generate circular polarization, but will typically yield elliptical

polarization.  This is when one axis has an intensity greater than the other.  Circular polarization occurs when both axes have equal power and as a result at any moment in time the root mean square of the intensity on each axis is constant.  To generate equal intensity on each axis the polarization angle of the incident light must be at 45° to each axis.[54]

Testing of the degree of circular polarization is accomplished with transmission measurements through a linear polarizer.  As the polarizer is rotated the minimum and maximum transmission is recorded.  The difference between the maximum and minimum over the average of the two yields the fraction of the power that is not circularly polarized.  Measurements for the system constructed showed that 3.2% of the power was not circularly polarized.  Ideally, this value would be lower, but the use of a laser diode results in a spectrum of wavelengths.  Although the width of the spectrum is narrow it does affect the results.  From section 3.7 the OD variation with linear polarized light is 1.6 to 2.3, which translates to a 20% signal fluctuation.  Knowing that 3.2% of the beam is acting as linearly polarized light the fluctuation could be 0.6% of the transmission.  This translates to a dose error of 1% and 0.5% at 50 and 150 cGy respectively.  This polarization error could be significantly reduced with additional modification of the system.  A simple method of achieving this would be to use a single mode optical cable.  This allows the undesirable wavelengths to escape and would also add the benefit of decreased light coherence.

5.2.3  Measurement beam width

The resolution necessary for the EBT digitizer is relatively low as the optical density gradient for films measuring IMRT fields is limited.  Measuring the distance in a beam penumbra from 80 – 20 %, which is the area with the greatest dose change, of the maximum dose is approximately 3 mm.  Actual distance is dependent of factors such as depth, MLC type and focal spot size.  Having four to five measurement points in this distance would yield an accurate representation of the dose.  Therefore, a beam width of 0.6 mm would achieve the desired results.

A less complex method of calculating the beam width will suffice, because a high degree of accuracy is not necessary.  Film measurements were performed off of the beam waist as the width at the waist will be too small and as a result the divergence can be neglected.  A lens with a focal length of 50 cm was used to focus the beam.   Using similar triangles, the beam width (w) at the measurement point some distance d beyond the beam waist is found using the initial laser beam radius (r) and the focal length (f) of the lens. The beam width at the output of the laser is 2.5 mm, so to yield a beam with of 0.6 mm d must be 12 cm.

$$w = 2d\frac{r}{f}$$

**Equation 28 – Formula for determining beam width, w.  Where d is the distance beyond the beam waist, r is the radius of the laser beam and f is the focal length of the lens.**
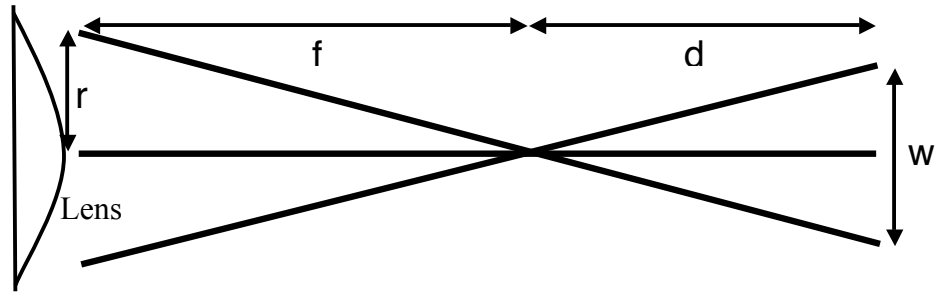
**Figure 56 – Geometrical drawing for determination of beam width, w.  Where d is the distance beyond the beam waist, r is the radius of the laser beam and f is the focal length of the focusing lens.**

Using a beam profiler the beam shape is determined at the measurement point of 12 cm beyond the beam waist or 62 cm from the lens.  Figure 57 shows the results from the measurement with the intensities normalized to the maximum intensity found.  The X and Y profiles are very similar, but not identical.  This is most likely caused by the initial laser beam no being a truly circularized beam.  Even with the X profile being slightly broader, 90.9% of the power is found within the 0.6 mm diameter of the desired beam width for the X axis and 93.9% for the Y axis.  The standard method for determining beam width is defined by the distance between where the intensity falls to $1/e^2$ or 13.5% of the maximum intensity.[55]  This is found to be 0.699 and 0.635 mm for X and Y respectively.  While slightly larger than the desired width, these are certainly acceptable due to the low resolution needed.
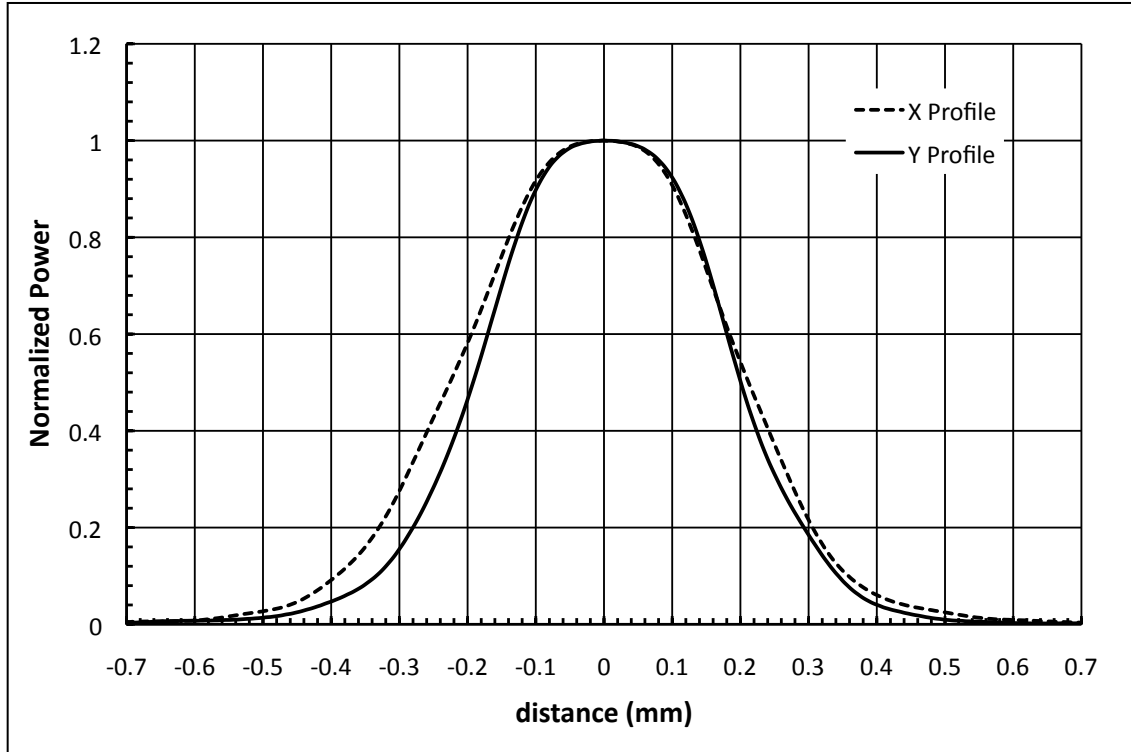
**Figure 57 – Measurement beam profiles for the x and y axis at the measurement point.**

5.2.4  Light scatter and collection

As previously discussed EBT film has a constant degree of light scatter, but it scatters light anisotropically due to the fibers in the active layer.  To get a true measure of the attenuation within the film it is necessary to have all light that passes through the film be collected and included as part of the signal.  It is difficult to collect all the transmitted light, because some of the photons scatter at a very high angle.  The best method to measure the greatest amount of light is through the use of an integrating sphere.  However, difficulties arise when trying to place the integrating sphere close to the film as it may collide with transport mechanisms.  Moving the sphere away from the film prevents this from happening, but a much smaller percentage of the light is measured.

An option that was implemented in the EBT digitizer was to use an aspherical singlet lens with a focal length of 18 mm and a diameter of 24 mm. The distance from the lens at which an object will appear in focus is found using Equation 29 and the size of the image is determined using the magnification in Equation 30.[56] Placing the lens at 20 mm from the film yields a final image size of 1.25 mm at film to image distance of 88.5 mm on the 5 mm diameter photodiode. It may seem that placing the lens at 2 mm beyond the focal length would cause the image distance to be much longer, but the back focal length of 11.4 mm must be taken into account. Back focal length is the distance from the lens to the focal point and is always less than the focal length. The detector is at about 39 mm from the lens, which is less than the calculated lens to image distance, s", of 49 mm. This causes this image on the detector to be out of focus, but for the purpose of the digitizer it does not need to be in focus. Having the detector closer also causes the illuminated region on the detector to be larger than the image, and is found to be 3.7 mm in diameter. As a result power is spread more uniformly across the detector.

$$\frac{1}{s''} = \frac{1}{f} - \frac{1}{s}$$

**Equation 29 – Thin lens approximation for lens to object distance, where f is the focal length and s" and s are the distances from the lens to image and object to lens.[56]**

$$M = \frac{s''}{s}$$

**Equation 30 – Formula for the magnification of an imaged object where s" is the lens to image distance and s is the object to lens distance.[56]**

# 6   EBT digitizer performance

## 6.1   Introduction

Many of the typical tests used to analyze a digitizer include measurement of the point spread function, modulation transfer function, noise and low contrast resolution.  These are not essential for measurement of high energy x-ray doses as the dose gradients are low and dose accuracy is more important than noise in the measurement value as it also includes the effects that the film introduces.

Ultimately, the desired output of a digitizer yields high dose accuracy for a specific measurement location.  The tests performed analyze the ability of the EBT digitizer to yield the exposure doses of the films.  All test are also compared against the Epson 10000XL, as it could be argued to be the best commercially available digitizer for EBT film.   Additionally, no dose measurements are performed above 300 cGy, because the vast majority of IMRT QAs will have dose levels below 300 cGy.

## 6.2   Response curve

When analyzing film, the sensitometric curve is essential as it provides the sensitivity of the film to an exposure of radiation.  For digitizers it is important to know the output response for a given input, which is usually an optical density. Combining the important factors for the film and digitizer as a system, the input is

dose while the output at a point is the numeric value that the digitizer yields. For convenience, the output of the digitizer at a point is called the pixel value.

In determining the response curve for a film digitizer system the film is exposured to a known dose. To simplify the number of scans and film necessary, a single film was exposed to doses of 17.1, 41.8, 64.7, 97.8, 129.8, 159.3, 200.1, 244.1 and 289.5 cGy using an MLC file that automatically generates the pattern. A scanned image of the exposed film is shown in Figure 58. The exposure was made with the Brainlab m3 multileaf collimator that has 3 mm MLCs in the center and 5 mm on the edges. Each square has an approximate size of 1.8x1.8 cm. Squares on the edges are 1.8x1.9 cm as the MLCs that are 5 mm prohibit an exact 1.8 cm. Regardless, PTW (Freiburg, Germany) pinpoint ion chamber measurements allow for the determination of the dose in each square, so uniform size is not important.
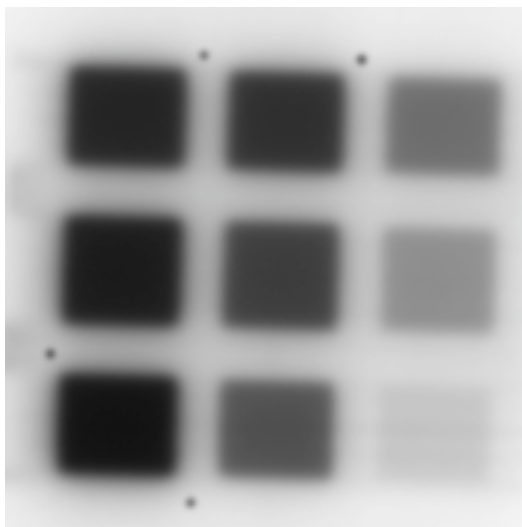


**Figure 58 – Calibration film with dose exposures from 17 to 290 cGy. Each exposed square is approximately 1.8 cm square.**

After exposure, films were scanned on the EBT digitizer and the Epson 10000XL. The average pixel value of the center 0.5x0.5 cm region in each square was recorded and the results are shown in Figure 59 as the response curve of the film and digitizer system. The EBT digitizer shows greater response as its light source is paired with the peak absorption wavelength of the EBT film as opposed to the Epson that uses a general red light, but the exact central wavelength and bandwidth are not known, as Epson will not release this information. The stronger response has the propensity to yield more accurate results, as the curve, for the conversion from pixel value to dose, is more tolerant to fluctuations in pixel value. The change in pixel value per cGy exposure for the EBT digitizer is found to be 604 and 29 PV/cGy for 17 and 290 cGy respectively. Similarly, the Epson 10000XL was found to be 162 and 44 PV/cGy. While the EBT digitizer showed a much greater slope for low doses, at high doses it was found to be less than the Epson. Even though the slope is greater for the Epson at high doses, the slope to noise ratio for the Epson is poorer as will be described in the next section. Where the noise is determined by the standard deviation in the pixel values of the measured area. The poorer ratio means that the accuracy in the measured dose is less.

There are two explanations for the larger slope at high doses on the Epson, as the change in light intensity must be greater on the EBT digitizer. At some point before the image is written to a file the output of the Epson could have a function applied that increases contrast at high optical densities. This

could be implemented in hardware or software. A log amplifier would be an example of hardware implementation. The other cause could be that the signal on the EBT digitizer is attenuated so much that the absolute change in light is less even if the percent change is more.
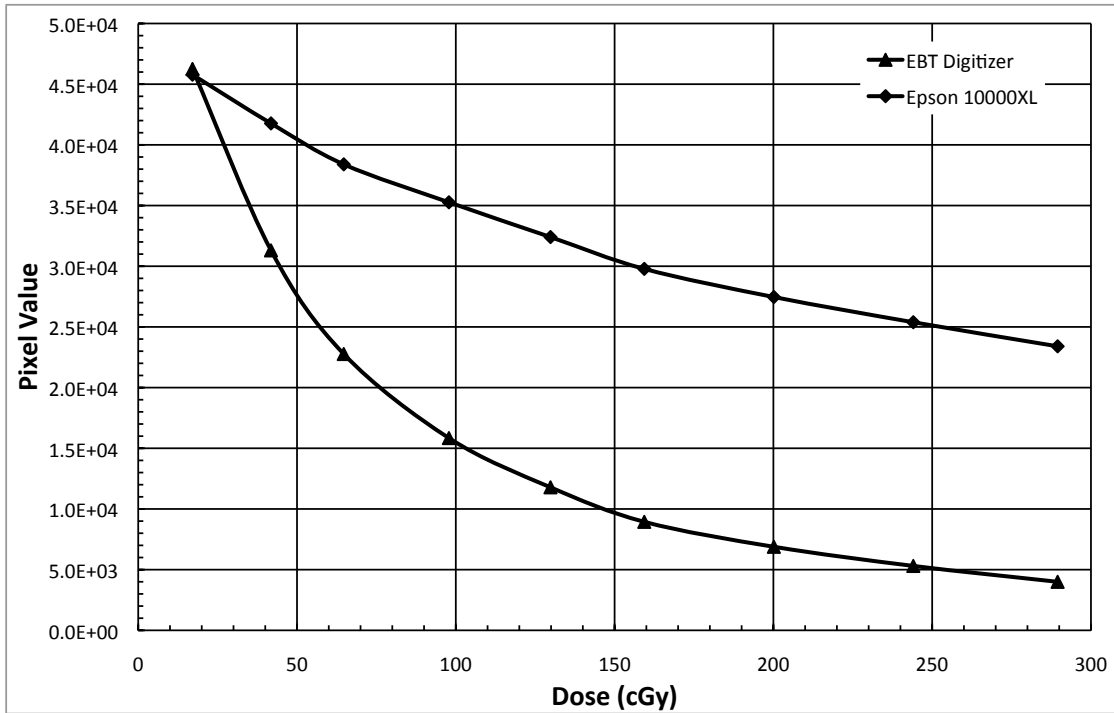


**Figure 59 – Response curve for the EBT digitizer and Epson 10000XL for a dose range of 17 to 290 cGy.**

## 6.3   Dose resolution

Previous measurements of the response curves are important, but the desired goal is high accuracy in the measured doses. Using the data from the response curves along with the standard deviation in the pixel values of the measured regions, a dose resolution was derived. Error in dose measurement was found by multiplying the slope of the response curve by the standard

deviation.  Scans taken at 50 dpi yield 100 pixels for each 5x5 mm measurement region.
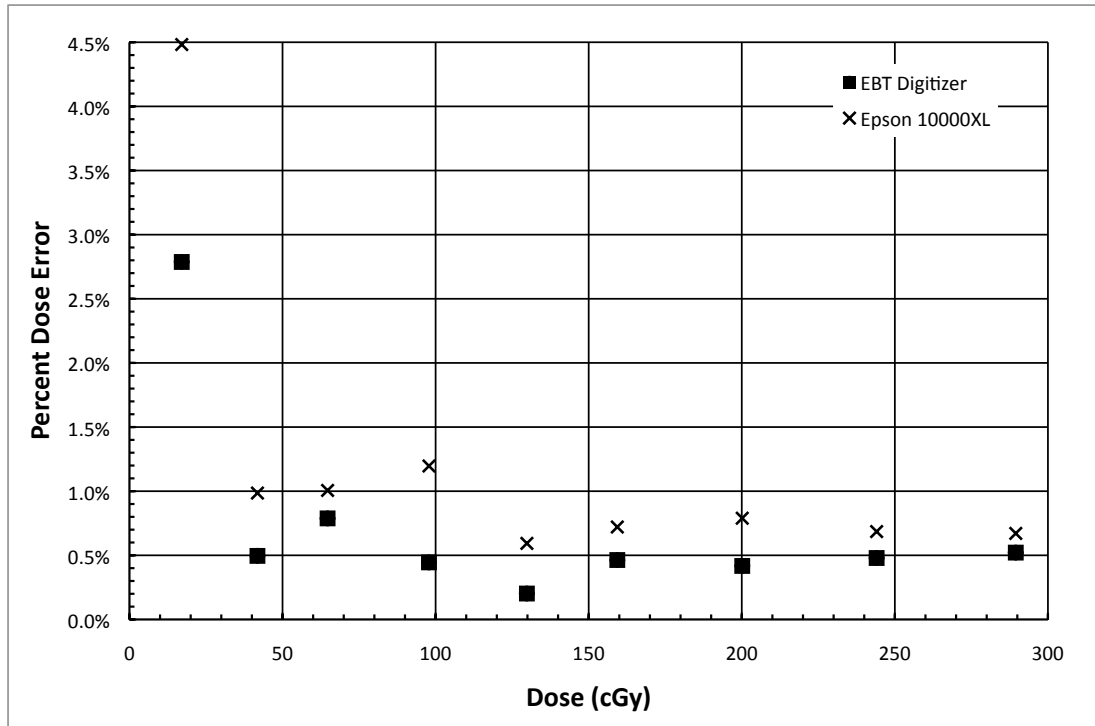


**Figure 60 – Dose error as a function of dose.  Displayed as a percentage of the dose value.**

Figure 60 and Figure 61 show the measurement error for doses between 17 and 290 cGy.  Error is displayed in both cGy and as a percentage of the measurement dose to demonstrate two aspects of the results.  For dose values below 50 cGy a significantly greater error results.  Doses above 150 cGy demonstrate increased error as well.  These are the dose values that yield optimal results for IMRT QAs.  While all film measurements will have dose values below 50 cGy, it is important to understand that those values are not as accurate. Comparing the two digitizers, all dose values yield at least 25% less error for the EBT system and are frequently under 0.5%, which is below the targeted 1.5%.  It

should be noted that at doses above 300 cGy the percent dose error will become

larger as response curves are approaching a slope of 0.
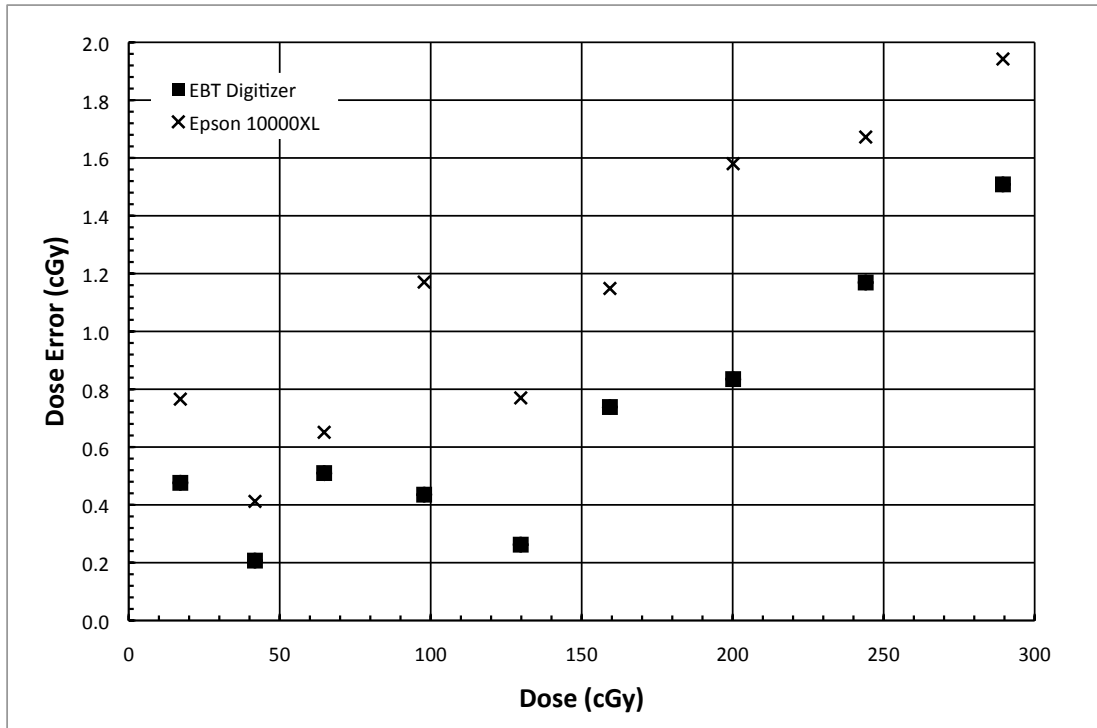


**Figure 61 – Dose error as a function of dose in cGy.**

## 6.4 Flatness profiles

As discussed in section 3.9 and shown in Figure 34 the light scattered by

the film has a significant affect on the profile taken from a scan, when a light

source illuminates a large area. By design the EBT digitizer illuminates a single

pixel at a time to eliminate the artifact. Figure 62 shows the results taken from

unexposed films. Each profile is normalized to the average value of the profile to

account for the differences in the pixel values for the digitizers. The Epson

10000XL shows a difference between the minimum and maximum value of

1.22% compared to 0.56% for the EBT digitizer. These results show a very significant gain in performance and are unfairly favoring the Epson scanner. The slope of the response curve for the EBT digitizer at 17 cGy is 3.7 times that of the Epson. This amplifies the fluctuations in the profiles used in comparison. To generate an equal comparison the corrected profile reduces the variations by 3.7.
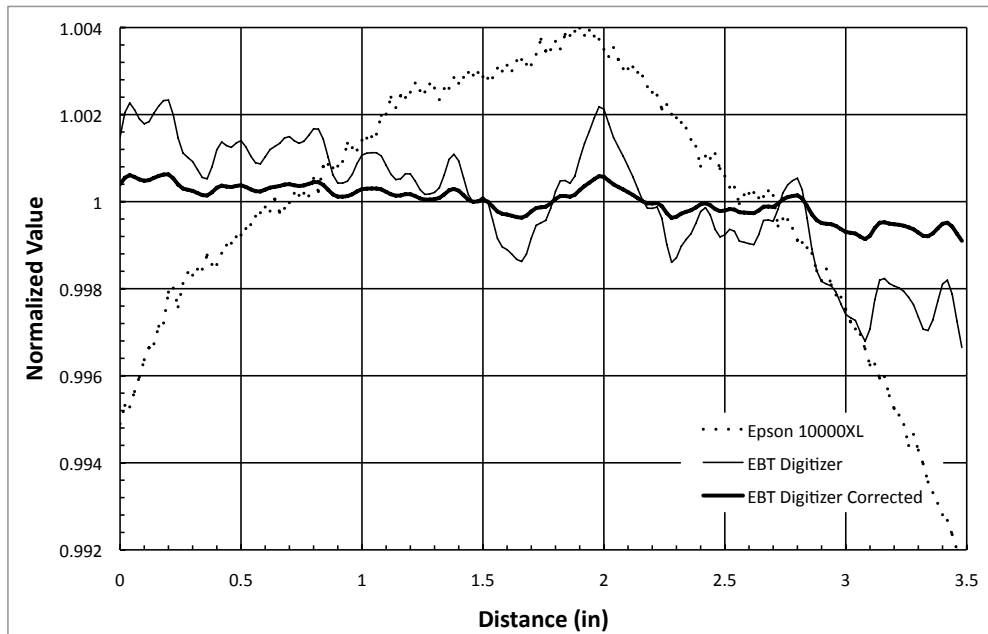


**Figure 62 – Profiles taken from unexposed films scanned on the EBT digitizer and the Epson 10000XL. A corrected profile scan accounts for the greater sensitivity of the EBT digitizer and yields an equal comparison.**

## 6.5 IMRT QA performance

### 6.5.1 IMRT QA analysis

Various techniques are used in film verification of IMRT. The first consideration is the delivery method used. Fields can be separated on individual films from a fixed gantry angle perpendicular to the plane than contains the film. While this technique yields the greatest accuracy and the ability to specify which

field is the cause of errors it is ultimately tedious and expensive. Combining the fields onto a single film eliminates the expense and has considerable time savings, although it could be difficult to determine the origin of errors in the measured doses.

After exposure the films are digitized and converted to dose. The measured doses must be compared against the expected doses calculated by the treatment planning system. There are three major algorithms used to analyze measured to calculated dose agreement. Determining the difference between the computed and measured dose at every position is the dose difference technique.[57] In regions where the dose gradients are small, the dose difference technique has the capability of yielding accurate results. The problem arises when the gradients are large and a slight shift in the positional accuracy can yield large dose differences. This leads to the rise of a distance to agreement method[58] where the closest distance in which two doses are equal is determined. Although beneficial in high dose gradients, distance agreement fails to yield good results when gradients are low. In search of a suitable method to analyze dose patterns, a calculation that combines the dose difference and distance to agreement was formed and is called the gamma function.[59]

Analysis is completed on a computer, so software algorithms must be implemented to perform the calculations. There are many commercially available software packages that are able to perform the functions. For example, FilmQA is a software package owned by International Specialty Products that is capable

of analyzing films. It takes scanned images of the IMRT and calibration films, converts them to dose and performs comparisons using the mentioned algorithms.

FilmQA also implements techniques that reduce the artifacts introduced by scanners through the use of unexposed background films. One method increases the flatness across a film through measuring the profiles in a fashion analogous to what is shown in Figure 62. Although this is desirable when performing IMRT QA it hides artifacts introduced by the scanners. The reduction of artifacts is not desirable while performing comparisons of two scanners. To bypass the artifact removing features of FilmQA, exposure doses on films are calculated in a program called ImageJ, distributed by the National Institutes of Health. Calibration films shown in Figure 58 were used to generate a pixel value to dose conversion function. The scripting language in ImageJ applied the calibration function to the scanned images and the resulting two dimensional doses were saved in tiff files. FilmQA imported the tiff files and perform the to be shown profile and gamma analysis, without implementing corrections.

To compare the two digitizers performance, two IMRT plans were created using Brainlab (Feldkirchen, Germany) Brainscan 5.2 treatment planning system for use on a Varian (Palo Alto, CA) 6EX linear accelerator with a Brainlab m3 multileaf collimator. This combination allowed for the exposure of small fields, necessary for the 3.5" film limitation of the EBT digitizer, while still achieving significant beam modulation using the smaller leaves of the m3. While not actual

clinical cases, the IMRT plans generated simulated prostate and head and neck patients plans by scaling the fields smaller.

## 6.5.2  IMRT plan analysis

### 6.5.2.1  Profiles

. One technique is the examination of profiles across the dose plane. Typically, profiles are taken from calculated and measured doses and compared. Any significant difference found would be questioned as a delivery or calculation error.  In evaluating the performance of the EBT digitizer profiles from it and the Epson 10000XL are compared against calculated doses and each other.  Before profiles are extracted spatial adjustments are performed to prevent alignment errors from being contributed to digitizer performance.  In all profiles generated the green line represents the calculated dose, the red line is the measured dose by the EBT digitizer and the black line is measured by the Epson scanner.  The blue line at the bottom of each profile comparison graph is the difference between each profile.  While three horizontal profiles and three vertical profiles for each film analyzed was completed the amount of graphs and redundant information make it unnecessary to show all data.  Both vertical and horizontal profiles across the central axis are displayed in Figures Figure 63 - Figure 68.

Several observations can be drawn from examining the profiles.  The most obvious is probably the greater noise levels in the Epson scanner.  Looking at any profile where there is a region of lower dose gradient, the noise becomes evident through the quick fluctuations.  The vertical profiles are perpendicular to

the 3 mm leaves of the MLC.  This makes it impossible for peak to peak dose fluctuations to have distances less than 6 mm.   Therefore, any fluctuation separated by less than 6 mm are most likely due to digitizer errors or film in homogeneities.   It should be noted that it is possible for profiles parallel to the MLC leaves to have fluctuations at a greater frequency.

Further analysis shows that the Epson scanner tends to have a greater difference between the peaks and valleys with sharper dose gradients than both the EBT digitizer and Brainlab calculated doses.  This is most evident on the vertical profiles of Figure 65.   Most likely greater variations are more representative of the actual dose distribution as Brainlab uses a pencil beam calculation model, which is known to overestimate dose contribution due to scatter,[60] which results in increased doses in the valleys.   The 0.6 mm measurement spot size of the EBT digitizer could be prohibiting it from yielding the same results as the Epson scanner.
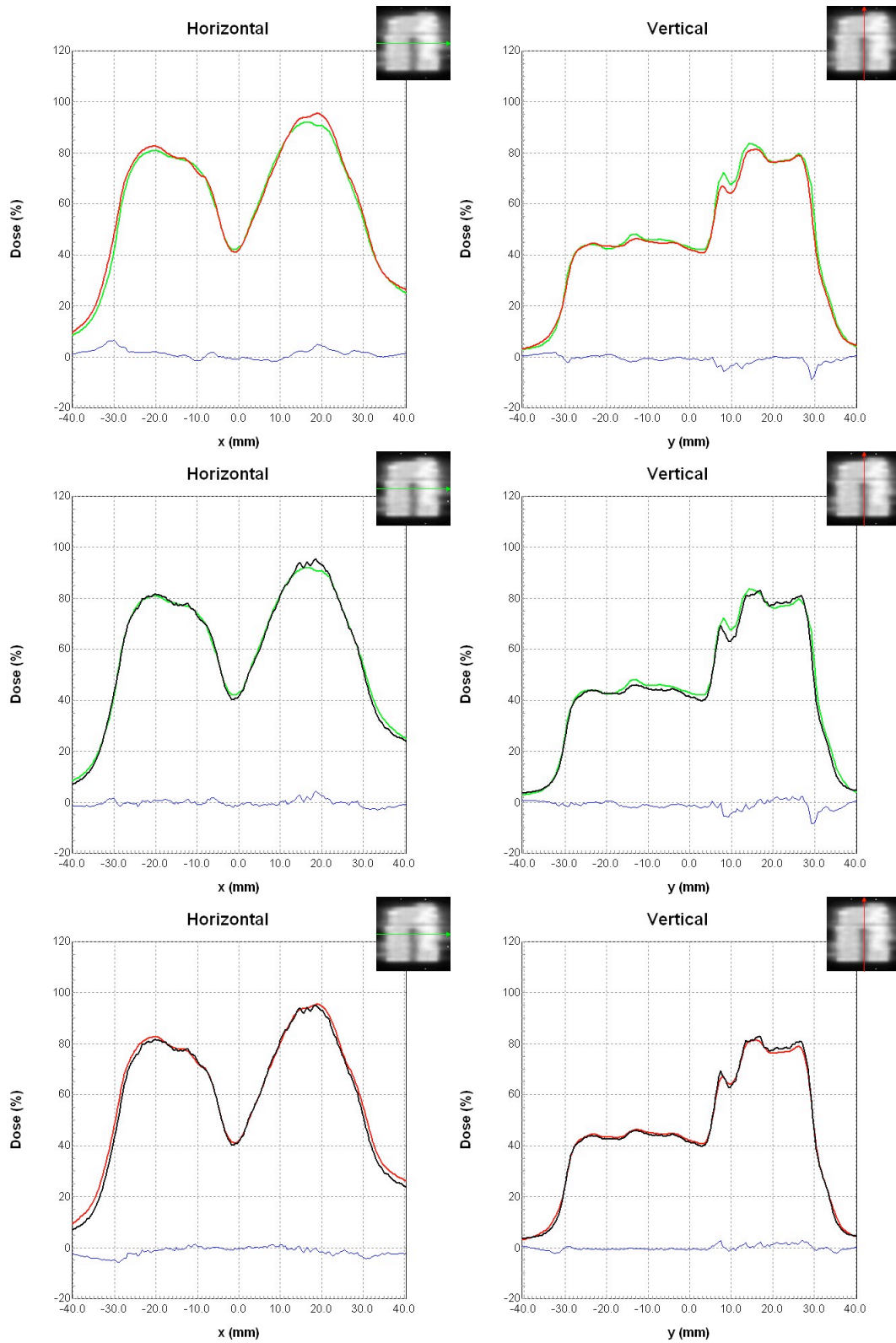
**Figure 63 – Profiles for the combine head and neck field. Green represents the Brainlab calculations, red is the EBT digitizer measurements and black is the Epson measurements. The profile location is shown as the line on the dose map in the corner of each profile.**

112
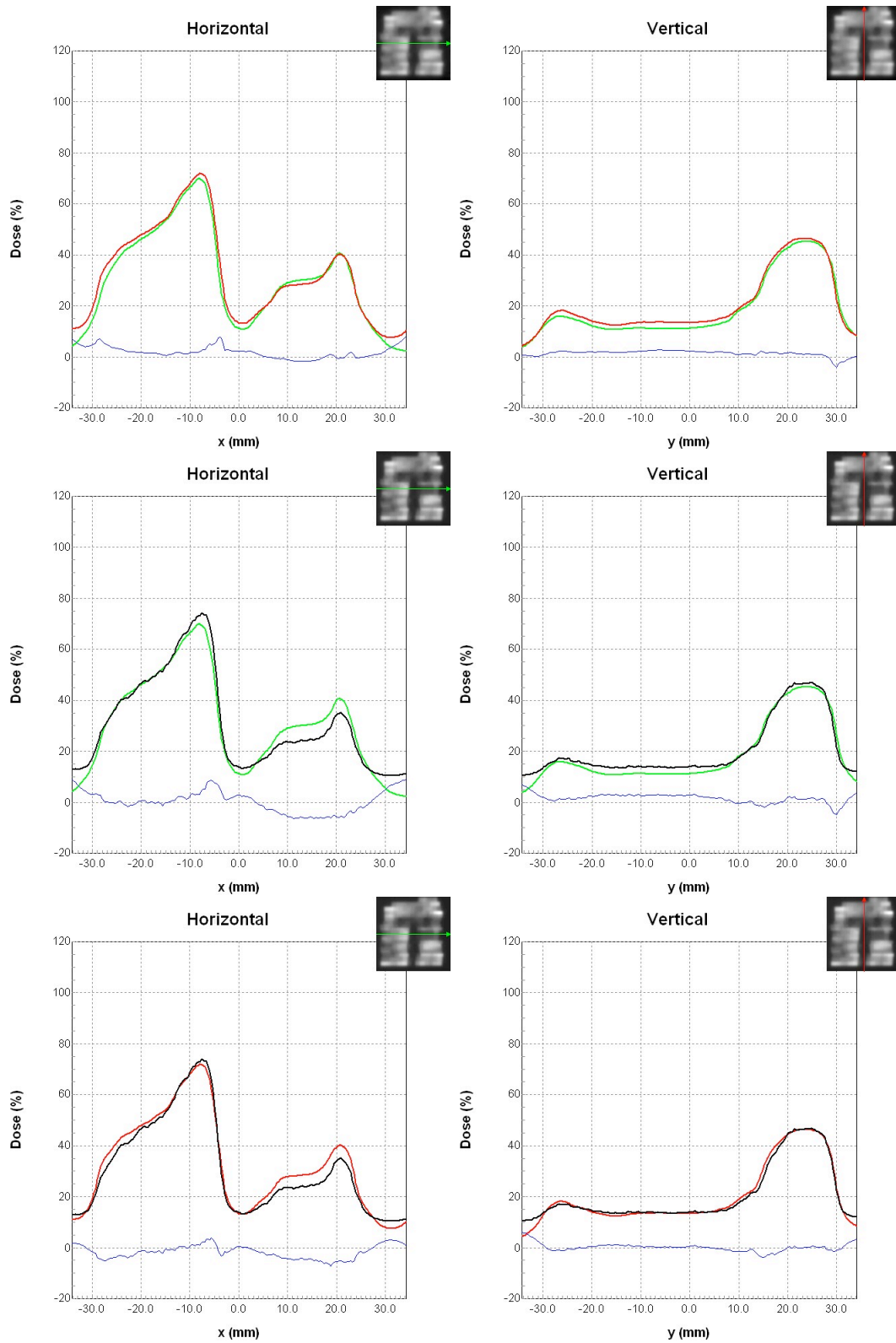
**Figure 64 – Profiles on field 1 of the head and neck study. Green represents the Brainlab calculations, red is the EBT digitizer measurements and black is the Epson measurements. The profile location is shown as the line on the dose map in the corner of each profile.**

113
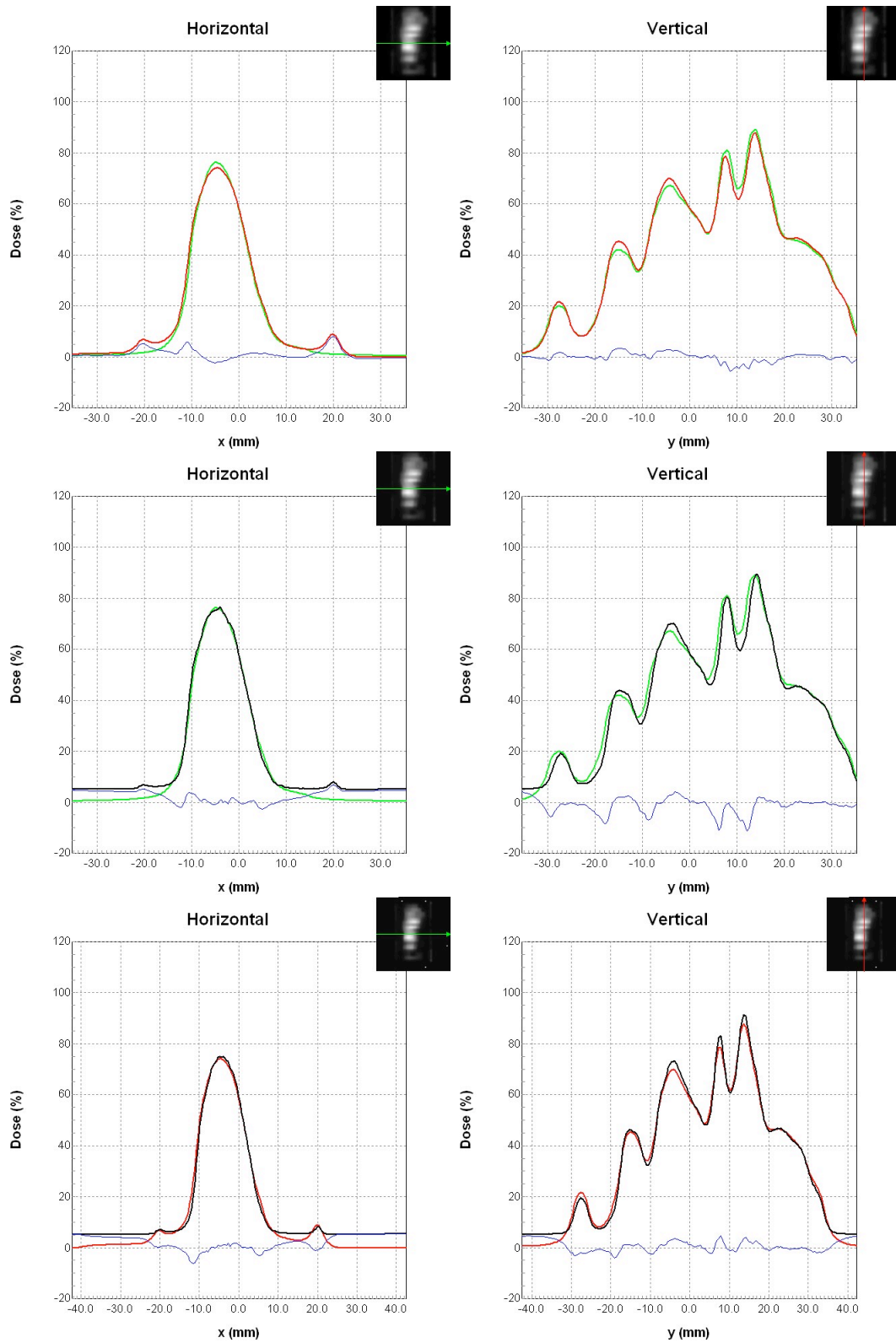
**Figure 65 – Profiles on field 2 of the head and neck study. Green represents the Brainlab calculations, red is the EBT digitizer measurements and black is the Epson measurements. The profile location is shown as the line on the dose map in the corner of each profile.**
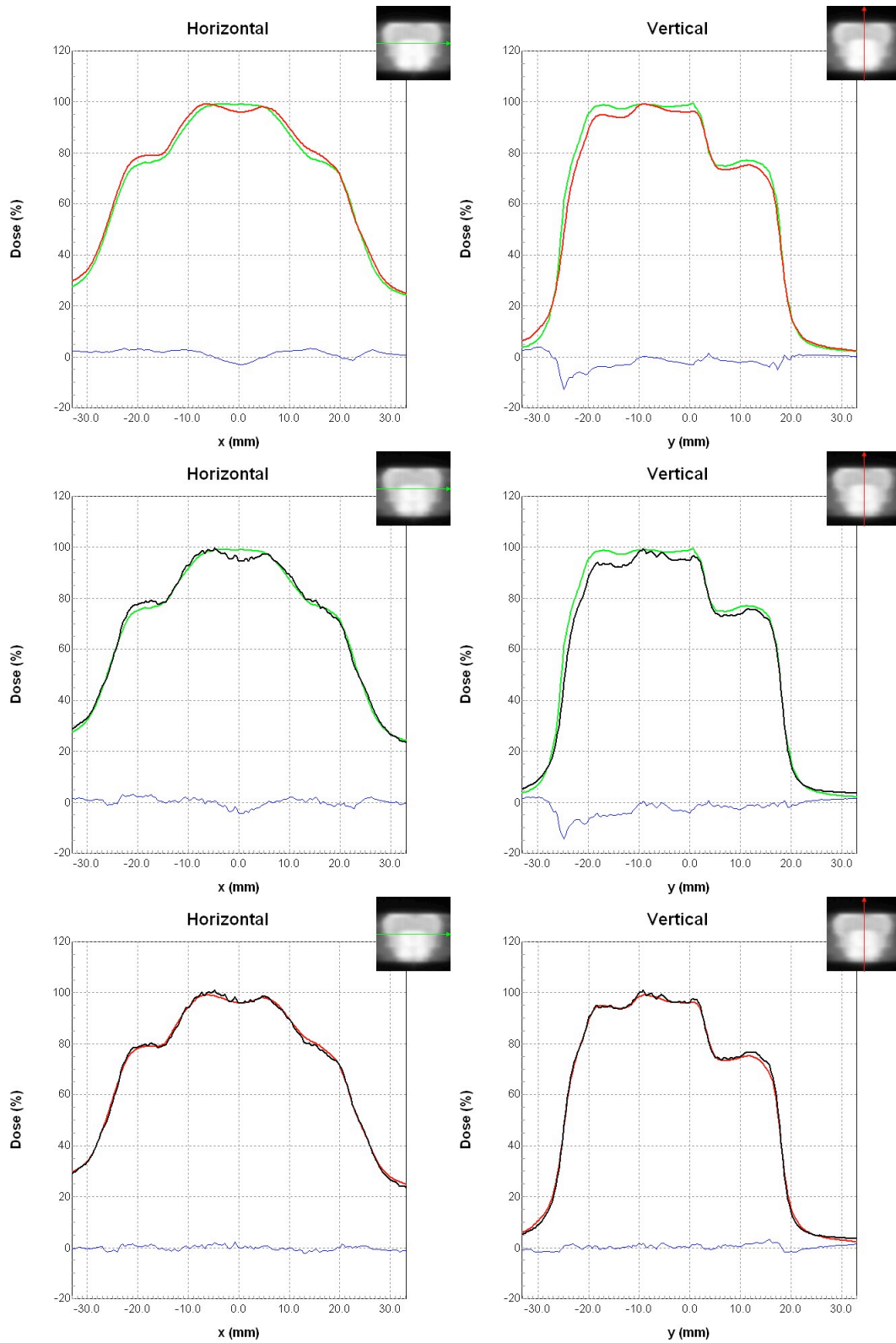
114

**Figure 66 – Profiles for the combine prostate field. Green represents the Brainlab calculations, red is the EBT digitizer measurements and black is the Epson measurements. The profile location is shown as the line on the dose map in the corner of each profile.**

115

**Figure 67 – Profiles on field 1 of the prostate study. Green represents the Brainlab calculations, red is the EBT digitizer measurements and black is the Epson measurements. The profile location is shown as the line on the dose map in the corner of each profile.**

116

**Figure 68 – Profiles on field 2 of the prostate study. Green represents the Brainlab calculations, red is the EBT digitizer measurements and black is the Epson measurements. The profile location is shown as the line on the dose map in the corner of each profile.**
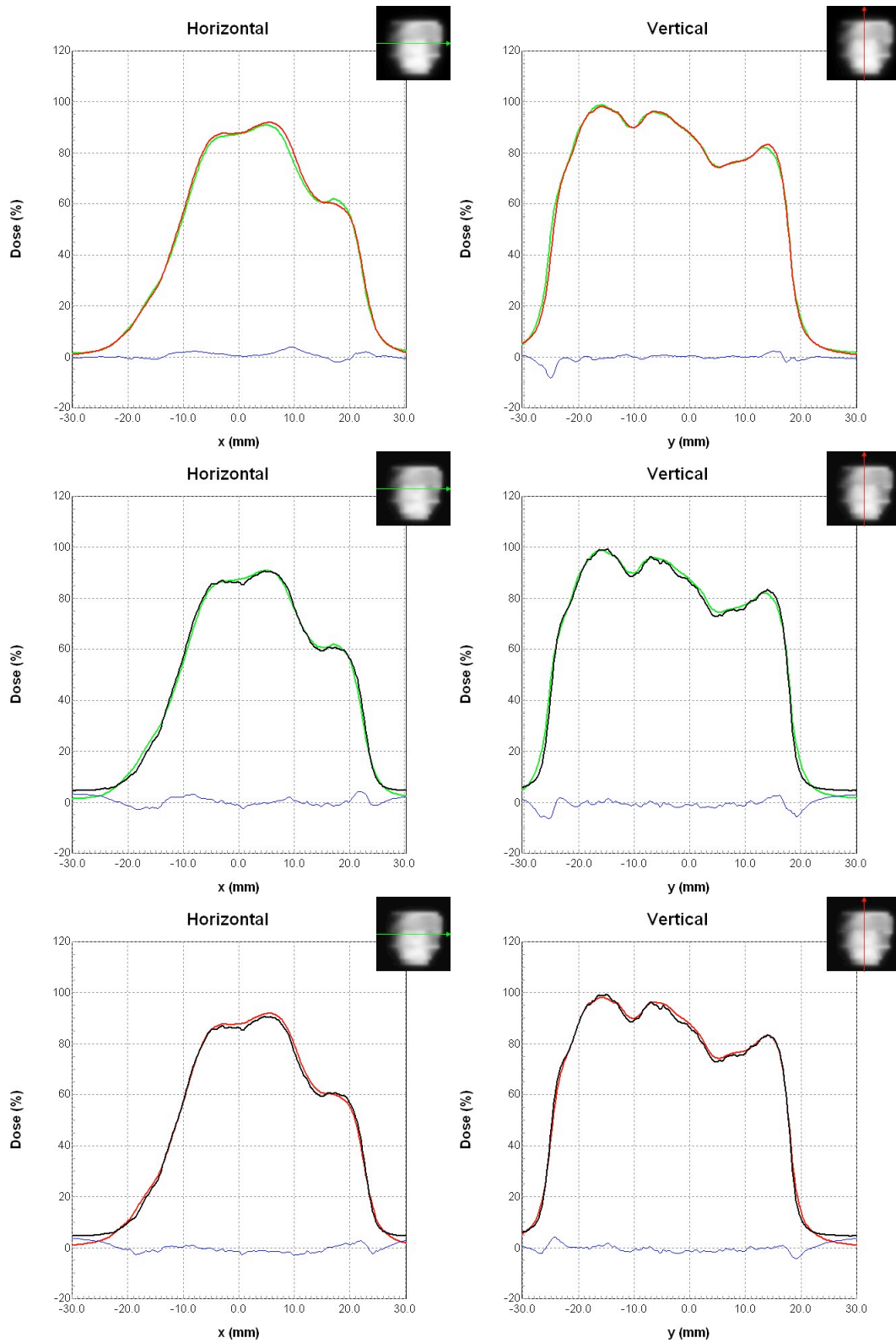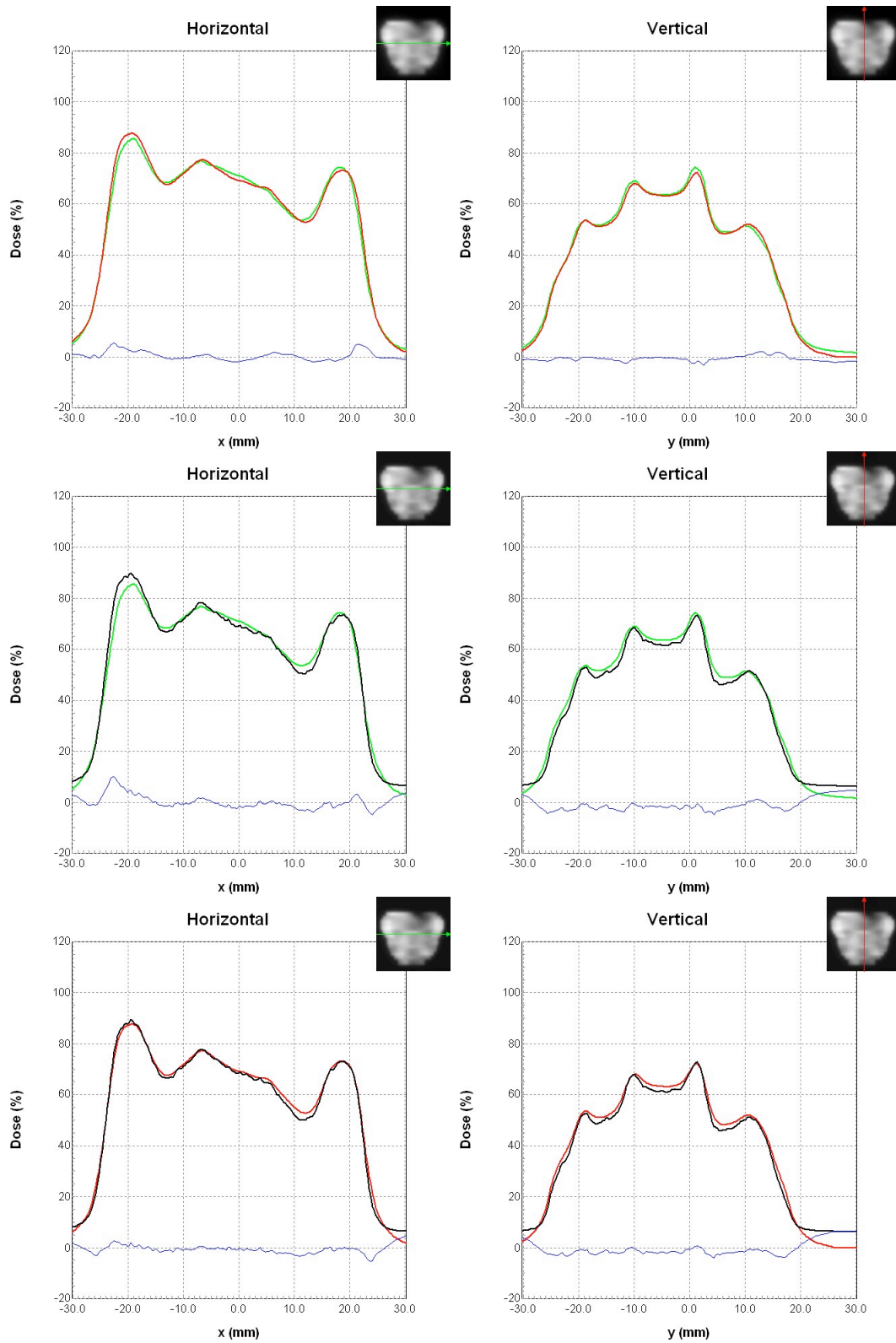
117

6.5.2.2   Gamma function

All gamma function analysis was implemented at 2% dose difference and 1 mm distance to agreement.  Typical clinical values use 3-5% and 2 – 3 mm.[61] Tighter tolerances allows the differences between the EBT digitizer and the Epson 10000XL to be shown clearly.

Gamma maps of the films exposed to the complete plan are shown in Figure 69.  While the percentage of pixels passing are very similar, the Epson achieves slightly better results, with the EBT digitizer getting 94% and 95.5% for the Epson.  Even thought the results appear slightly better for the EBT digitizer it is difficult to determine which performs superiorly, because the calculated doses are not a gold standard as they include errors.  Notice that the Epson comparison seems grainier.  This is due to the higher noise level in the Epson scans. Interestingly, greater noise levels artificially improve the performance of the gamma function.[62]   This is mostly accomplished through the distance to agreement component to the gamma function.  Increased noise levels generate artificial dose fluctuations, making it so that a position within the 1 mm tolerance will have the same dose value.  It is therefore necessary to use some degree of human judgment to determine the digitizer that performs superiorly.

Results for two single fields measurements are shown in Figure 70 and Figure 71.  In both cases the EBT digitizer generates better results.  It should be noted that all low doses on the Epson in the single field cases are found to have gamma values above tolerance.  This could be attributed to a pixel value to dose

conversion curve that is inaccurate for low doses.  This is unlikely because, the combined field analysis does not demonstrate the same effect.  In most cases the low dose regions are ignored for the Epson scanner and can be depicted by the red box in the gamma map showing region of interest used.  Comparing the results of the single fields, the EBT digitizer yields better results.  The dose patterns are shown in the top right corner of each gamma analysis.  Examining where the gamma function fails with respect to the dose distribution, the Epson has higher dose errors in regions with significant dose values.

The EBT digitizer in Figure 71 shows two regions in the low dose area that fail on both sides of the dose pattern.  The Epson would exhibit the same errors, but the entire area outside of the field fails which hides the regions on either side. These are caused by leakage through the MLC where the leaves from bank A abut against those from bank B.  This could have been avoided by closing the jaws, but does not interfere with the results.
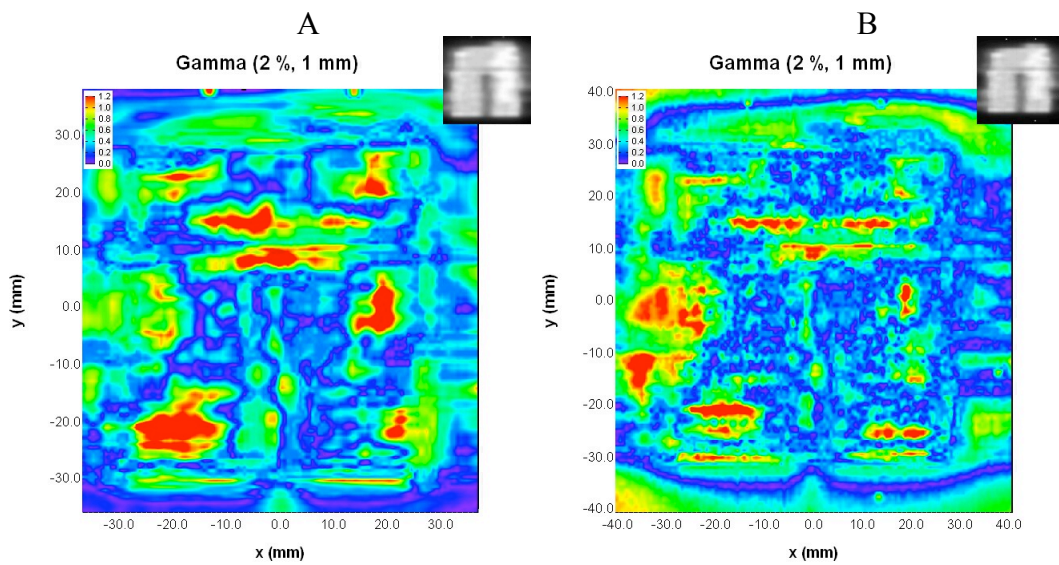


**Figure 69 – Head and neck combined field gamma analysis.  A) is the EBT digitizer with a 94% passing and B) is the Epson 10000XL with 95.5% passing using 2% and 1 mm criteria.**

119
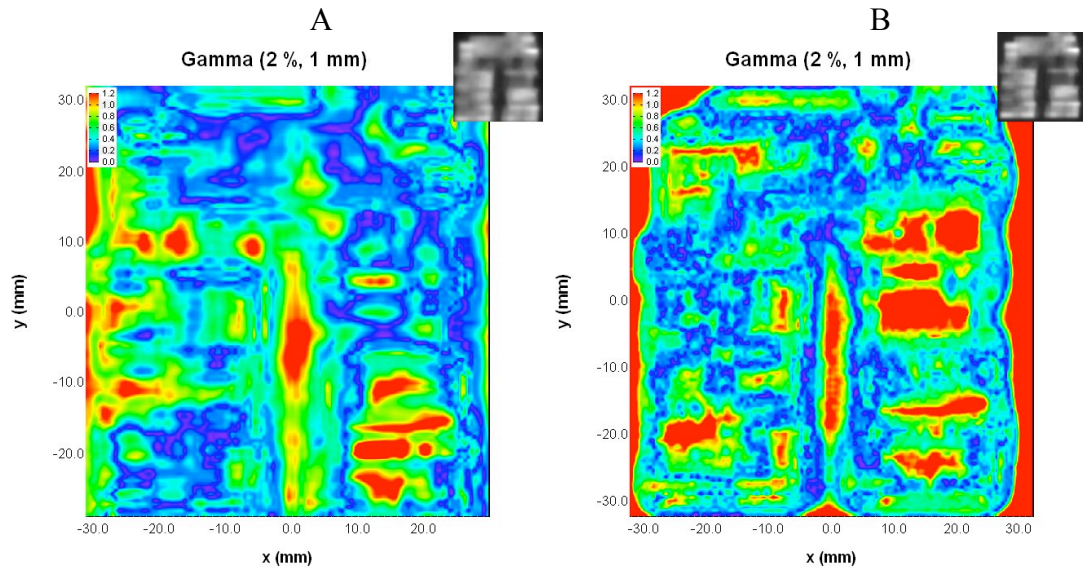
**Figure 70 – Head and neck field 1 gamma analysis. A) is the EBT digitizer with a 92.2% passing and B) is the Epson 10000XL with 80.8% passing using 2% and 1 mm .**
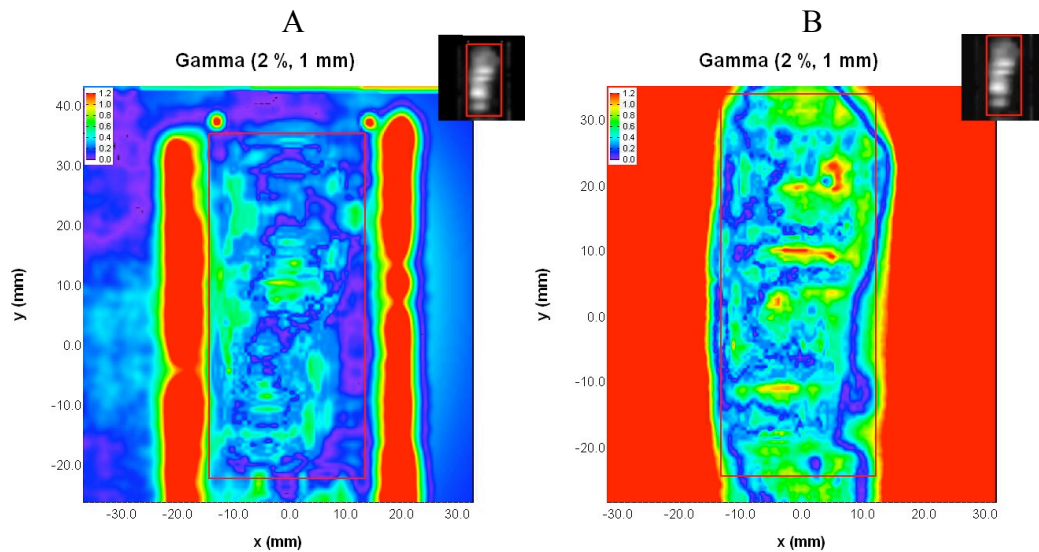


**Figure 71 – Head and neck field 2 gamma analysis. A) is the EBT digitizer with a 100% passing and B) is the Epson 10000XL with 98.1% passing using 2% and 1 mm .**

Similar conclusions can be drawn for the prostate simulation as were found for the head and neck example. Noise for the Epson is still larger, low doses on the single fields do not match the calculated values and the single field analysis shows better results for the EBT digitizer.

**Figure 72 – Prostate combined field gamma analysis. A) is the EBT digitizer with a 96.6% passing and B) is the Epson 10000XL with 96.8% passing using 2% and 1 mm criteria.**



**Figure 73 – Prostate field 1 gamma analysis. A) is the EBT digitizer with a 99.7% passing and B) is the Epson 10000XL with 99.5% passing using 2% and 1 mm criteria.**
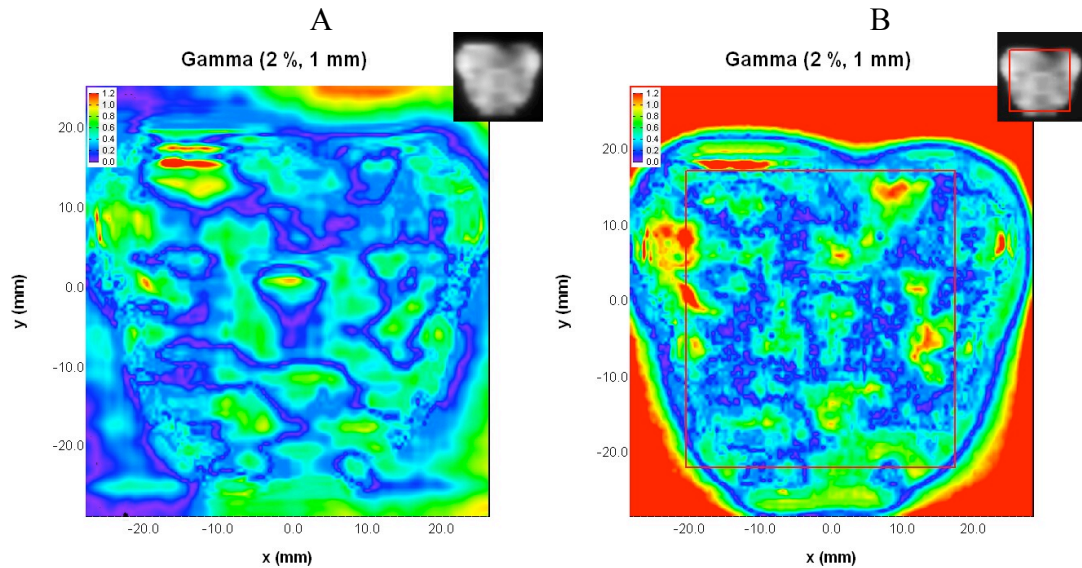
**Figure 74 – Prostate field 2 gamma analysis. A) is the EBT digitizer with a 98.8% passing and B) is the Epson 10000XL with 98.2% passing using 2% and 1 mm criteria.**
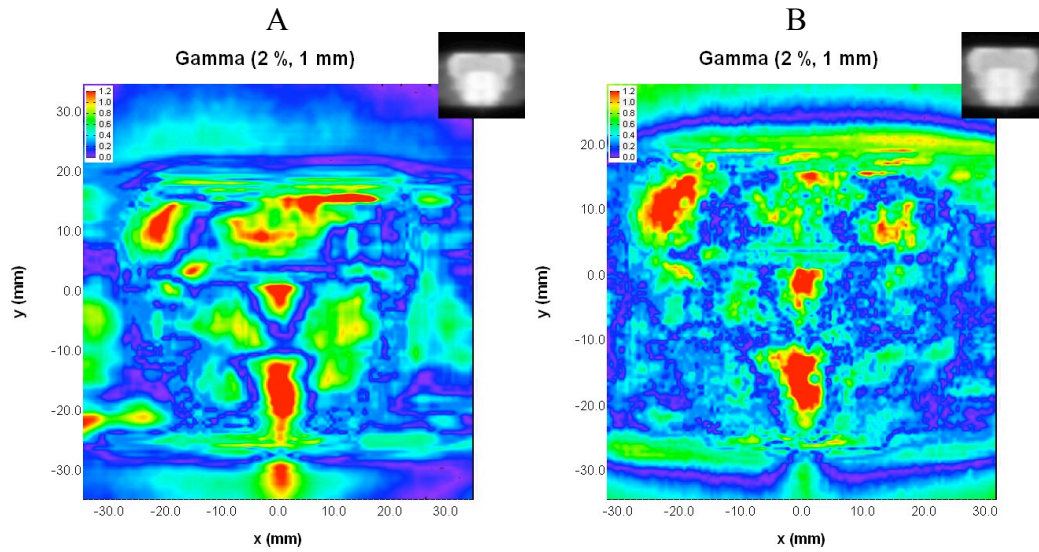
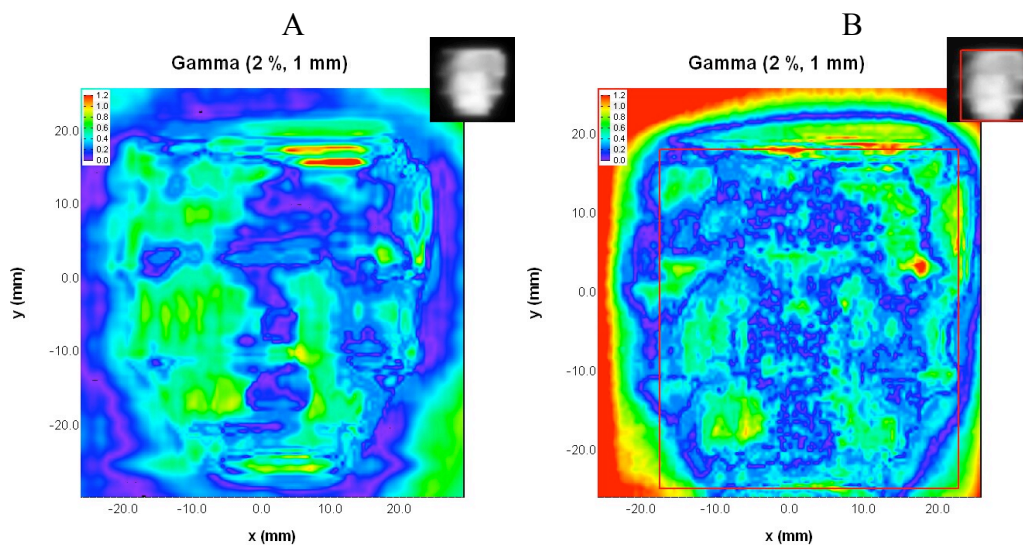## 6.6 Film orientation sensitivity

Section 5.1 suggested a rotating platform design for a fast scanning technique. If a beam were to have perfectly circular polarized light, rotating the film in the process of scanning should have no affect on the final output. It was found that 3.2% of the light remained linearly polarized on the EBT digitizer. To determine the feasibility of having a rotating platform design, a film was exposed to 100 cGy, scanned with rotations of 0°, 30°, 60° and 90° and converted to dose using the ImageJ software. Pin pricks in the film allowed for consistent reorientation regardless of the scan angle.
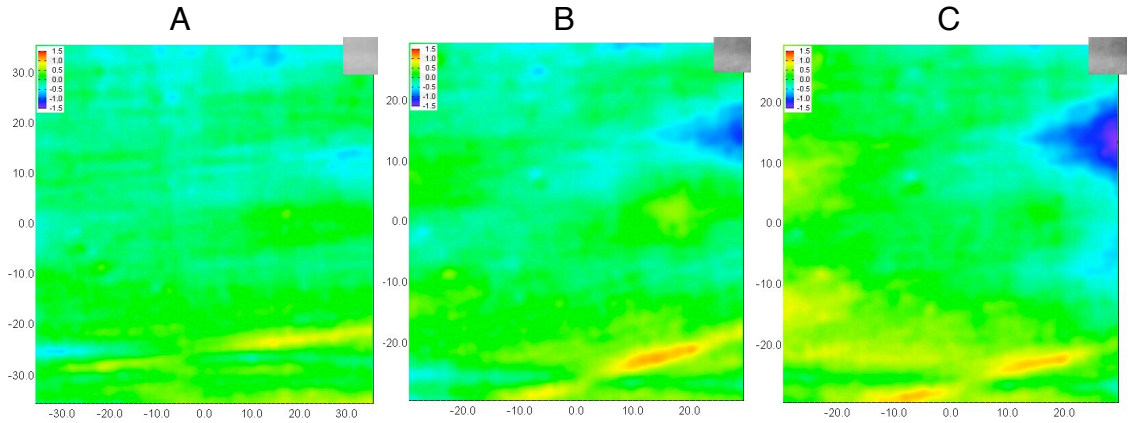
**Figure 75 – EBT digitizer rotated scan comparison. The 0° is compared against A) 30°, B) 60° and C) 90° using a dose difference function. A 1% tolerance yields passing percentages of 100, 99.4 and 98.5 respectively.**
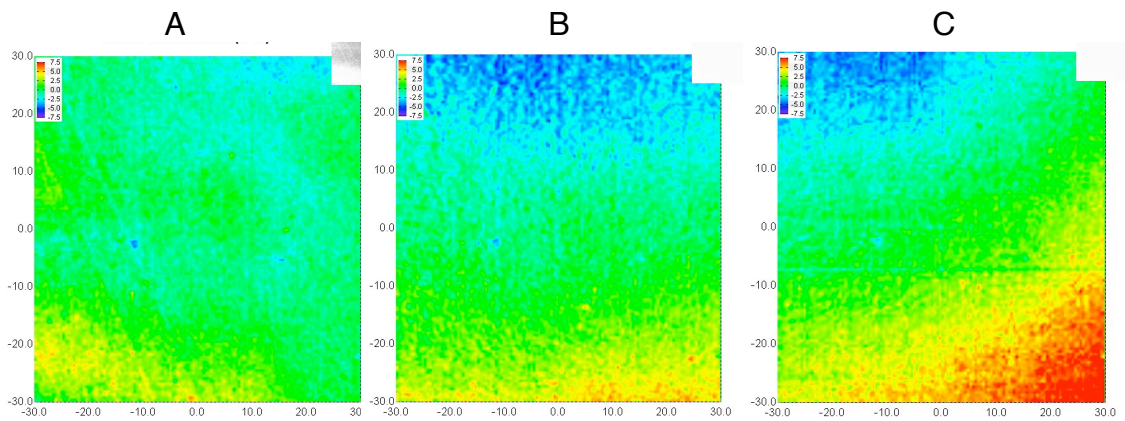


**Figure 76 – Epson 10000XL rotated scan comparison. The 0° is compared against A) 30°, B) 60° and C) 90° using a dose difference function. A 5% tolerance yields passing percentages of 100, 98.9 and 87.8 respectively.**

Comparing the different scan angles using a dose difference technique allowed for an examination of how the measured dose varies with scan angle. The 0° angle is compared against the other three to allow for a progression in the dose difference with each scan angle. Figure 75 shows the results using a 1% dose difference. In the worst-case scenario of the 90° scan orientation 1.5% of the pixels are outside the 1% tolerance. Examining a 0.5% tolerance on the 30° scan yields 20% of the pixels failing and continuing to 90° results in more than 50%. The goal of the digitizer was to have one standard deviation of the pixels to

123

be within 0.5%. That means that the current degree of circular polarization is not circular enough. To accomplish a greater degree of circular polarization it is necessary to select a narrower band of wavelengths as discussed in section 5.2.2.

The same analysis was repeated on the Epson 10000XL. Instead a 5% tolerance is used and the results are shown in Figure 76. A higher tolerance is used, as the results are far worse than the EBT digitizer. The 90° scan orientation shows that 12.2% fail the 5% criteria. The cause of the poor performance is due to two affects. The first cause is light scatter, which Figure 32 shows how it alters the calibration curve. The same calibration curve is used for all scan orientations, so errors were introduced as the calibration curve was not adjusted according to the angle. Additionally, profiles in the direction of the CCD show a decrease in pixel value as demonstrated in Figure 62. The rotation of the film causes a rotation in the direction in which a reduction in the pixel value occurs. Therefore, dose differences are found to be more towards the edges of the film for the Epson scanner.

## 6.7 Discussion

Throughout the entire research project an overlying goal was the generation of IMRT QA system based on Gafchromic EBT film. Many QA techniques in use were either based on outdated technology or provide less than

124

desirable data to accurately perform analysis of the dose distributions. Examples of this are radiographic film, which requires a film processor that is not available in many clinical settings, and two dimensional arrays that have discrete measurement points at distances of no less than 5 mm.[8,9] The use of Gafchromic EBT film allows every clinic to perform IMRT QAs at minimal expense and yields high accuracy.

Research showed that a major source of dose measurement error was introduced as part of the digitizing process. It was hypothesized that better results could be obtained using a digitizer that was specifically designed for EBT film. The primary sources for error in commercially available digitizers are the observed sensitivity, noise levels, polarizing artifacts and light scatter affects. While not every analyzed digitizer demonstrated effects from all of the mentioned error sources, they all exhibited at least one.

To achieve better results a custom designed digitizer based on a circular polarized 635 nm light source that illuminated a single measurement point was implemented. The EBT digitizer did show improvements over other digitizers, but there are still performance gains possible. Continuing work on the digitizer would primarily be focused on the light source. Better results are obtainable if the light source is circularly polarized to a greater extent. In the current form 3% of the light intensity is not circularly polarized. Elimination of the linearly polarized light should be possible through utilizing a narrower bandwidth of wavelengths. Possible methods for removing undesirable wavelengths are through the use of a

material where the index of refraction is dependent on the wavelength. Refracting the light through the material will separate the wavelengths spatially and could therefore be removed. Another possibility is through the use of a single wavelength fiber optic. This technique would only internally reflect the desired wavelengths and eliminate the undesirable light. Additionally, the fiber optic would break up the coherence of the light and help to reduce the possibility of moiré patterns.

Another area to continue research is the reduction of scan times. The current technique of moving the film in both the vertical and horizontal directions yields scan times much too long for practical use. One possible technique to use is through a scanning motion with continual movement, such as a drum scanner or rotating platform design. Another possibility is through intelligent scanning. Regionally changing the resolution of a scan based on the gradient of the optical density on the film would greatly reduce the number of measurement points. The reduction in scan time should be proportional to the reduction in the number of measurement points. Another possibility is the following of isodose lines on a film. This eliminates the need to scan an entire film, but may not yield enough data for effective analysis.

# 7   Conclusions

Implementation of IMRT requires a quality assurance program that verifies the accuracy of the doses being delivered.  One of the possible techniques utilizes International Specialty Products' Gafchromic EBT film.  It allows for an IMRT QA program that can be established for minimal initial investment.  EBT film is a radiochromic film, which are known for inter and intrasheet variations that prohibit dose measurement accurate enough for IMRT QA.  Manufacturer claims state that EBT film is an acceptable film for accurate dosimetry of IMRT dose patterns.

Many studies were performed to assess the quality and properties of EBT film.  Uniformity tests showed that inter and intrasheet variations had typical errors of less than 1%.  Radiation sensitive films have a tendency to have a varied response based on the exposure energy.  High energy radiation fields have a spectrum of energies that vary based on exposure setups, such as field size and depth.  Research performed and found in the literature shows that there was not detectable energy dependence.  Therefore, no special procedures must be performed to account for various exposure techniques.

Radiographic films have uniform light absorption across the visible wavelengths.  Many radiochromic films have major and minor absorption peaks at 674 and 614 nm.  EBT film maintains a similar absorption curve to EBT film, but the peaks are 635 and 583 nm.  To achieve the greatest sensitivity a measurement light source at 635 nm should be utilized.  Film temperature during

measurement can have a significant affect on the measured dose. A shift in temperature from 18 to 26 °C causes the major peak to decrease in absorption by 0.05 OD when exposed with 8 Gy. Similar results were found at lower dose levels. Another property observed with absorption spectrum measurements is the sensitivity to linear polarized light. A film exposed to 3 Gy displays a 0.8 OD variation in absorption at 635 nm when the orientation of the linear polarized light is rotated 90°.

Experiments analyzing the effectiveness of commercially available digitizers established the strengths and weaknesses to various digitizing techniques. Due to EBT film's absorption spectrum, a measurement light source predominately in the 635 nm region will yield the greatest sensitivity. The use of a light source that illuminates the measurement film in an area larger than a single pixel can result in scattering artifacts. This causes effects such as a decrease in pixel value towards the edges of the scanner region, and possibly a general increase or decrease in measured values depending on the rotation of the EBT film.

Design of a digitizer specifically for use with Gafchromic EBT film began in the electronics stage with the amplifier. A dual stage linear amplifier resulted in noise levels that yielded dose precision at or below 0.5% for doses up to 6.5 Gy. Other amplifier designs considered are the composite and log. Better results may be achievable using one of these designs, particularly at the high dose levels for the log amplifier. Further research was not performed, as the results

obtained from the dual stage amplifier were acceptable. Continued research would look into obtaining increased performance from a different amplifier configuration.

The optics system is a major component in the accurate measurement of EBT film. Increased sensitivity seen through using the narrow bandwidth of a laser is offset with the affects of coherent linearly polarized light. The use of optics to generated circularly polarized light from a laser diode, help to eliminated the artifacts generated through the use of a laser. Measurement showed that 97% of the light power was circularly polarized. This yields estimated dose errors up to 1% for 50 cGy. Better performance should be achievable through a beam that has a greater degree of circular polarization. In the case of the EBT digitizer this was hindered by wavelengths other than 635 nm. These wavelengths can be removed through a number of techniques, one of which is a single mode fiber optic. This is a possible goal for future studies.

Final design of the EBT digitizer utilized two linear stages that translated the film in the XY plane. All test results compared the EBT digitizer to the Epson 10000XL. One of the greatest deterrents in obtaining accurate dose measurements is amount of noise present in a system. The EBT digitizer had more than 25% decrease in noise in all tested dose values, which spanned from 0 to 300 cGy. At doses above 50 cGy the maximum observed measurement error was no more 0.5%. A large contributor to the decreased noise levels is due to the increase of the observed sensitivity when using a 635 nm light source.

Performing scans of EBT film rotated at 0, 30, 60 and 90° with respect to the digitizer display the effectiveness of the circular polarization. When comparing the 0 and 90° scans, 1.5% of the pixels show a dose difference of more than 1%. Considering that 0.5% is due to noise within the digitizer the circularly polarized light can effectively remove artifacts due to polarization.

Analysis of the EBT digitizer performance during IMRT quality assurance is completed on two IMRT cases. Comparisons are completed using both profiles and the gamma function. The most notable difference in both the profiles and the gamma functions are the apparent noise levels, which are most easily seen in the low dose gradient regions. This is extremely important, as the ultimate desire in IMRT QA is to determine the accuracy of the dose distributions. Another observation is that the Epson digitizer yielded greater differences in the peaks and valleys on the profiles. It is probable that the Epson displayed more accurate results and could point to the need for a smaller spot size for the EBT digitizer.

There were two major goals throughout the entire research project. The first was to study the newly introduced Gafchromic EBT film, and determine if it was a suitable dosimeter for use in IMRT quality assurance. Consistency in dose measurement is the most important aspect in any system where comparative measurements must be performed. Findings showed EBT film is accurate enough for IMRT quality assurance.

A second desire was to improve on the ability to digitize the doses measured by EBT film. It is important to remember that commercially available digitizers could already accomplish film measurements with accuracy great enough for IMRT quality assurance. Therefore, any improvements would not be so significant that results yielded new findings or dramatically differences. If it did, the digitizers currently in use would not be acceptable. Having the perspective of the available digitizers being adequate the increases seen in the performance of the EBT digitizer are significant.

Ultimately, using Gafchromic EBT film with the EBT digitizer will yield more accurate results than other digitizers. In the clinical setting this allows for a greater percentage of passing IMRT QAs that should yield positive results. This scenario is when the doses output by the treatment planning system do match the delivered distributions. Therefore, a failing QA will have a greater probably of being caused by a setup or calculation error. The end result is that IMRT QAs will have a greater specificity and fewer unnecessary repeats will be performed.

# Bibliography

[1] IMRT Collaborative Working Group, "Intensity modulated radiotherapy: Current status and issues of interest," International Journal of Radiation Oncology Biology and Physics 51, 880-914 (2001).

[2] IMRT Subcommittee of the AAPM Radiation Therapy Committee, "Guidance document on delivery, treatment planning and clinical implementation of IMRT," Medical Physics 30, 2089-2115 (2003).

[3] D Law, "Quality Assurance of Intensity-Modulated Radiotherapy," Seminars in Radiation Oncology 12, 219-228 (2002).

[4] D Litzenberg, J Moran and B Fraass, "Verification of dynamic and segmental IMRT delivery by dynamic log file analysis," Journal of Applied Clinical Medical Physic 3, 63-72 (2002).

[5] J Li, j Dempsey, L Ding, C Liu, J Palta, " Validation of dynamic MLC-controller log files using a two-dimensional diode array," Medical Physics 30, 799-805 (2003).

[6] W Lou, J Li, J Yang, S McNeely, C Ma, "Dosimetry Validation of IMRT Treatment Plans Using MLC Log Files," International Journal of Radiation Oncology Biology Physics 60, S590-S591 (2004).

[7] W Lou, J Li, R A Price, L Chen, J Yang, J Fan, Z Chen, S McNeeley, X Xu, C Ma, "Monte Carlo based IMRT dose verification using MLC log files and R/V outputs," Medical Physics 33, 2557-2564 (2006).

[8] B Poppe, A Blechschmidt, A Djouguela, R Kolhoff, A Rubach, K C Willborn and D Harder, "Two-dimensional inonization chamber arrays for IMRT plan verification," Medical Physics 33, 1005-1015 (2006).

[9] B Poppe, A Djouguela, A Blechschmidt, K Willborn, A Ruhmann, D Harder, "Spatial resolution of 2D ionization chamber arrays for IMRT dose verification: single-detector size sampling step width," Physics in Medicine and Biology 52, 2921-2935 (2007).

[10] E Spezi, A L Angelini, F Romani, A Ferri, " Characterization of a 2D ion chamber array for the verification of radiotherapy treatments," Physics in Medicine and Biology 50, 3361-3373 (2005).

[11] M Wendling, R J W Louwe, L N McDermott, J-J Sonke, M van Herk, B J Minjheer, "Accurate two-dimensional IMRT verification using a back-projection EPID dosimetry method," Medical Physics 33, 259-273 (2006).

[12] W Ansbacher, "three-dimensional portal image-based dose reconstruction in a virtual phantom for rapid evaluation of IMRT plans," Medical Physics 33, 3369-3382 (2006).

[13] B. Warkentin, S. Steciw, S. Rathee, and B. G. Fallone, "Dosimetric IMRT verification with a flat-panel EPID," Medical Physics 30, 3143–3155 (2003).

[14] B. M. C. McCurdy, K. Luchka, and S. Pistorius, "Dosimetric investigation and portal dose image prediction using an amorphous silicon electronic portal imaging device," Medical Physics 28, 911–924 (2001).

[15] S. Pai, I. Das, J. Dempsey, K. Lam, T. LoSasso, A. Olch, J. Palta, L. Reinstein, D. Ritt, E. Wilcox, "TG-69: Radiographic film for megavoltage beam dosimetry," Medical Physics 34, 2228 – 2258.

[16] N. Dogan, L Leybovich, A Sethi, "Comparative evaluation of Kodak EDR2 and XV2 film for verification of intensity modulated radiation therapy," Physics in Medicine Biology 47, 4121 – 4130 (2002).

[17] D Baltas, L Sakelliou, N Zamboglou, The Physics of Modern Brachytherapy for Oncology, Taylor and Francis Group, 443 (2007).

[18] C Danciu, B Proimos, J Resenwald, B Mijnheer, "Variation of sensitometric curves of radiographic films in high energy photon beams," Medical Physics 28, 966 – 974 (2001)

[19] Unknown, "Summary of Gafchromic film product line," http://www.ispcorp.com/products/dosimetry/content/gafchromic/content/home/radiotherapy.html

[20] Unknown, "Gafchromic HS radiochromic dosimetry films for high energy photons," http://harpellassociates.com/ISP/gaf-hs-conspefo.pdf

[21] Unknown, "Garchromic HD-810 radiochromic dosimetry film and D-200 pre-formatted dosimeters for high-energy photons," http://www.ispcorp.com/products/dosimetry/content/gafchromic/content/products/hd810/conspefo.html

[22] Unknown, "Gafchromic MD-55 Radiochromic Dosimetry film for high-energy photons," http://www.ispcorp.com/products/dosimetry/content/gafchromic/content/products/md55/conspefo.html

[23] L Reinstein, G Gluckman, H Amols, "Predicting optical densitometer response as a function of light source characteristics for radiochromic film dosimetry," Medical Physics 24, 1935 – 1942 (1997)

[24] A Rink, I Vitkin, D Jaffray, "Energy dependence (75 kVp to 18MV) of raduichromic films assessed using a real-time optical dosimeter," Medical Physics 34, 458 – 463 (2007)

[25] L Reinstein, G Gluckman and A Meek, "A rapid colour stabilization technique for radiochromic film dosimetry," Physics in Medicine and Biology 43, 2703 – 2708 (1998)

[26] E Efstathopouls, L Costaridou, O kocsis and G Panayiotakis, "A protocol-based evaluation of medical image digitizers," The British Journal of Radiology 71, 841 – 846 (2001)

[27] Unknown, "Gafchromic EBT self-developing film for radiotherapy dosimetry," http://online1.ispcorp.com/_layouts/Gafchromic/index.html

[28] Personal conversations with David Lewis from International Specialty Products.

[29] A Meigooni, M Sanders, G Ibbott and A Szeglin, "Dosimetric characteristics of an improved radiochromic film," Medical Physics 23, 1883 – 1888 (1996)

[30] W McLaughlin, Y Chen, C Soares, A Miller, G Van Dyk and D Lewis, "Sensitometry of the response of a ne radiochromic film dosimeter to gamma radiation and electron beams," Nuclear Instrumentation and Methods in Physics Research 302, 165 – 176 (1991)

[31] PR Almond et al., "AAPM's TG-51 protocol for clinical reference dosimetry of high-energy photon and electron beams," Medical Physics 26, 1847-1870 (1999)

[32] I Ali, C Costescu, M Vicic, JF Dempsey, JF Williamson, "Dependence of radiochromic film optical density post-exposure kinetics on dose and dose fractionation," Medical Physics 30, 1958-67 (2003)

[33] MJ Butson, T Cheung, PK Yu, "Absorption spectra analysis of exposed FWT-60 radiochromic film," Physics Medicine and Biology 49, N377-81 (2004)

[34] NL Childress, L Dong and II Rosen, "Radiographic film calibration for IMRT verification using automated MLC fields," Medical Physics 29, 2384-90 (2002)

[35] T Cheung, MJ Butson, PK Yu, "Post-irradiation colouration of Gafchromic EBT radiochromic film," Physics Medicine and Biology 50, N281-5 (2005)

[36] S Devic, J Seuntjens, G Hegyi, E Podgorsak, C Sores, A Kirov, I Ali, J Williamson and A Elizondo, "Dosimetric properties for improved Gafchromic films for seven different digitizers," Medical Physics 31, 2392 – 2401 (2004)

[37] L Reinstein, G Gluckman and H Amols, "Predicting optical densitometer response as a function of light source characteristics for radiochromic film dosimetry," Medical Physics 24, 1935 – 1942 (1997)

[38] G Gluckman and L Reinstein, "Comparison of three high-resolution digitizers for radiochromic film dosimetry," Medical Physics 29, 1839 – 1846 (2002)

[39] J Kalef-Ezra and K Karava, "Radiochromic film dosimetery: reflection vs transmission scanning," Medical Physics 35, 2308 – 2311 (2008)

[40] Unknown, "Effects of light scattering by films on the performance f CCD scanners," http://online1.ispcorp.com/_layouts/Gafchromic/index.html

[41] T Bortfeld, W Schlegel and B Rhein, "Decomposition of pencil beam kernels for fast dose calculations in three-dimensional treatment palnning," Medical Physics 20, 311 – 318 (1993)

[42] A Ahnesjo, M Saxner and A Trepp, " A Pencil beam model for photon dose calculation," Medical Physics 19, 263 – 273 (1992)

[43] W Trzeciakowski, A bercha, F Dybala, R Bohdan, P Adamiec and O Mariani, "Pressure and temperature tuning of laser diodes," Phsica Status Solidi 244, 179 – 186 (2006)

[44] S Pai, I Das, J Dempsey, K Lam, T LoSasso, A Olch, J Palta, L Reinstein, D Ritt and E Wilcox, "TG-69: Radiographic film for megavoltage beam dosimetry," Medical Physics 34, 2228 – 2258 (2007)

[45] Unknown, "Analog devices AD549 specification sheet," http://www.analogdevices.com

[46] J Graeme, Photodiode Amplifiers Op Amp Solutions, McGraw-Hill 1996

[47] J Karki, "Active Low-Pass Filter Design," Texas Instruments file SLOA049B, September 2002

[48] Unknown, "Noise analysis in operational amplifier circuits," Texas Instruments file SLVA043A, 1999

[49] K Mitzner, Complete PCB Design Using OrCAD Capture and Layout, Newnes 2007

[50] I Amidror, The Theory of the Moiré Phenomenon, Springer 2007.

[51] J Sneddon, Advances in Atomic Spectroscopy, Elsevier 2000

[52] Unknown, http://universe-review.ca/R12-03-wave.htm

[53] G Fowles, Introduction to Modern Optics, Courier Dover Publications 1989

[54] Unknown, "Basic polarization techniques and devices," Meadowlark Optics Inc, 2005

[55] F Dickey and S Holswade, Laser Beam Shaping: Theory and Techniques, CRC Press 2000

[56] Unknown, Melles Griot Optics Giude, http://www.mellesgriot.com/products/optics/toc.htm

[57] E Mah, J Antolak, J Scrimger and J Battista, "Experimental evaluation of a 2D and 3D electron pencil beam algorithm," Physics in Medicine and Biology 34, 1179 – 1194 (1989)

[58] K Higstrm, M Mills, J Meyer, J Palta, D Mellenberg, R Moez and R Fields, " Dosimetric evaluation of a pencil-beam algorithm for electrons employing a two-dimensional heterogeneity correction," International Journal of Radiation Oncology Biology and Physics 10, 561 – 569 (1984)

[59] N Childress and I Rosen, "A software tool for the quantitative evaluation of 3D dose calculation algorithms," Medical Physics 25, 1830-1836 (1998)

[60] T knoos, C Ceberg, L Weber and P Nilsson, " The dosimetric verification of a pencil beam based treatment planning system," Physics in Medicine and Biology 39, 1609 – 1628 (1994)

[61] E Wilcox, G Daskalov, L Nedialkova, "Comparison of the Epson Expression 1680 flatbed and the Vidar VXR-16 Dosimetry PRO film scanners for use in IMRT dosimetry using Gafchromic and radiographic film," Medical Physics 34, 41 – 48 (2007)

[62] D Low and J Dempsey, "Evaluation of the gamma dose distribution comparison method," Medical Physics 30, 2455 – 2464 (2003)